Universidad Nacional de Colombia - Sede Medellín

Master Thesis

A methodology for the measurement of carbon monoxide concentration during *in-situ* combustion with tunable diode laser

Author:
Juan E. Duque

Supervisor:
Alejandro Molina

A thesis submitted in fulfilment of the requirements for the degree of M.Sc. Chemical Engineering

in the

Bioprocesos y Flujos Reactivos
Facultad de Minas, Departamento de Procesos y Energía

August 2016

UNIVERSIDAD NACIONAL DE COLOMBIA - SEDE MEDELLÍN

Abstract

Facultad de Minas

Departamento de Procesos y Energía

A methodology for the measurement of carbon monoxide concentration during *in-situ* combustion with tunable diode laser

by Juan E. Duque

A TDL system is reported to monitor carbon monoxide (CO) concentration under conditions similar to those of laboratory-scale tests used to characterize the behaviour of a heavy crude oil during in situ combustion (ISC). The TDL-CO sensor uses a DFB diode laser operating over the spectral range of the rotational transition R(11) of the CO-2ν-vibrational band, where simulations of spectral absorption bands for CO, CO_2 and H_2O show minimal spectral interference. The absorption spectra were calculated using HiTran 2008 Database, under typical conditions of temperature of 150°C to 800°C, pressures from 1 atm to 5 atm and major species compositions observed in ISC characterization experiments. CO-concentration measurements were conducted in a static-glass cell, of *Duran*® borosilicate glass 3.3 with a pathlength of 3.81cm, to validate the CO sensor architecture under controlled laboratory environments. A calibration curve of CO was obtained by quantifying the optical density at the line center of R(11) for a concentration range between 0.7%$_{mole}$ to 3.4%$_{mole}$ which reached a R-squared of 0.9986. High-pressure and temperature experiments were carried out in a custom-designed combustion chamber with optical access, which has two optical wedged sapphire windows (2°) to avid etalon effects. CO-absorption spectra were validated by a comparative study with HiTran Database while a free-calibration methodology using scanned-wavelength direct absorption TDL was investigated for future characterizing experiments of ISC. Typical Signal to Noise Ratios (SNRs) were above 40, although for the static glass cell a value of SNR = 14 was observed. The linestrengths for R(11) of $\nu^{'} = 2 \leftarrow \nu^{''} = 0$ were also measured and validated with HiTran. The calibration experiments showed the potential of 2.3 μm TLD-CO sensor for non-invasive, in-situ combustion monitoring of CO generated at conditions to those of ISC experiments.

Acknowledgements

I sincerely thank my advisor Prof. Alejandro Molina, who offers me the opportunity to study in such a wonderful research group.

To the Facultad de Minas for the scholarship "Exencion de Derecho Académicos" during 2013-II, 2014-I.

To Colciencia and Ecopetrol by funding the research program "Herramientas tecnológicas para incrementar factor de recobro de crudos", project 1118-531-30561 "Caracterización mediante técnicas láser de las reacciones químicas de petróleo crudo durante combustión in situ".

Contents

List of Figures

List of Tables

To my family

Chapter 1

Introduction

1.1 Motivation

Research efforts have been carried out to improve the recovery factor of heavy-crude oil by the use of the ISC process for non-conventional reservoirs. Improvements of the heavy oil recovery method and deeper knowledge of the chemical reactions that take place from the combustion phenomena in ISC are based on the accuracy of the characterization methods used by the $Oil\&Gas$ companies [1]. The driving force of the growing demand for improving efficiency and optimal-operation conditions for the oil industry in ISC projects comes from both environmental and economic concerns because of the environmental impact generated by any pollutant emissions and the high-operational costs from an inefficient ISC process. Some flue gases produced during ISC such as CO and H_2S are important atmospheric pollutants that generate harmful effects on human health and, therefore, are subject to stringent regulations mandates regarding emission controls [2].

In traditional combustion systems, carbon monoxide (CO) is considered a species that can be used to assess the efficiency of the combustion process. CO is mainly generated during ISC [3] because of incomplete combustion. CO is a toxic pollutant which is strongly regulated.

Traditional extractive sampling methods used in ISC experimental tests at lab-scale suffer from long response times which could favor secondary chemical reaction by intrusiveness of the physical-sampling probes. There is then a strong motivation for developing an in-situ sensor of CO as target molecule during lab-scale ISC experiments.

Conventional methods to measure species concentration such as ex situ gas analyzers in ISC experiments use invasive sampling which tend to disturb the flow field generating shock structures and may by affected by secondary reactions in the sampling probe [4]. However, laser-based diagnostics can provide non-invasive, real-time, in situ and accurate measurements for CO-monitoring during in situ combustion experiments [5].

There is a set of measuring techniques which render accurate results, but a calibration procedure is required, while other primary-measuring methods operate free-calibration but they are not suit to for field or in-situ measurements. For example Gas Chromatography (GC) and Mass Spectroscopy (MS) are very precise measurements techniques, unfortunately, these methods cannot be applied for real-time, sample-free and non-invasive measurements. In Fourier Transform Infrared (FTIR) spectroscopy the spectral lines show limited resolution and the path-length cannot be accurately known because of the lack of directionality of the laser beam from the radiation source [6].

Tunable Diode Laser Absorption Spectroscopy (TDLAS) is an alternative particularly suitable for difficult conditions such as combustion processes where the specific-species detection by non-invasive, real-time and in-situ are important [7]. As TDLAS is an optical technique, it does not have operational problems of sample extraction such as condensation and chemistry and time delay along the extractive line. TDLAS has been successfully implemented in several combustion-test facilities with excellent results [8]. An appropriate understanding of the main combustion phenomena and CO-generation during ISC at lab-scale tests can be obtained with a TDL-CO sensor, giving in a future the availability to install a TDL sensor for gaseous emission control in ISC projects.

This thesis describes in details the design and construction of a TDL-CO sensor using the R(11) transition of the $CO - 2\nu$ for the measurements of carbon monoxide at similar conditions of those characterizing ISC experiments of a heavy crude oil. The sensor was evaluated at pressure and temperatures similar to those of ISC experimental tests in a custom-designed combustion chamber for a range of CO concentration expected relevant to ISC.

1.2 Objectives

1.2.1 Main objective

To develop a methodology to measure the carbon monoxide concentration at conditions similar to those of ISC characterizing-experiments by Tunable Diode Laser Absorption Spectroscopy.

1.2.2 Specific objectives

- To design and build an experimental setup for the evaluation of the carbon monoxide concentration with Tunable Diode Laser Absorption Spectroscopy at conditions similar to those of ISC characterizing experiments.
- To validate the developed CO-measurement methodology with changes in temperature, pressure, and water and carbon dioxide concentration typical of ISC.

1.3 Scope and contribution

This research work describes the development of a methodology for CO-sensing using a designed TDL-sensor at similar conditions of ISC experiments. The experimental data obtained during the laser-based measurement in a static-glass cell and a custom-designed combustion chamber proved the reliability of the CO sensor. Free-calibration and calibration curves showed the potential of the optical technique. The effect of pressure and temperature on the sensor's ability to measure CO was also addressed. The developed sensing system includes an interface in LabView for data acquisition and a code in MatLab that converts the complex laser signals to CO concentration.

1.4 Thesis outline

This thesis is arranged into chapters as follows:

1) **Chapter 2** describes the fundamental theory of in situ combustion and laser absorption spectroscopy and the diagnostic methods to carry out laser-based measurement of carbon monoxide. The theory and implementation of direct absorption (DA) spectroscopy technique is discussed for the methodology and TDL-sensor designed in this work.

2) **Chapter 3** describes in detail the absorption spectra of CO, CO_2 and H_2O and the selection of the vibrational bands using HiTran 2008 database. An analysis was carried out in the order to choose an appropriate absorption line of CO without interference from neighboring compounds. The spectral analysis includes the main gases produced during ISC and interference by hydrocarbons.

3) **Chapter 4** outlines the overall sensor architecture as well as the pitch and catch assemblies of the TDL-sensor. The experimental hardware for the sensor and the equipment is described in detail. An interface in LabView was designed to acquire data signals from LabView while an algorithm for data processing in both free-calibration and calibration methods is explained.

4) **Chapter 5** presents the development of a TDL-sensor with a distributed-feedback (DFB) laser at 2.3 μm. The validation procedure includes the verification of background interference and the validation of spectroscopic parameter such as line-strength, under controlled conditions in a static-glass cell. Calibration and calibration-free curves at room conditions showed the viability of the TDL-sensor.

5) **Chapter 6** demonstrates CO sensing in a practical field environment of high pressure and high temperature of a custom-designed combustion chamber with optical access. The experimental conditions and sensor location are described. An experimental validation using CFD was implanted with good results when non-uniform temperatures are obtained over the line-of-sight.

Chapter 2

Theory and background

2.1 Chapter outline

Chapter 2 described the availability of heavy crude oil over the world and the potential of Colombia to explore petroleum reservoirs by means of in situ combustion (ISC) process. A brief explanation of ISC was conducted in order to clarify the high production of carbon monoxide, which can be above 3%. With the purpose of enhance the characterization methods, chapter 2 showed the disadvantage of the currently methods used for gas analysis. To developed reliable measures during ISC tests, several successful projects of laser diagnostic techniques are shown, where tunable diode laser absorption spectroscopy (TDLAS) provided appropriate performance even during field-measurements of combustion environments. Detail information of spectroscopic theory was carried out.

2.2 Petroleum overview

The future availability of crude oil, which is considered as the most efficient primary source of non-renewable energy, remains an ongoing debate because it plays an important role on the world economy stability. The depletion of non-renewable resources of crude oil within the next 50 years is the reason why governments are increasingly looking to invest in research projects that to use cutting-edge technologies for oil exploration. However, the idea of time for oil depletion is mainly based on the extraction of conventional oil reservoirs. It is estimated that, until now, more than 30% of the total of the conventional oil has been recovered However, this value is as low as 10% for non-conventional reservoirs [9].

Heavy and bitumen crude oil reservoirs are usually seen as one of the non-conventional energy sources most abundantly-scattered over the world. Reserves of heavy-crude oil are estimated to be ∼3396 billion barrels crude original oil (BBCO) in place [10], while bitumen reservoirs have an estimated amount of ∼5505 BBCO in place [10]. The global reserves of unconventional crude oil are usually calculated as three times 3010 BBCO in place, those reported for conventional oil [11]. The Middle East has more than 50% of conventional crude oil, and about 30% of existing heavy crude oil on earth. However, most of the heavy crude oil reserves and more than 80% of natural bitumen are located in the Americas. Canada and Venezuela alone have natural sources of heavy oil that exceed the conventional reservoirs in the world. Increases in the oil-recovery factor of unconventional crude oil would allow that several Latin American governments meet their internal demand.

North and South America along with Middle East have more than 80% of the heavy oil reserve in the world. The Campeche basin of Gulf of Mexico has 45% of the heavy crude oil of American continent, while 45% of all the world reserves are located in the major basin: i) Arabian, ii)Zafgros and iii) East of Venezuela. The main reserves of heavy crude oil are located in Venezuela, where both the East of Venezuela and Maracaibo basis have the 27% of global heavy oil of earth crust, while around 80% of bitumen-global reserves are located in the American continent in both Western Canada and Eastern Venezuela basis.

Colombia is currently positioned as the fourth oil producer in Latin America after Venezuela, Mexico and Brazil. Unconventional basins of both natural bitumen and heavy oil are located in the east and middle of Colombian region. Figure 2.1 shows the Colombian reservoirs and its geographic location. The Maracaibo basin is considered the largest reservoir of heavy oil with, approximately, 322 BBCO in place. Barinas-Apure is located in almost 70% of the Colombian territory with about 9.19 BBCO in place. The Putumayo basin is in the Ecuadorian border and an estimated reserve of 42.4 BBCO is shared with that country. Many of the unconventional reservoirs are located in border areas with both Venezuela and Ecuador. However, Colombia has own resources such as Middle, and Upper Magdalena and Yari basin with approximately 18.6 BBCO waiting for an appropriate exploitation [10].

2.3 *In-Situ* combustion (ISC)

In-situ combustion (ISC) is a thermal oil recovery method used for extracting the fluid from unconventional reservoirs [12]. The propagation of a combustion front along the

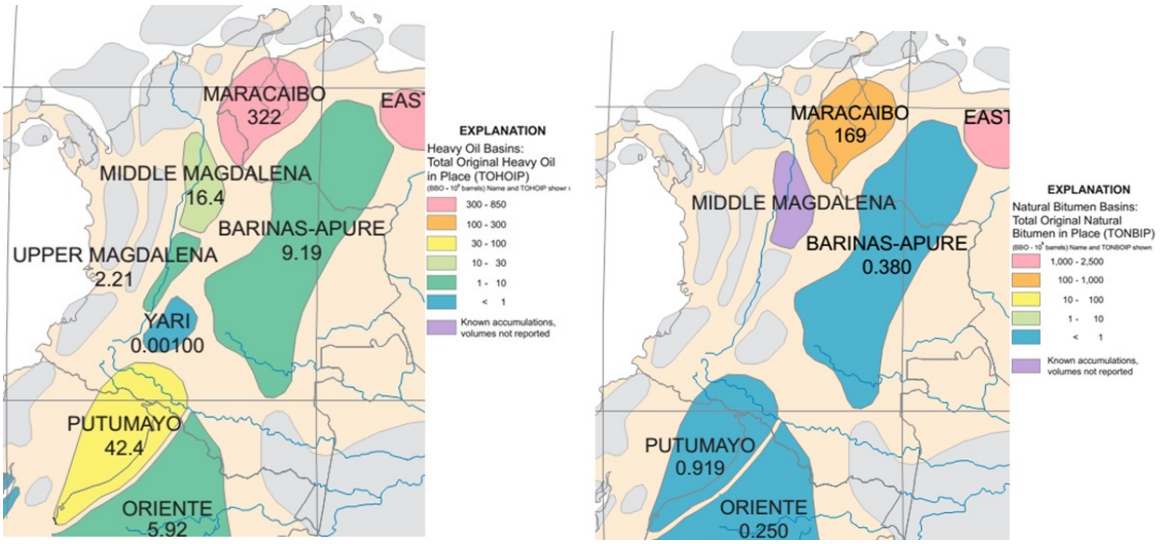

(A) (B)

FIGURE 2.1: A)Heavy oil reservoirs and B)Natural bitumen reservoirs in Colombia

oil reservoir generates enough heat to reduce the viscosity of the original fluid. By continuous injection of air, the combustion front moves and reduction of oil viscosity is sustained. This movement of the combustion starts from the ignition of a portion of the original oil in the vicinity of the injection wells and finishes close to the production wells. The combustion front play an important role in ISC as the oil viscosity is continuously suffering changes because of thermal effects. A natural phenomena that resembles the propagation of the combustion front of ISC is the hot zone of a burning cigarette. Furthermore, molecular breaking, because of the elevated temperatures, takes place. This generates increases on the recovery factor of unconventional reservoirs because an easier extraction of the upgraded oil can be carried out [13]. The burning of hydrocarbons due to combustion phenomena between air and oil leads to a higher reservoir pressure which together with flue gases and carrier water, acts as drainage mechanism that drives the upgraded oil to the production wells. The air that has been injected to the reservoir replaces natural reservoir fluids because of the density difference between the flue gases generated during ISC and the air from the injection wells.

Multiple chemical reactions as well as several phenomena of both heat and mass transfer take place during the propagation of the combustion front inside the oil reservoir. The passage of the combustion front forms six feature zones of ISC, each of them with unique saturation and temperature as illustrated in Figure 2.2 [14]. Zone I represents the region wherein coke deposition occurs, this burned zone records high temperatures due to its proximity to the combustion front considered as the zone with the highest reactivity of the ISC process. Highly-exothermic reactions are conducted in the combustion front through the burning of coke deposited in Zone I. The perfect phenomenon

of combustion during ISC occurs when the coke generated by both reaction mechanism of oxidation and thermal cracking is deposited on the porous rock of the burner zone. In Zone I, which is saturated with air, high temperature oxidations is carried out by a combustion front moving towards producing wells, and leaving behind a sweep zone with coke deposited for a later burning. Thus, the deposition, burnt and formation of coke group a natural cycle that describes the propagation of the combustion front inside the oil field when an ISC process is developed. Next to the coking zone is located the area with vaporized-liquid gas such as flue gases, steam and light hydrocarbons. ISC temperature after the vaporized zone drops to the saturation temperature, and a hot water bank is generated. An oil bank is close to the production wells, wherein a portion of the oil is upgraded by mixing with heavy hydrocarbons [13].

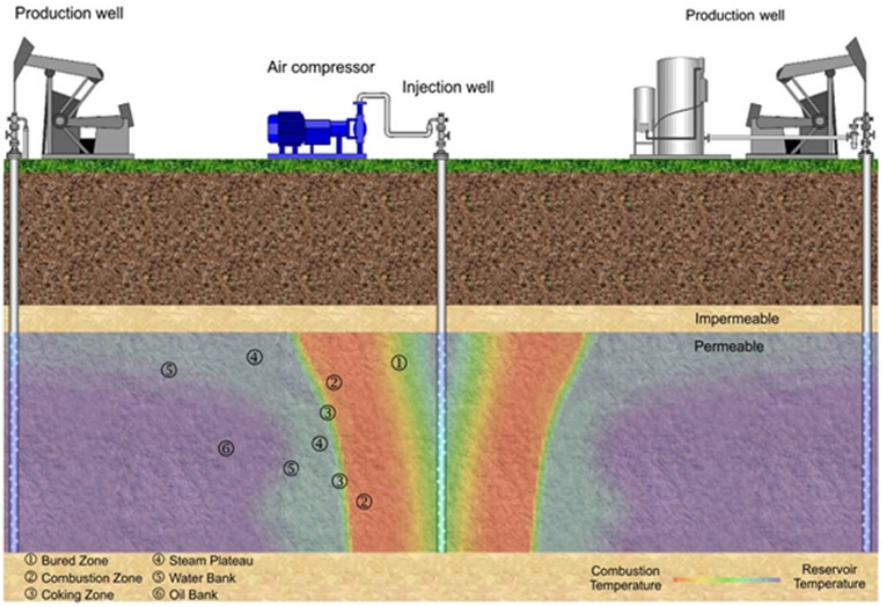

FIGURE 2.2: Sketch of a typical in situ combustion process.

ISC takes place from the native reservoir temperature to temperatures as high as 800 $°C$ [13]. Oxidation and thermal cracking reactions take place during ISC because of the presence of different states of matter in the porous matrix of the reservoir rock. Low temperature oxidations (LTO) are considered as heterogeneous reactions (gas/liquid) with high production of carboxylic acids, aldehydes, ketones, alcohols, and hydrocarbons all of these generated at temperatures up to 350 $°C$. Thermal cracking reactions occur between 300 $°C$ and 400 $°C$ with a production of hydrocarbons with low carbon numbers. During this reacting stage the deposition of an immobile fraction previously referred as coke is accomplished [15]. High temperature oxidation (HTO) occurs when heterogeneous reactions and coke combustion are carried out in a temperature range of 380 $°C$ to 800 $°C$, mainly generating water vapor and carbonaceous oxides such as CO_x [16].

The gas-effluent emissions from ISC have large amount of carbon monoxide (CO) compared with those obtained in typical combustion processes. CO is considered as a key molecule to monitor the combustion efficiency by following the progress of a target-combustion reaction. In addition, CO is a highly toxic and lethal compound for human health. Inhalation may cause death if exposure limits of 9 ppm in 8 hours or 35 ppm during an hour are exceeded. Therefore, a detailed knowledge of the production of CO is mandatory for environmental regulations and safety but also as a key factor for reducing operational costs as CO relates to combustion efficiency.

Carbon monoxide is mainly generated during ISC in the HTO stage as described by the mechanism proposed by Thomas et al. [17], where lab-scale ISC tests of heavy crude oil showed a concentration range of CO from 1.6% to 2%. The Reaction R1 below shows how these authors propose CO formation from ISC coke.

$$Coke_{(s)} + 1.1(O_2 + 3.76N_2)_{(g)} \rightarrow 0.9(CO_2)_{(g)} + 0.1(CO)_{(g)} + 0.6(H_2O)_{(g)} + 4.6(N_2)_{(g)} \quad \text{R1}$$

2.4 ISC characterizing methods for gas analysis

Efficiency improvements of ISC process are mainly attributed to the technological innovations developed in the lab-scale experimental tests. Although, ISC is considered a mature recovery method, there is a poor knowledge of the combustion phenomena. A deficit of the ISC community is the lack of detailed information of the chemical mechanisms. Kapadia et al. [18] and Liu et al. [19] have provided empirical reactions mechanisms with limitations to reproduce the nature for the chemical of the ISC.

Oxidation phenomena and reaction kinetics for oil/rock systems are determined by ramped temperature oxidation (RTO) tests [20]. In a RTO experiment, a specified amount of oil is charged to a reactor flow and undergoes a linear temperature increase over the experimental time generating a uniform heating of the saturated-oil cores, while a flow of either air or oxygen flows through the reactor. RTO tests provide valuable information as experiments take place under controlled conditions with records of production of fluids, coke and flue gases.

Combustion tubes are carried out to study the advance of the combustion front. Operational parameters such as the necessary reservoir air-flow to maintain a selfpropagation of the combustion front, recovery factor, pressure drop and production of flue gases are

important experimental results obtained from combustion tubes. In the experimental setup the combustion begins at one end of the reactor, which is usually stainless steel with several meters long and few centimeter in diameter. A packed bed is saturated with oil and water and located along the tube length[21]. Semi-quantitative measurements are conducted by characterization methods with a lower complexity than those outlined below. Thermogravimetric analyses (TGA/DTA) as well as differential scanning calorimetry quantify the thermal stability by monitoring the weight changes using a reference sample. Heat of reaction, amount of deposited coke, minimum temperature of combustion front and kinetic parameters can be obtained with these experimental tests [22] [23].

The lab-scale setups used to characterize ISC use intrusive probes and gas analysis systems to monitor the generation of different species. However, these devices may perform erroneous measurements when aerodynamic changes around the measuring volume caused by the intrusiveness of a physic probe are important. Furthermore, the reactive compounds may undergo secondary reactions caused by the generation of both concentration and temperature gradients as well as poor quenching.

Gases from ISC experimental test at lab-scale are traditionally measured with extractive probe and non-dispersive infrared (IR) analyser. However, delivering and conditioning a hot, moisture-saturated flue gas to an analyser can be a tedious process requiring a complex sampling manifold that needs to be well maintained. This sampling manifold may involve a long delay time, and CO in our case may be lost in the sampling manifold owing to many mechanisms particularly at high-temperature conditions. Furthermore, non-dispersive devices employ a wideband IR ration source over the spectral range of the CO vibrational bands. Such instruments are potentially subject of spectral interference from the major combustion products. In addition, gas analyzers that require extractive gas sampling such as chromatography have low temporal resolution and long delay time.

This research used for the first time for lab-scale ISC experiments a method of laser diagnostic for CO sensing under typical lab-scale conditions of ISC tests that, in principle, should not be affected by the various drawbacks that the traditional ex-situ measurements experience and that were described above..

2.5 Laser diagnostics for species-specific sensing

Laser diagnostic methods are currently the most important experimental tool for understanding of combustion. Laser techniques can be applied directly in practical combustion systems to study details of the complex interaction of chemical kinetics and transport processes and act as sensors in active control loops to improve fuel efficiency and reduce the environmental effects of combustion. The main advantage of optical methods is attributed to noninvasive interaction that occurs between the laser light and matter. Real-time measurements with high spatial and spectral resolutions provide detailed information on highly complex reactions such as combustion phenomena [7].

Measurements of concentration, temperature, pressure and particle velocity can be obtained using optical methods such as laser diagnostic techniques [24]. Tunable diode laser absorption spectroscopy (TDLAS) provides a valuable method for characterizing combustion gases and operating parameters. Temperature and concentration have been measured by TDLAS in hostile environments of industrial processes such as waste combustors and pressurized gasifiers. Most optical methods based on absorption spectroscopy, such as TDLAS and Cavity ring-down spectroscopy (CRDS), perform quantitative measurements along the line-of-sight of the laser beam [25]. However, CRDS has greater complexity than TDLAS due to operational cost as well as complexity in processing and acquisition of signals [26]. Various laser-based methods have been implemented with absorption spectroscopy to characterize the combustion. Variety of laser diagnostic methods that implement linear and nonlinear optics are the subject of experimental research for the monitoring and detection of species. However, many laser techniques have limitations for measuring carbon monoxide in ISC. Fluorescence methods such as planar laser induced fluorescence (PLIF) and laser induced fluorescence (LIF) developed a visual mapping with concentration contours [27], therefore, a coupling to quantitative methods must be carried out. Methods of elastic scattering such as laser Rayleigh scattering (LRS) and induced polarization such as spontaneous Raman spectroscopy (SRS) have low detection limits, while CARS and CRS have both high complexity and experimental costs.

TDLAS has measured carbon monoxide concentration in hostile conditions of temperature and pressure. Monitoring of chemical species via laser-based techniques has been developed on an industrial-scale equipments such as waste combustors, coal gasifiers, scramjets, pulse detonation engines (PDEs), IC engines and aerojets [28]. Although different scenarios of laser diagnostics were successfully developed to characterize combustion, very few optical methods are used in the oil community.

The second overtone vibrational band of carbon monoxide, $\upsilon' = 3 \leftarrow \upsilon'' = 0$, corresponding to wavelengths near $1.55\mu m$, is the spectral region most widely used for tuning diode laser for carbon monoxide monitoring. Accessibility to telecommunication laser is considered an advantage when working in this spectral range. However, the vibrational band 3υ has line-strength values lower than the fundamental and first overtone vibrational bands. Furthermore, high spectral interference caused by vibrational bands of water steam (H_2O) and carbon dioxide (CO_2) limit the characterization of CO using rotational transitions belonging to 3υ. Low line-strengths give low absorption values of target compound yielding that tunable diode laser absorption spectroscopy via direct absorption is not enough sensitive to detect the target molecule. Therefore, frequency modulation spectroscopy techniques have been mainly used at 3υ vibrational band for a higher detection limit. Tunable diode laser absorption spectroscopy with wavelength modulation spectroscopy (TDLAS-WMS) has been the most implemented method. On the other hand, measurements of CO at fundamental band $\upsilon' = 1 \leftarrow \upsilon'' = 0$, corresponding to wavelengths near to $4.6\mu m$, are currently the subject of study. The highest line-strength and absorption values of carbon monoxide are achieved in this spectral region. Limitations of temperature control of diode laser used in the Mid-Infrared (MIR) have generated problems for industrial-scale implementation. However, lasers than can operate at wavelength corresponding to MIR under industrial conditions, such as external cavity quantum cascade lasers (EC-QCLs), are more expensive than lasers that work at near infrared (NIR). The 2υ vibrational band, corresponding to the first overtone, $\upsilon' = 2 \leftarrow \upsilon'' = 0$, is considered as a prominent region to characterize carbon monoxide. This band provides isolated carbon monoxide rotational transitions from interference of (H_2O) and CO_2 as well as proper line-strengths and accessibility to commercial lasers working at NIR wavelengths such as distributed feedback (DFB) lasers.

Different CO rotational transitions belonging to the 2υ vibrational band have been implemented in the tuning of a diode laser to characterize carbon monoxide using direct and modulated absorption spectroscopy. Several absorption lines of CO such as R(4), R(6), R(9), R(10), R(12), R(15) and R(30) have been commonly used in TDLAS which have appropriate line strength and small interferences by neighbouring compounds.

Gabrysch et al. [29] used the 3υ vibrational band of CO for simultaneous detection of CO and (CO_2) concentration. TDLAS by direct absorption (DA) and WMS were implemented for monitoring two target compounds at wavelengths near $1.578\mu m$. The CO rotational transitions belongs to the second overtone vibrational band, while the absorption line of CO_2 is from a combination vibration band $2\upsilon_1 + 2\upsilon_2 + \upsilon_3$. Gabrysch et al showed that in some cases the need to use more than one diode laser for sensing two molecules can be avoided by a careful selection of absorption transition lines, where

a minimum detectable of concentration for CO was 500 ppm and 800 ppm for CO_2 by using TDLAS-DA, while for TDLAS-WMS an improvement was obtained in which the minimum detectable concentration for both CO and CO_2 is about 10 ppm. Engelbrecht developed a diode laser spectrometer for simultaneous sensing of CO and CO_2 by using P(7) and P(30) as the absorption lines. These absorption features were selected based on criteria such as proximity between transitions and little interference of neighboring compounds. Concentration detection limits using TDLAS-WMS for CO and CO_2 were 5.1 ppm and 9.1 ppm. Excellent versatility, stability and flexibility between optical devices were the most important results by using an optical fiber system instead a free-space system.

Wang et al. [30] reported CO concentration measurements using TDLAS-DA and TDLAS-WMS with DFB diode laser in both exhaust and the immediate post flame regions of an atmospheric pressure flat flame burner operating on ethylene and air. The first overtone of CO was regarded as the spectral region where the measurements were carried out. The R(15) absorption line was the spectral region selected to obtain concentration values of CO in the exhaust duct, while R(30) was used at the immediate post flame, both R(15) and R(30) belong to R-branch of the first overtone. The concentration detection limit corresponding to wavelengths near to $2.3\mu m$ in the exhaust duct using TDLAS-DA was 1.5 ppm to 460 K, while using TDLAS-WMS the detection limit in the exhaust duct was 0.1 ppm. Nicolas et al. [31] used TDLAS-WMS at an astigmatic multipass cell, with an optical pathlength of 100 m. An excellent concentration limit was achieved to carbon monoxide of 0.3 ppm by using both R(12) and R(9).

TDLAS-DA has been implemented when an appropriate absorption of target compound is possible. Conditions under which the experiments will be carried out such as pressure, temperature, optical path are the parameters than influence the detection limits of the compound. ISC has an abundant production of carbon monoxide from heavy oil between 10° and 20° API, about $2\%_{mol}$ dry basis. This mole fraction of carbon monoxide can give a good light-matter interaction and appropriate values of absorption of target compound are obtained.

2.6 Spectroscopy theory

In this section the necessary background theory of absorption spectroscopy is described. A brief explanation of the characteristic phenomenon of light-matter interaction is given. The molecular absorption transitions for CO are studied explaining the vibrational

modes in the near and middle infrared regions. The TDL theory to quantify a target molecule concentration via Beer-Lambert and broadening mechanisms is detailed in order to introduce the equations used in this thesis.

2.6.1 Ligth-matter interaction

Absorption spectroscopy is rooted in phenomena of quantum theory because the interactions between radiation and matter occur in discrete amounts called quanta. This energy amount governs the changes in energy levels of an atom when an interaction with a photon is achieved. Due to quantization of energy levels, only certain transitions take place between modes of internal energy of a molecule such as nuclear, rotational, vibrational and electronic. Electromagnetic radiation, by means of a laser light, and matter can interact when the wavelength of the laser emission resonates with a characteristic motion of a molecule. An energetic excitation from a lower state to a higher state generates an absorption transition when matter absorbs a photon. However, the matter can also emit a photon giving an emission line which consists of a transition from an excited level to a lower level.

Discrete differences between energy levels, $\Delta E = E_2 - E_1$, are transitions that generate an absorption spectra. Three key parameters are present in an absorption spectra: i) transition position, ii) line-strength and iii) transition shape. The transition position is determined by the energy difference of quantum levels where the absorption transition takes place which is described by Planck′s law. Line-strength is based on the relative population of molecules in the different energy states, which is governed by Boltzman statistics at a given temperature, where some energy states can be more populated than other transitions resulting in the absorption of more photons by highly populates states.

Each of the quantum levels is associated with a molecular microscopic movement. Electronic, vibrational and rotational movements are represented by different quantum numbers. Depending on the quantum number, the transition can be used to group the absorption spectrum in: i) electronic system (rovibronic), ii) vibrational bands (rovibrational) and iii) pure rotational lines. Different types of transitions between quantum states occur in different regions of wavelength. Rovibronic transitions need more energy therefore occur in the UV and visible region. Rovibrational transitions require less power than electronic system taking place in IR region, while the pure rotational lines are carried out at microwave region. This thesis focuses on the study of rovibrational transitions of CO located in the NIR region.

2.6.2 CO molecular spectra

Carbon monoxide is a heteronuclear diatomic molecule with a permanent electric dipole moment because of the positive charge on one side and negative on the other with a simple fundamental vibrational mode of stretching. The constant movement of the electric dipole moment via rotations and vibrations increases the possibility of absorption of electromagnetic radiation by CO.

Molecular vibrations of CO are carried out in the infrared region leading to changes in the electric dipole moment. These molecular movements, which occur at characteristic frequencies, create the possibility to resonance with electromagnetic waves which generate energy transitions via absorption in these frequencies an thus vibrational absorption bands.

2.6.3 Quantitative absorption spectroscopy theory

Absorption spectroscopy is based on a physical phenomenon wherein a target molecule can absorb electromagnetic radiation as function of wavelength in a specific-spectral range in this research. TDL uses the absorption spectrum for tuning a diode laser in an isolated absorption line to develop measurements of carbon monoxide concentration; however, it can also be applied to determine temperature, pressure and even particle velocity in hazardous environments. In a TDL setup, a collimated laser beam is directed through a gaseous medium to posterior being detected by a detector. The CO absorbs photons from the diode laser when the frequency of the photons resonates on a part with an absorption transition of CO. Therefore, if the emitted wavelength from the diode laser is tuned over an absorption transition, an absorption phenomenon takes place. By measuring the incident and transmitted intensities as a function of the wavelength along the absorption line, the absorption transition can be measured and a CO concentration inferred.

2.6.3.1 Beer-Lamber law

TDL technique implements the absorption spectrum of a target molecule to develop quantitative measurements such as concentration by using the Beer-Lambert law. When a laser beam of a collimated-monochromatic radiation of radiant power $I(\lambda)$ crosses through an homogeneous absorbing gas of thickness Z, the transmitted radiation $I(\lambda, Z)$ has a radiant power given by Eq 2.1.

$$I(\lambda, Z) = I(\lambda) \times exp(-k(\lambda, T)Z) \tag{2.1}$$

where $k(\lambda, T)$ is the absorption coefficient of the matter obtained from Eq 2.2. For measurements of high resolution spectroscopy in gas phase, the absorption coefficient is determined by the line-strength $S_i(T)$ of the substance in an absorption transition i, the partial pressure P_{CO} and a the line-shape function $\phi(\lambda, T, P, X_B)$.

$$k(\lambda, T) = S_i(T) \times \phi(\lambda, T, P, X_B) \times P_{CO} \tag{2.2}$$

Replacing Eq 2.2 in Eq 2.1 yields a new mathematical relation, Eq 2.3, known as Beer-Lambert law and that describes light-matter interaction.

$$I(\lambda, Z) = I(\lambda) \times exp(-S_i(T) \times \phi(\lambda, T, P, X_B) \times P_{CO} \times Z) \tag{2.3}$$

The spectral absorbance, $k \times Z$, is referred as absorption (α) or optical density (OD), Eq 2.4, which is highly implemented in laser diagnostic reports.

$$OD \equiv \alpha\,(\lambda) \equiv -\ln\left[\frac{I(\lambda, Z)}{I(\lambda)}\right] = S_i\,(T) \times \phi\,(\lambda, T, P, X_B) \times P_{CO} \times Z \tag{2.4}$$

The dimensionless product $\alpha\,(\lambda)$ is defined as absorbance, Eq 2.5, and is often used to describe the absorption level. In the optically thin limit, $\alpha\,(\lambda) \ll 1$, the absorbance is equal to absorption.

$$1 - \frac{I(\lambda, Z)}{I(\lambda)} = 1 - exp\,(-\alpha\,(\lambda)) \approx 1 - (1 - \alpha\,(\lambda)) \tag{2.5}$$

Thus,

$$\alpha\,(\lambda) = -\ln\left[\frac{I(\lambda, Z)}{I(\lambda)}\right] \tag{2.6}$$

Combining Eq 2.3 and Eq 2.4 and equaling $Z = L$, Eq 2.7 is obtained.

$$\alpha\,(\lambda) = S_i\,(T) \times \phi\,(\lambda, T, P, X_B) \times P \times X_{CO} \times L \tag{2.7}$$

The last mathematical relation allows to express results of the measured gas in mole fraction. The amount of fraction has the advantage of being independent of external

conditions. Since the lineshape function ϕ is normalized such that $\int_{-\infty}^{\infty} \phi(\nu)\, d\nu \equiv 1$, the spectrally-integrated absorbance, $A_{line}[cm^{-1}]$, which is the area underneath the absorption lineshape, can be used to obtain species concentration by Eq 2.9.

$$\int_{-\infty}^{\infty} \alpha(\nu)\, d\nu = S_i(T) \times X_{CO} \times P_{Total} \times L \tag{2.8}$$

$$X_{CO} = \frac{1}{S_i(T) \times P_{Total} \times L} \int_{-\infty}^{\infty} \alpha(\nu)\, d\nu = \frac{1}{S_i(T) \times P_{Total} \times L} \times A_{line} \tag{2.9}$$

2.6.3.2 Line-strength

Radiative transfer theory for two states of a vibrational-rotational system delivers the definition of the spectral linestrength given by Eq 2.10, which illustrates that linestrength of a specific transition depends on two major factors: the population of the lower quantum state by Boltzman's function and the probability of the transition which depends on specific spectroscopic constants associated with that particular transition.

$$S_i(T_{ref}) = \frac{8 \times \pi^3}{3 \times h \times c} \nu_{0,i} \frac{I_a \times g'' \times exp\left(\frac{-c_2 \times E_i''}{T_{ref}}\right))}{Q(T_{ref})} \times \left[1 - exp\left(-\frac{c_2 \times \nu_{0,i}}{T_{ref}}\right)\right] \times \Re_i \times 10^{-36} \tag{2.10}$$

$S_i(T_{ref})$ is the linestrength for the i-transition based on a reference temperature, commonly 296 K, h is the Planck's constant, C is the speed of light in vacuum, $\nu_{0,i}$ is the central wavenumber of spectral transition, I_a is the natural isotopic abundance, c_2 is the secondary radiation constant $c_2 = \frac{h \times c}{k_B}$ where k_B is the Boltzmann's constant, E_i'' is the lower state energy, $\Re_i$ is the weighted transition moment squared and g'' is the state statistical weight. $\Re_i$ is independent of both temperature and isotopic abundance and can, therefore, be considered the real molecular property. The term $exp\left(\frac{-c_2 \times E_i''}{T_{ref}}\right)$ in Eq 2.10 accounts for the ratio of Boltzman populations, and the fourth therm on the right is the effect of stimulated emission.

Two preconditions are important when using 2.10. First, when local thermodynamic equilibrium is assumed, the population between states is governed by the Boltzman statistic. Second, the linestrength is weighted according to the natural terrestrial isotopic abundances. The linestrength $S_i(T)$ for a particular transition i can be converted from the radio of linestrength with 2.10 at temperature T and T_{ref}, rendering the following equation,

$$S_i(T) = S_i(T_{ref}) \frac{Q(T_{ref})}{Q(T)} exp\left[-\frac{h \times c \times E_i''}{k_B}\left(\frac{1}{T} - \frac{1}{T_{ref}}\right)\right] \frac{\left[1 - exp\left(\frac{h \times c \times \nu_{0,i}}{k_B \times T}\right)\right]}{\left[1 - exp\left(\frac{h \times c \times \nu_{0,i}}{k_B \times T_{ref}}\right)\right]} \tag{2.11}$$

$Q(T)$ is the internal partial function for CO, which is function of temperature and can be obtained by using Eq 2.12 .The coefficients are listed in Table 2.1 from HiTran database for carbon monoxide.

$$Q(T) = a + (b \times T) + (c \times T^2) + (d \times T^3) \tag{2.12}$$

TABLE 2.1: HiTran96 coefficients for the partition function of CO.

Coefficients	70≤T≤500 K	500<T≤1500 K	1500<T≤3005 K
a	0.227758	0.90723	0.63418
b	0.36290	0.33263	0.20760
c	-0.74669	0.11806	0.10895
d	0.14896	0.27035	0.19844

The linestrength of transitions, which reflects the net result of both absorption and stimulated emission, depends on the optical transition probability and the molecular populations of the upper and lower states. The probability of optical transition is a fundamental parameter that depends on the wave functions of the upper and lower state. However, the populations of the upper and lower states are functions of temperature. In the work developed in this thesis, the local thermal equilibrium can be assumed and the molecular population distributions of different energy states are determined by the local gas temperature. In the ranges of temperatures, as high as 600K, and pressures, up to 4 atm, of this research, the population distribution is always within the limits of non-degeneracy and can be satisfactorily described by Boltzmann statistics.

2.6.3.3 Line-shape function

Uncertainties in the energy of an absorption transition i with a central line position $\nu_{0,i}$, produce a finite spectral width with a Gaussian lineshape according to the Heisenberg's principle.

The lineshape function ϕ reflects the relative absorption coefficient variation with wavelength or wavenumber due to different broadening mechanisms. Although numerous physical mechanisms influence the shape function of lineshape function, there are two

main broadening mechanisms considered for combustion research such as collisional broadening by pressure and Doppler broadening by thermal motion.

2.6.3.3.1 Doppler broadening. When a molecule has a velocity component in the same direction as the beam of light, there will be a shift in the wavenumber at which it will absorb a photon. This effect, called Doppler shift, is carried out because of the constant motion of molecules of any gas with random velocities described by a Maxwellian velocity distribution function. The distribution function leads directly to a lineshape function with a Gaussian form given by Eq 2.13.

$$\phi_D(\nu) = \frac{2}{\Delta\nu_D}\sqrt{\frac{ln(2)}{\pi}} \times exp\left[-4 \times ln(2) \times \left(\frac{\nu - \nu_0}{\Delta\nu_D}\right)^2\right] \tag{2.13}$$

The Doppler halfwidth (FWHM) $\Delta\nu_D$ is given by

$$\Delta\nu_D = \nu_0\sqrt{\frac{8 \times k_B \times T \times ln(2)}{m \times c^2}} \therefore \Delta\nu_D = \nu_0\left(7.1623 \times 10^{-7}\right)\sqrt{\frac{T}{M}} \tag{2.14}$$

Doppler broadening is function of temperature by Doppler halftwidth (FWHM) and is not dependent on the mole fraction of species. The term $\nu - \nu_0$ quantifies the spectral distance to the center line for the transition i, T is the temperature in K and M is the molecular weight in g/mol.

2.6.3.3.2 Collisional broadening. Molecular interactions cause life-time reductions of an excited energy state because of disturbances that occur during the collision. Reductions in life-time of a molecule in an energy level j lead to higher levels of uncertainty, thus generating an absorption lineshape following an Lorentz function.

$$\phi_c(\nu) = \frac{1}{2 \times \pi} \times \frac{\Delta\nu_c}{(\nu - \nu_0)^2 + \left(\frac{\Delta\nu_c}{2}\right)^2} \tag{2.15}$$

where $\Delta\nu_c$ is the FWHM for collisional broadening which is modelled as the product of the pressure system and the sum of each mole fraction of the interfering species B multiplied by the broadening coefficient 2γ.

$$\Delta\nu_c = P \times \sum_B x_B \times 2\gamma_{A-B} \tag{2.16}$$

As the likehood of collision increases at higher pressures collisional broadening dominates at elevated pressures typically $p \geq 0.1atm$. Therefore, collisional broadening is

important in the development of this thesis since experiments with pressure conditions as high as 4 atm were carried out.

2.6.3.3.3 Voigt profile. In the common case in which both Doppler and Collisional broadening are significant and neither can be neglected, the appropriate lineshape will be a combination of the two. A Voigt profile is a convolution of Doppler and Collisional broadening which is used in TDLAS experiments in combustion environments when temperatures and pressures are high..

$$\phi_V(\nu) = \int_{-\infty}^{\infty} \phi_D(u) \times \phi_C(\nu - u)\, du \tag{2.17}$$

$$\phi_V(\nu) = \frac{2 \times ln(2)}{\pi^{3/2}} \frac{\Delta\nu_C}{\Delta\nu_D^2} \int_{-\infty}^{\infty} \frac{e^{-t^2}}{\left(\sqrt{ln(2)} \times \frac{\Delta\nu_C}{\Delta\nu_D}\right)^2 + \left(\sqrt{4 \times ln(2)} \times \frac{\nu - \nu_0}{\Delta\nu_D} - t\right)} dt \tag{2.18}$$

where t is the integral variable and a is the damping constant:

$$t = \frac{2 \times \sqrt{ln(2)} \times u}{\Delta\nu_D} \tag{2.19}$$

$$a = \frac{\sqrt{ln(2)}\Delta\nu_C}{\Delta\nu_D} \tag{2.20}$$

The a parameter indicates the relative significance of Doppler and collisional broadening, with a increasing as the effect of collisional broadening increase. The integral can be calculated using standard mathematical routines.

2.6.4 Quantitative measurements of species concentration

2.6.4.1 Direct absorption sensing strategies

Direct absorption techniques have been extensively used for non-intrusive in-situ gas measurements such as temperature, pressure, species concentration and particle velocity. This section is focused on methods for measuring concentration of gaseous species using direct absorption spectroscopy in systems with tunable diode lasers.

2.6.4.1.1 Fixed-wavelength direct absorption spectroscopy The method of fixed-wavelength direct absorption uses the fractional-light transmission in a specific wavelength and infers gas conditions directly from the Beer-Lambert law. The wavelength of the diode laser is not tuned over the absorption-CO feature, the detection bandwidth is limited by the sampling rate of the detector and the data acquisition system. Therefore, high sampling rates should be developed in fixed-wavelength DA.

For schemes of fixed wavelength the absolute wavelength of laser emission must be accurately known and precisely controlled. Wavelength monitors with precise control of temperature and current of the laser are used to understand the behaviour of laser emissions, also to help to prevent long term wavelength drift. The use of these devices increases costs of the experimental setup and demands complex sensors with appropriate operations on harsh environments.

The wavelength of the laser is adjusted to the linecenter of the absorption transition through precise control of both temperature and current of the driver. Concentration measurements are carried out when the laser emission in the absorption peak are performed. However, this technique requires a reference intensity of zero absorption and a laser emission locking for stabilization. In the presence of broadband absorption and scattering loss, more lasers are required to distinguish between the intensity loss due to the distinct absorption transition versus other absorption or light scattering. In addition, accurate modelling of ϕ_ν depends on knowledge of complex interactions of the thermal motion and collision processes. Therefore, the uncertainty in the measured concentration using fixed-wavelength strategy is relatively large.

2.6.4.1.2 Scanned-Wavelength direct absorption spectroscopy Scanned wavelength direct absorption spectroscopy has been implemented for most measurements TDLAS assemblies with direct absorption measurements, without modulation are often quite simple and yield low detection limits.

For a diode laser, wavelength scanning is typically accomplished by temperature stabilizing the laser and modulation of the injection current with a sawtooth or triangular waveform. This causes a simultaneous ramping of the laser intensity and wavelength. A laser can then be wavelength-tuned over the spectral range of an absorption transition, producing the detected signal shown in the intensity vs time of Fig 2.3 A). Using a baseline fit and applying Beer-Lambert law the detected signal can be converted to absorbance, as shown in Fig 2.3 B), which in turn can be used to determine properties of the absorbing species such as temperature and mole fraction.

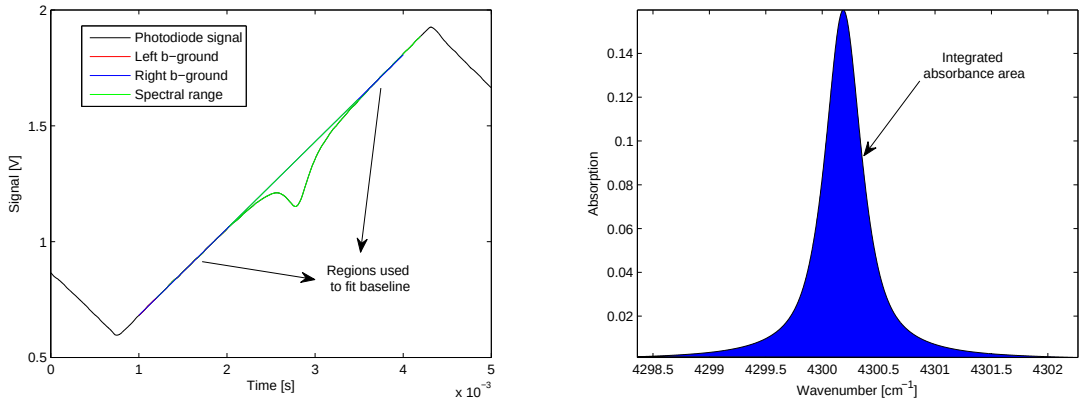

(A) (B)

FIGURE 2.3: A)Photodiode signal with feature absorption and baseline and B) integrated absorption area.

The incident laser intensity is known as baseline and can be: i) experimentally measured if the incident beam is split into two beams, one that directs the measuring field and other directly to a reference photodiode, ii) mathematically adjusted using portions of non-absorption in the absorption scan, when the lines are sufficiently isolated such that these portions are available. When none of these approaches is possible, the addition of a reference path for monitoring the variation of the laser intensity provides another solution to the expense of a more complicated system and potential errors from etalons. In general, particular care should be taken to the baseline of direct absorption measurements, particularly for in-field measurements.

The scanned-wavelength (SW) method has advantages such as i) provides easy data processing as the line shape function is normalized to 1 and broadening coefficients are not necessary to be calculated and ii) the scanning-range covered by the diode laser over the target transition is easily obtained; therefore, precise information of the absolute wavelength is not necessary.

The technique is relatively easy to use by means of integration of the absorption lineshape; however, it needs data from linestrength. Broadening coefficients for lineshape function are not necessary to infer concentration. The technique has some disadvantages: i) the bandwidth of the sensor can be limited to several kHz as the wide laser scanned range needs to reach non-absorption regions, ii) the procedure for obtaining baseline is prone to errors when absorption is low, iii) less effective method for high pressure due to the lack of baseline as the collisional broadening blends the features. However,

the difficulties of the method of fixed wavelength are avoided using scanned wavelength since the method distinguishes attenuation of intensity due to different characteristics of absorption and scattering loss.

Chapter 3

Quantitative spectroscopy of CO absorption transitions in the NIR

3.1 Chapter outline

Absorption simulations were carried out for the first-,second- and fundamental band of carbon monoxide at typical lab-scale conditions of ISC experimental tests. HiTran database 2008 was used to simulate spectroscopic parameters such as line-strength and absorbance while the CO and the major ISC-flue gases concentrations were obtained by a stoichiometric analysis of the coke-oxidation reaction in the HTO stage by the reaction mechanism proposed by Thomas et al [17]. The absorption spectra considered the non-excited states. The R-branch of the $CO-2\nu$ was chosen because of the high absorption values and minimal interference by CO_2 and H_2O. A spectral analysis showed an increasing behaviour of the absorption spectra when the pressure raised. A higher temperature increases the last part of the R-branch, above ∼R(15), but decreases the signal in the spectral range below ∼R(15). The rotational transition R(11) of the R-branch of $CO-2\nu$ was chosen as the best option to perform laser-based optic diagnostics by TDL because of excellent line strength behaviour and isolation features from neighbouring compounds. A final analysis was conducted to corroborate the viability of the R(11) when hydrocarbons are present when measuring CO.

3.2 Introduction

The absorption of electromagnetic radiation from a monochromatic-light source is carried out when a target molecule is monitored by the Tunable Diode Laser (TDL) technique,

wherein average-molar concentrations are obtained along the optical pathlength over a CO-spectral specific region. Detailed-spectroscopic analysis for carbon monoxide and most abundant ISC-combustion products must be developed to performed CO measurements by using TDLAS without any spectral interference from neighbouring compounds. Furthermore, choosing an appropriate absorption transition provides a first thought of the optic-experimental setup and the viability to use modulation techniques.

3.3 Determination of molar-fraction concentrations for the major gaseous compounds generated during ISC.

The gaseous composition on wet basis for the main products in ISC-characterizing experiments was determined with a stoichiometric analysis that considered the kinetic mechanism for the coke-oxidation reaction proposed by Thomas et al[17]. The coke reaction at high temperature oxidation (HTO) was considered as the most relevant in HTO thermal-stage as it contributes with the major production of carbonaceous oxides during combustion. This thesis assumed as typical molar fraction concentrations for lab-scale ISC experiments for CO, CO_2 and H_2O those obtained by using Thomas' reaction.

A stoichiometric analysis base on R1 determined as the minimum values of percentage molar fraction on wet basis for carbon monoxide, carbon dioxide and water vapour 1.62%, 14.52% and 9.10% respectively. These values are in the range of experimental data obtained in ISC characterizing tests for heavy oils with API gravity between 8° and 20°.

3.4 Simulation of absorption spectra

The HiTran 2008 database was used to simulate the absorption spectra of CO, CO_2 and H_2O in the order to perform spectroscopic analysis that provides different candidate spectral regions free of overlapped-spectral interference but with high absorption values to carry out CO measurements by laser-based diagnostics with TDLAS. High-Resolution Transmission Molecular Absorption (HiTran) is a spectroscopic database widely used in the combustion community in spectral studies that predicts possible behaviours of the feature-absorption lines when changes in experimental conditions such as temperature and pressure are conducted. Although, HiTran database is rooted to simulate the absorption, transmission and emission of light in the atmosphere, excellent results have been obtained to emulate light-matter interactions in combustion environments.

As outlined in Chapter 2, the ISC process at lab-scale characterizing experiments have been studied under different conditions, particularly at various ranges of temperature and pressure. This thesis developed a spectral study for temperature varying between 423.15 K and 1023.15 K, and pressure from 1 atm up to 20 atm. Regarding the optical pathlength, it was chosen to be 0.0381 m as this is the diameter of a typical synthetic-reservoir core. The line-shape function was fitted to be a Voigt profile, which adequately represent spectral broadening by thermal motion and collisional phenomena.

Absorption spectra of CO, CO_2 and H_2O were obtained in a spectral range that covers the three CO-vibrational bands for the purpose of knowing the absorption profiles and the CO-absorption regions affected by neighbouring absorption bands along the electromagnetic spectrum. CO has three vibrational absorption bands. Since the highest ISC temperature was lower than the characteristic vibrational temperature of carbon monoxide, $T \ll \theta_{v,CO} \rightarrow 1023K \ll 3125K$, the CO-hot bands were not taken into account. Therefore, the simulated CO-vibrational bands were the fundamental band, $v^{'} = 1 \leftarrow v^{''} = 0$, the first-overtone,$v^{'} = 2 \leftarrow v^{''} = 0$, and the second-overtone, $v^{'} = 3 \leftarrow v^{''} = 0$. Thus, the analyzed range covered the region from 1815.57 cm^{-1}, which is the end of the fundamental band, to 6416.81 cm^{-1}, the beginning of the second-overtone.

3.5 Selection of the CO-vibrational absorption band

As previously outlined for the CO-vibrational bands, the vibrational absorption bands for gaseous molecules were selected to be those originating from a non-excited state, this is, those to have a vibrational quantum number equal to zero in the lower-state. Hot bands do not play an important role at typical ISC conditions as its line-strength values are weaker than those obtained for the fundamental bands. However, special care was taken for water as it presents a characteristic vibrational temperature of the second vibrational mode that is lower than typical ISC temperatures ($\theta_{v_2} = 960 < 1073K$).

The line-strengths were obtained for a reference intensity at room temperature making use of radiative transfer theory, while the Beer-Lambert law was used to quantify the absorption fitting the line-shape as a Voigt profile.

To develop accurate and species-specific measurements of carbon monoxide by TD-LAS, three evaluation criteria for the absorption spectra should be satisfied: *i.* minimal spectral interference from neighboring molecules ensures specific-species sensing of the target molecule as none feature-absorption line foreign to the CO will take place during

experimental tests. Thus, isolated and non-overlapped regions are good candidates. *ii.* High intensity is one of the most important factors and high enough values simplify the system as direct absorption may be sufficient for the measurements. *iii.* Accessibility to commercial diode lasers, as quantum cascade lasers (QCLs) may be too expensive or not available in the desired spectroscopic range..

Carbon dioxide and water vapour are considered in this thesis as the most probably neighbouring compounds that can interfere during laser-based optic diagnostic. These gases are heteronuclear triatomic molecules that have more than one vibration mode. CO_2 has four vibrational modes with two degenerate vibrational mode because of linear nature. On the other hand, H_2O is a non-linear molecule with three vibrational modes. Table 3.1 reports some spectroscopic parameters such as characteristic vibration temperature and molecular vibrational frequency for carbon dioxide and water vapour. It is important to highlight how the second vibration mode from H_2O has a characteristic vibrational temperature that is lower than the ISC process and needs to be considered during absorption spectra simulations. Therefore, especial care was necessary to guarantee that water absorption does not take place over any selected CO-absorption region.

TABLE 3.1: Characteristic vibrational temperature of CO_2 and H_2O.

Molecule	Vibrational mode	Characteristic vibrational temperature (K)	Molecular vibrational frequency (cm^{-1})
CO_2	υ_1	$\theta_{\upsilon_1} = 4170$	$\omega_1 = 1330$
	υ_2	$\theta_{\upsilon_2} = 1820$	$\omega_2 = 667$
	υ_3	$\theta_{\upsilon_3} = 4290$	$\omega_3 = 2349$
H_2O	υ_1	$\theta_{\upsilon_1} = 1930$	$\omega_1 = 3652$
	υ_2	$\theta_{\upsilon_2} = 960$	$\omega_2 = 1585$
	υ_3	$\theta_{\upsilon_3} = 3390$	$\omega_3 = 3756$

The absorption spectra along the overall spectral range for the most abundant isotopes on earth of the target molecules, $^{12}C^{16}O$, $H^{16}OH$ and $^{16}O^{12}C^{16}O$, were simulated under conditions of 10 atm and temperatures of: Figure 3.1 A) 423 K, Figure 3.1 B) 600 K, Figure 3.1 C) 900 K and Figure 3.1 D) 1023K. All spectra were obtained simulating the vibrational bands listed for H_2O in Table 3.2 and for CO_2 in Table 3.3. Regarding hot bands for water vapor, just one vibrational band was chosen. As mentioned above, the CO-fundamental band located at 1815.573 cm^{-1} and 2316.048 cm^{-1} provide excellent absorption characteristics almost comparable to those of CO_2 and H_2O in the region between 3000 cm^{-1} and 4000 cm^{-1}. The figure does not show the first- and second-overtones, which are weaker than fundamental band by factors of 100 and 1000 respectively.

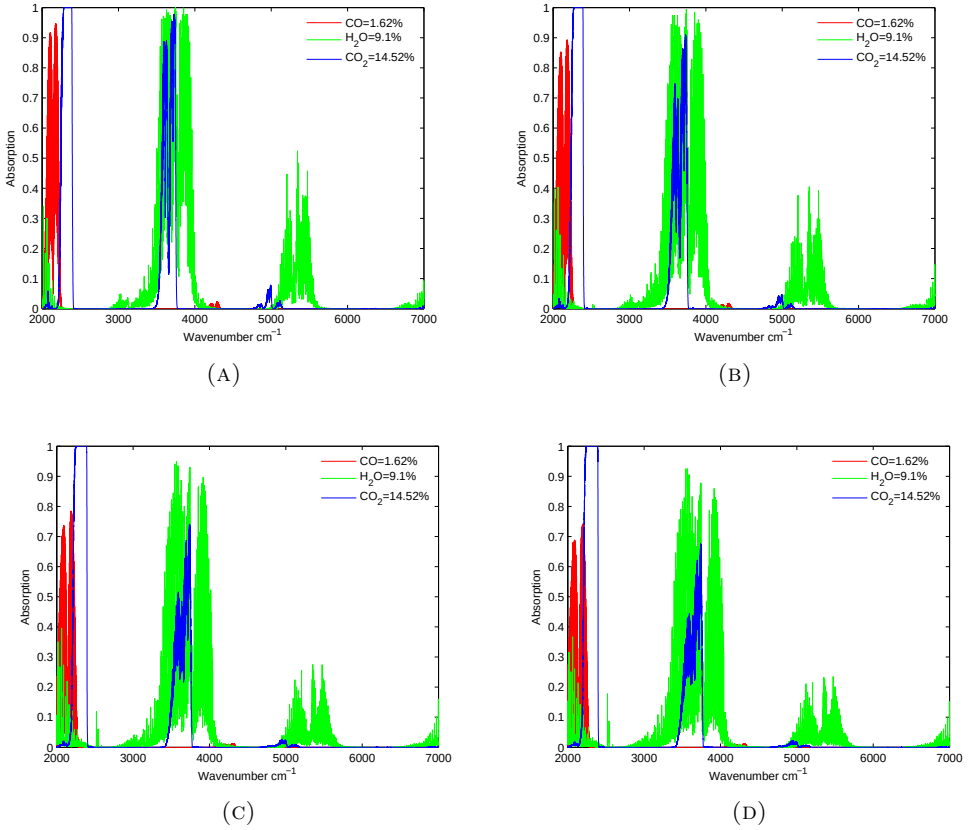

FIGURE 3.1: Simulated absorption spectra for CO, CO_2 and H_2O at P=10 atm and four temperatures: A) 423 K, B) 600 K, C) 900 K and D) 1023 K.

TABLE 3.2: Vibrational bands of water steam simulated for absorption spectra.

υ_1'	υ_2'	υ_3'	υ_1''	υ_2''	υ_3''	Symbol	Band name and vibrational mode
0	1	0	0	0	0	υ_2	Fundamental band. 2nd vibrational mode
0	2	0	0	0	0	$2\upsilon_2$	1st overtone. 2nd vibrational mode
1	0	0	0	0	0	υ_1	Fundamental band. 1st vibrational mode
0	0	1	0	0	0	υ_3	Fundamental band. 3rd vibrational mode
0	3	0	0	0	0	$3\upsilon_2$	2nd overtone. 2nd vibrational mode
1	1	0	0	0	0	$\upsilon_1 + \upsilon_2$	Combination band.1st and 2nd vibrational modes
0	1	1	0	0	0	$\upsilon_2 + \upsilon_3$	Combination bands. 2nd and 3rd vibrational modes.
0	4	0	0	0	0	$4\upsilon_2$	3rd overtone. 2nd vibrational mode
1	2	0	0	0	0	$\upsilon_1 + 2\upsilon_2$	Combination bands. 1st and 2nd vibrational modes.
0	2	1	0	0	0	$2\upsilon_2 + \upsilon_3$	Combination bands. 2nd and 3rd vibrational modes
2	0	0	0	0	0	$2\upsilon_1$	1st overtone. 1st vibrational mode.
1	0	1	0	0	0	$\upsilon_1 + \upsilon_3$	Combination bands. 1st and 3rd vibrational modes.
0	0	2	0	0	0	$2\upsilon_3$	1st overtone. 3rd vibrational mode.
0	1	1	0	1	0	-	Hot band

The location of the second-overtone of CO provides a spectral region easily accessible to telecommunication diode lasers as it is situated in the electromagnetic spectrum between 5958.59 cm^{-1} to 6417.81 cm^{-1}, near to 1.53 μm of the NIR. The availability of

TABLE 3.3: Vibrational bands of carbon dioxide simulated for absorption spectra.

v1	v2	l	v3	r	v1	v2	l	v3	r	Symbol	Band name
1	1	1	0	1	0	0	0	0	1	v1+v2	Combination band. 1st and 2nd vibrational modes
0	0	0	1	1	0	0	0	0	1	v3	Fundamental band. 3rd vibrational mode.
2	1	1	0	1	0	0	0	0	1	2v1+v2	Combination bands. 1st and 2nd vibrational mode
0	2	2	1	1	0	0	0	0	1	2v2+v3	Combination bands. 2nd and 3rd vibrational modes.
1	0	0	1	1	0	0	0	0	1	v1+v3	combination bands. 1st and 3rd vibrational modes.
1	2	2	1	1	0	0	0	0	1	v1+2v2+v3	Combination bands. 1st, 2nd and 3rd vibrational modes.
2	0	0	1	1	0	0	0	0	1	2v1+v3	Combination bands. 1st and 3rd vibrational modes.
0	1	1	2	1	0	0	0	0	1	v2+2v3	Combination bands. 2nd and 3rd vibrational modes.
3	0	0	1	1	0	0	0	0	1	3v1+v3	Combination bands. 1st and 3rd vibrational modes.
1	1	1	2	1	0	0	0	0	1	v1+v2+2v3	Combination bands. 1st, 2nd and 3rd vibrational modes.
0	0	0	3	1	0	0	0	0	1	3v3	2nd overtone. 3rd vibrational mode
2	2	2	1	1	0	0	0	0	1	2v1+2v2+v3	Combination bands. 1st, 2nd and 3rd vibrational modes.

commercial diode laser operating around that wavelength generated the first laser-based measurements of carbon monoxide by TDLAS.

At typical conditions of lab-scale experimental tests of ISC, the second-overtones of CO is almost overlapped by vibrational bands of carbon dioxide, and some background interference from H_2O was observed too, as it is evident in Figure 3.2. Although, some rotational transitions belonging to the R-branch of the second-overtone seem isolated from CO_2-spectral interference, no absorption transition was chosen at this region due to the poor absorption values, less than 1×10^{-4}, which implies the need to improve the sensitivity of the TDL sensor and further complicated the methodology by implementing modulation techniques such as wavelength modulation spectroscopy (WMS).

On the other hand, the fundamental vibrational band of CO provides excellent values of both line-strength and, consequently, absorptions as illustrate in Figure 3.3 under similar conditions to those used for the $CO - 2\nu$ simulation. Isolated rotational transitions and absorptions above 0.7 make this an appropriate vibrational band to characterize CO with absorption spectroscopy techniques. However, limitations of temperature control of the diode laser operating at these wavelengths, which are near 4.6 μm, have prevented

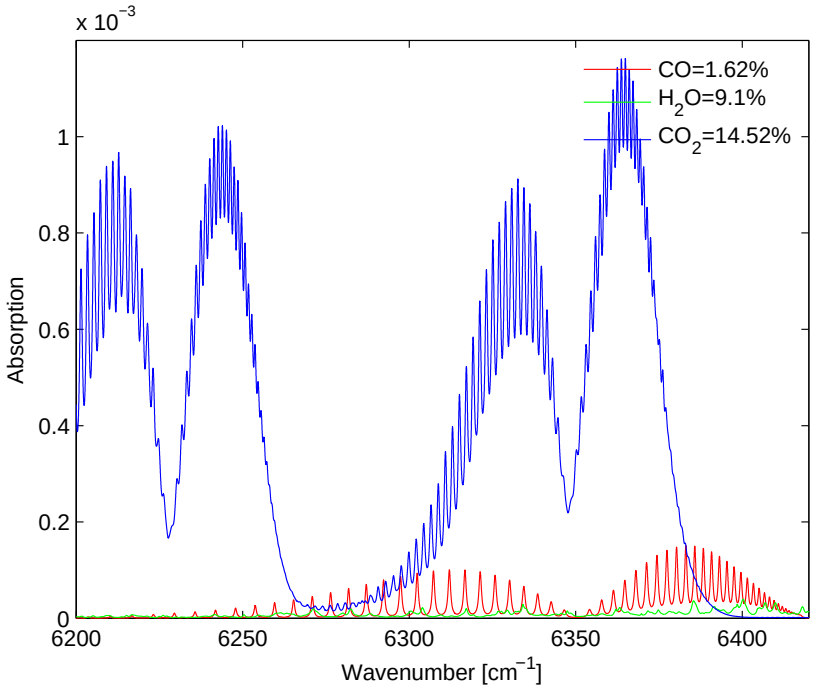

FIGURE 3.2: Simulated absorption spectra of the second overtone for CO at T=423.15 K, L=0.0381 m, and P=10 atm.

industrial production. The cutting-edge technology in laser-based optic diagnostics in combustions environments uses external cavity quantum cascade lasers (EC-QCLs) for sensing hydrocarbons in the MIR region. Unfortunately, these radiation sources are more expensive than those working in the NIR.

The first-overtone, CO-2ν, of carbon monoxide showed a larger quantity of spectral attributes than those obtained from the absorption spectra for both the first-and fundamental bands. Several spectral regions were found along of the 2ν band to have non-interference from most abundant flue gases of the ISC experiments. An advantage of the CO-2ν band to the other vibrational bands lies in the fact that CO_2 does not have any absorption phenomena over the region of the first overtone, which is located between 3887.18 cm^{-1} and 4360 cm^{-1}, and the fact that water vapour generates little background interferences without any appreciable spectral overlapping at typical concentration of ISC experimental tests. An absorption spectrum was carried out for the first overtone for the same temperature, pressure, pathlength and concentration used for both second-and fundamental bands. Figure 3.4 illustrates how absorption values up to 0.023 are obtained for rotational transitions belonging to the R-branch of CO-2ν. Although high interference from H_2O affects the P-branch, some absorption lines were found to be isolated. Since acceptable values for absorption were achieved, the 2ν-band seems an appropriate option for being the vibrational band to be study by direct

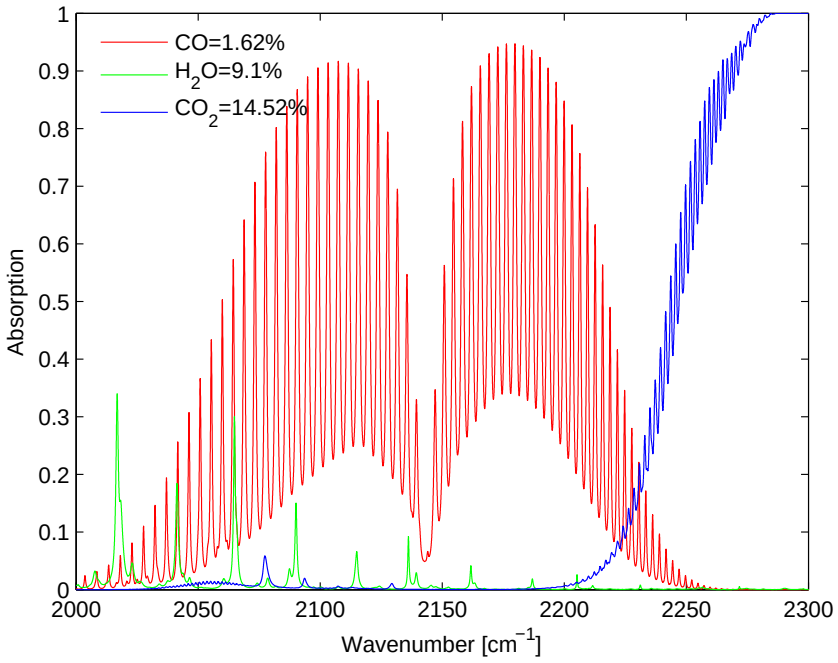

FIGURE 3.3: Simulated absorption spectra of the fundamental band for CO at T=423.15 K, L=0.0381 m, and P=10 atm.

absorption without the need to implement modulation techniques. In addition, the first-overtone is currently easily accessible to commercial diode lasers such as the Distributed FeedBack (DFB) diode lasers widely used with successful results in hazard-combustion environments.

The first-overtone of CO was simulated at different operational pressures in the order to know the spectral-absorption profiles at high-pressure conditions. Increases in working pressure led to greater absorption at the line-center of the rotational transition as shown in Figure 3.5. Three different-pressure scenarios were conducted over the first overtone at 600 K, 0.0381 m of optical path and 0.0162 mole fraction of CO for the purpose of quantifying broadening effects generates at high pressures. The Beer-Lambert law explains that the absorption coefficient is directly proportional to pressure and increases in pressure cause higher absorption. Unfortunately, the line-shape of the absorption lines broadens as the likelihood of particle collisions increases. However, absorption-spectral simulations showed that even at pressures as high as 20 atm a well-defined line-shape was achieved as illustrated in Figure 3.6. Regarding experiments at high pressure, the best option to carry out laser-based sensing was to propose an absorption line belonging to the R-branch of CO-2ν but located between 4280 cm^{-1} and 4310 cm^{-1} as the line-shapes at the center of the R-branch exhibited best features to develop the scanned-wavelength method, Fig 3.6.

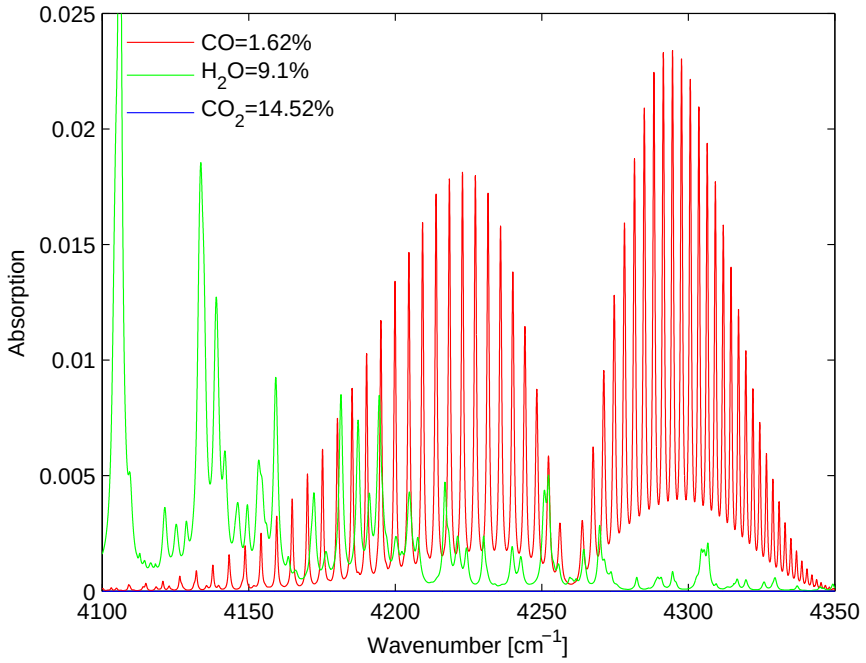

FIGURE 3.4: Simulated absorption spectra of the first overtone for CO at T=423.15 K, L=0.0381 m and P=10 atm.

Although laser diagnostic experiments at pressures above 4 atm were not conducted in this thesis, simulations suggests that under ISC conditions laser-based measurements of CO are possible. A successful research in a high-pressure and high-temperature coal gasifier support the viability to monitor the CO production in the R-branch, 2ν band using a TDL sensor exposed at condition up to 12 atm and 1200K.

Thermal effects on the spectral-absorption simulations, presented in Figure 3.7, illustrated the behaviour over the 1ν, 2ν and 3ν vibrational bands. The end of the R-branch, located between 4310 cm^{-1} and 4350 cm^{-1}, increased absorption with temperature. Contrary, the absorption lines located in region between 4260 cm^{-1} and 4310 cm^{-1}, registered a reduction in absorption with temperature.

Thermal and collision effects play an important role on the selection of an appropriate absorption line for CO-sensing at ISC lab-scale conditions. Previous spectral-absorption simulations showed that the worst scenario for the R-branch of CO-2ν is at high temperatures and low pressures. By using the blue-line spectrum in Figure 3.7 , which was evaluated at 1 atm and 1023 K, it can be guaranteed that under lab-scale experimental conditions of ISC characterizing tests, several rotational transitions have a well-defined line-shape with absorption values above 1×10^{-3} and direct absorption spectroscopy can be performed.

As high pressures generated increases in the absorption spectrum a new simulation was

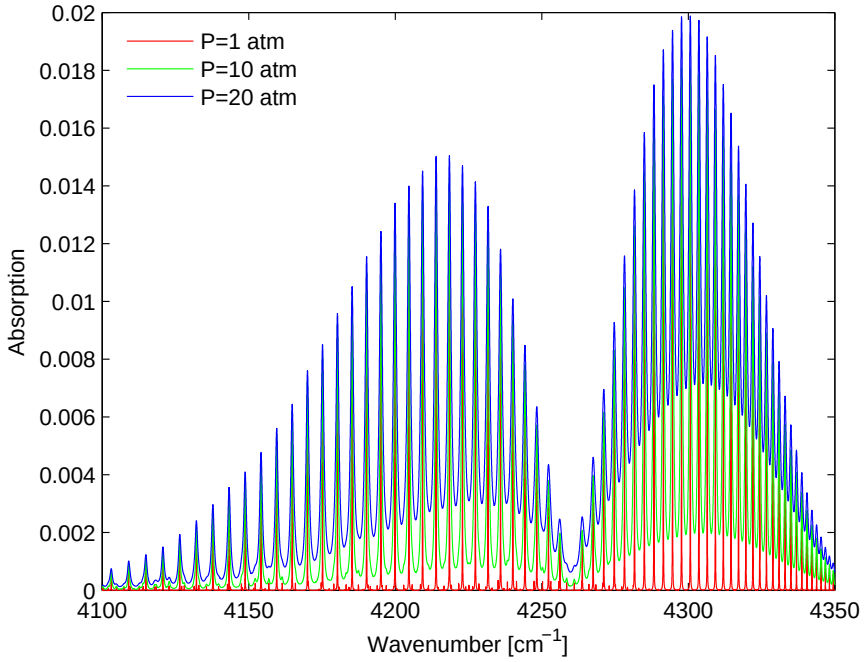

FIGURE 3.5: Simulated absorption spectra of the first overtone for CO at T=600 K and different pressures.

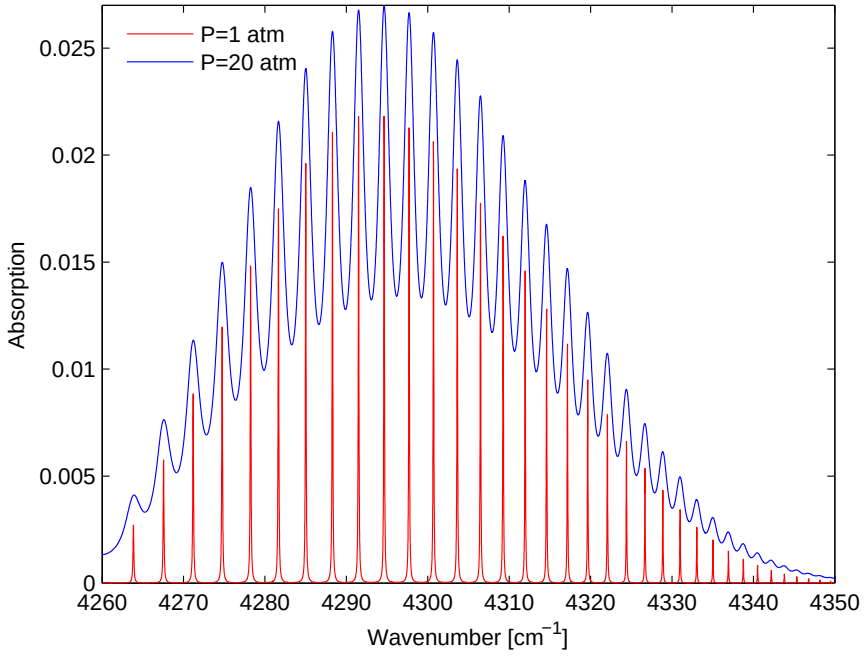

FIGURE 3.6: Simulated absorption spectra of the first overtone, R-branch of CO at T=423 K and different pressures.

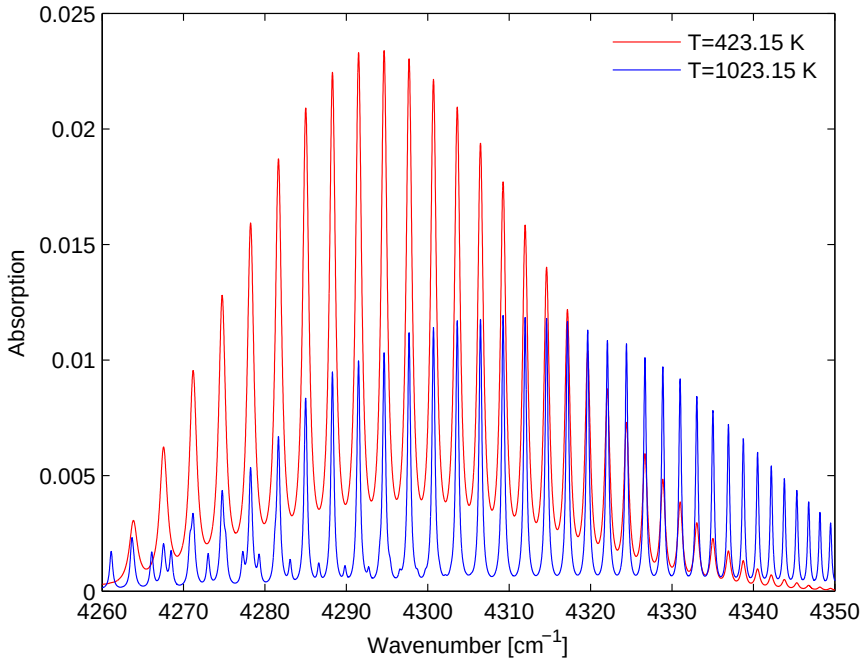

FIGURE 3.7: Simulated absorption spectra of the first overtone, R-branch of CO at P=1 atm and different temperatures.

carried out for understanding the background interference from water vapour. Prior knowledge by spectral simulations showed that the worst absorption behaviour for CO-2ν band was achieved at 1023K. For that reason, a spectroscopy analysis was needed to know how spectral interference affects the absorption spectrum of the first overtone under conditions of low absorption. A working pressure of 10 atm was chosen to provide high-spectral interference from H_2O. Although, some absorption regions over the R-branch of the CO-2ν band were not overlapped by the H_2O spectrum, considerable background interference was evident. The fact that the P-branch obtained the highest interference of the first overtone confirmed the non-election of this spectral area. Different research papers provided a strong foundation of rotational transitions used in successful measurements of carbon monoxide using TDL sensor in combustion environments. R(4), R(6), R(9), R(10), R(11), R(12), R(15) and R(30) from the CO-2ν band have been implemented in laser-based sensing because of its spectroscopic features such as high absorbance and no interference. Figure 3.8 illustrates the interference from water vapour over the firs-overtone of carbon monoxide as well as some absorption lines from literature. An important point is the fact that some absorption lines from the R-branch, e.g. R(10) and R(11) around 4300 cm^{-1}, are completely isolated from water vapor.

Figure 3.9 shows the molar fraction of CO, CO_2, H_2O and O_2 uptake of a simulation for a particular case of a RTO experimental test using the mechanisms of Thomas el. al. [17] widely used to represent the chemical behavior of a heavy-crude oil during ISC

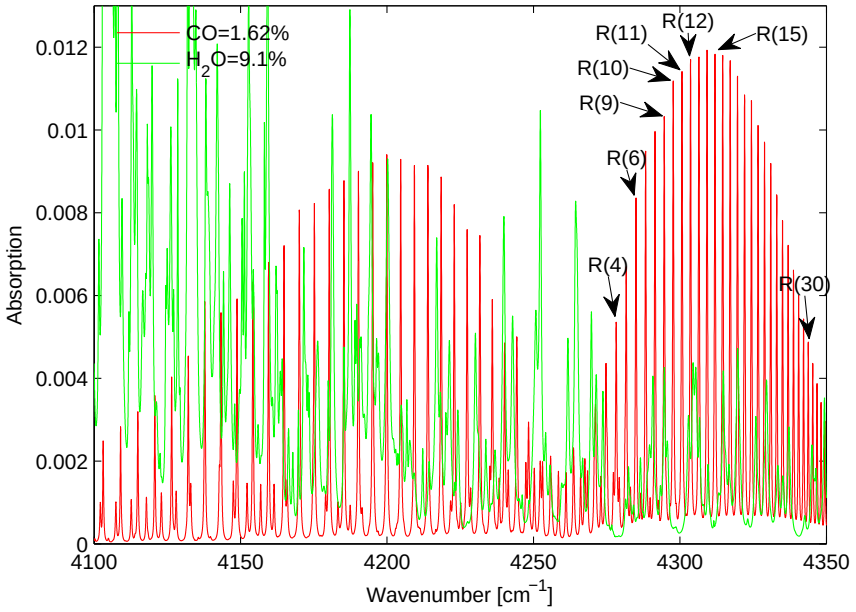

FIGURE 3.8: Rotational transitions isolated from interference of water vapour in the firs overtone of CO at T=1023 K and P=10 atm.

process. The simulation suggested that after 2.5 hours high temperature oxidations take place and the production of gaseous species such as CO, CO_2 and H_2O kicks off. Figure 3.10 confirmed that at a concentration of CO, the maximum obtained for this species in Figure 3.9 but lower than that typically reported in the literature [17], there is no interference from water vapor, at the maximum concentration in Figure 3.10, and, good absorption values are achieved.

As shown in previous spectral simulations different rotational transitions from the R-branch of $CO-2\nu$ appear to be appropriate for laser-based sensing of carbon monoxide. However, a line-strength analysis was carried out over the temperature range where carbon monoxide was considered to be generated during ISC lab-scale tests. This spectroscopic study provided accurate information of the thermal sensitivity that has those absorption transitions. Quantum parameters were taken from HiTran database 2008 for the following spectral lines: R(4), R(6), R(9), R(10), R(11), R(12), R(15) and R(30). The line-strength at a specific temperature was corrected by a reference temperature assumed to be 296 K, while the state-statistical weights of both lower and upper states were obtained by Equation 3.1, and the weighted-transition moment squared by Equation 3.2. The HiTran parameters were previously validated simulating a line-strength profile of a target rotational transition published as a case study.

$$g_n = ((2+J)+1) \times g_s \times g_i \tag{3.1}$$

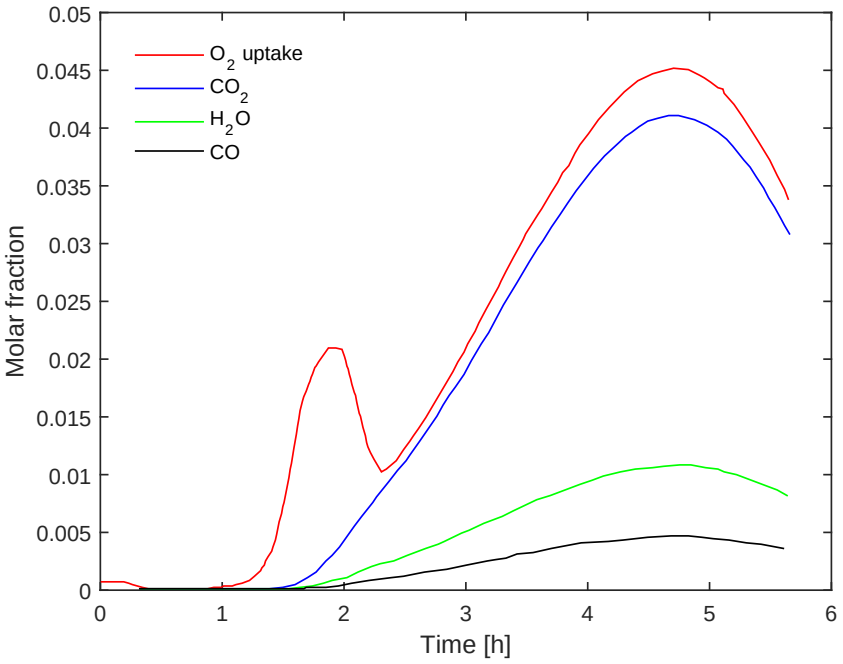

FIGURE 3.9: Mole fraction of the main gases produced during ISC process. Results for the simulation of ISC of a kinetic cell taken from reference [17].

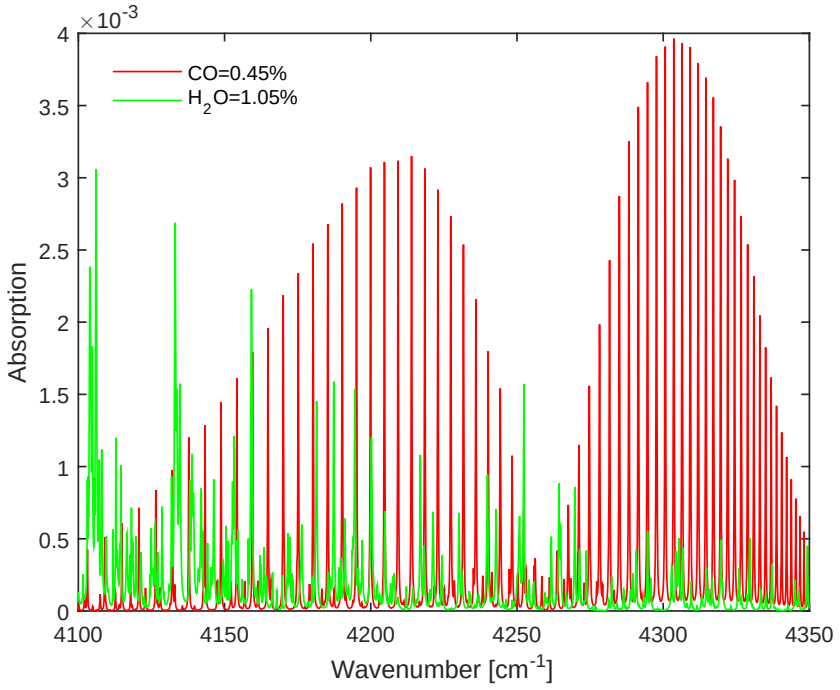

FIGURE 3.10: Absorption spectra of first overtone of CO at conditions of Belgrave simulations in Figure 3.9, T=798 K, P= 5 atm.

$$\Re_{n'n} = \frac{A_{n'n} 3h g_{n'}}{64\pi^4 \nu^3 g_n \times 10^{-36}} \tag{3.2}$$

where g_n is the state-statistical weight, J is the rotational-quantum number, g_s is the state-independent weight, g_i is the state-dependent weight, $\Re_{n'n}$ is the weighted-transition moment squared and $A_{n'n}$ is the Eistein coefficient for spontaneous emission.

Figure 3.11 illustrates the thermal effects over each line-strengths outlined above. The black-line profile from R(30) provides information regarding increases in absorption when the temperature goes up while some absorption lines such as R(9) decreases along the evaluated temperature. Although the R(30) had a positive slope during temperature increases, the maximum value reached, around 0.6, was lower than those obtained from the other absorption lines which were higher than 0.8.

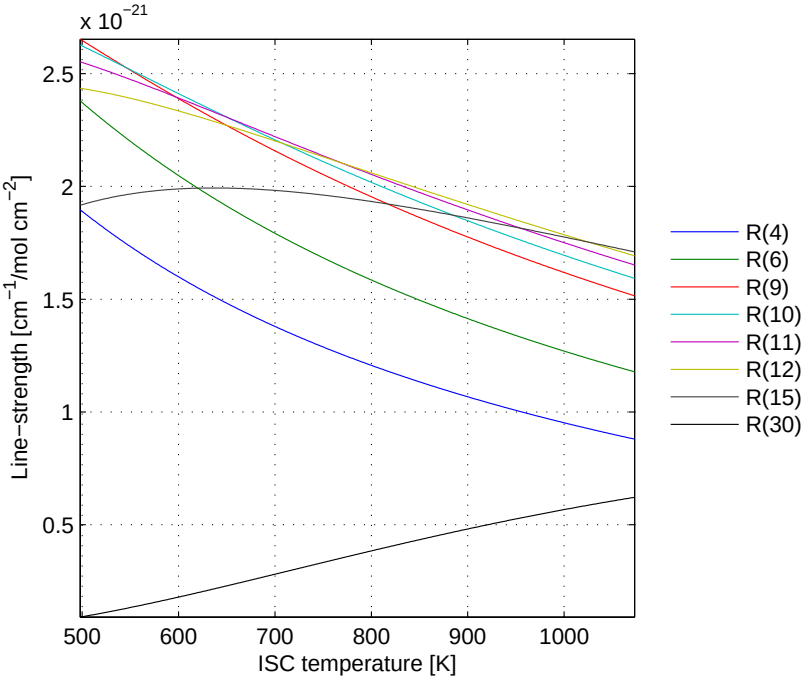

FIGURE 3.11: Line-strength variation with temperature for rotational transitions R(4) to R(30) from the first overtone.

The absorption lines R(10), R(11) and R(12) provide an stable behaviour of line-strength along the ISC temperature with highest values than R(4), R(6), R(9), R(15) and R(30). To choose the best absorption line, the area for each profile was calculated by integrating the line-strength function and evaluated between temperatures from 498K to 1073K. As mentioned above, some absorption lines generate a decline in absorption at high temperatures. However, absorption transitions located at the center of the R-branch such as lines from R(10) to R(12) exhibited the highest values of line-strength. By means of Figure 3.12 is shown that the R(10) from $CO - 2\nu$ has an integrated area of line-strength

of, around, 1.18×10^{-18}, which was the lowest value from the three-final absorption lines. During temperatures below to 650 K, R(10) showed a line-strength behaviour with values as high as $2.64 \times 10^{-26} \frac{cm^{-1}}{mol \times cm^{-2}}$, while R(11) and R(12) remained below. After almost the 700 K, the absorption line R(10) drop to values lower than R(11) and R(12), while R(12) kept the high amounts providing a higher integrated area of 1.19×10^{-18}. However, the absorption-rotational transition R(11) from the $CO - 2\nu$ remained stable with a temperature rise up to 1073K. The red-line profile showed a constant behaviour which kept in the middle between R(10) and R(11) giving an integrated area of 1.20×10^{-18}. Therefore, the rotational transition $J^{'} = 12 \leftarrow J^{''} = 11$, known as R(11), with a wavenumber at the line-center of 4300.7 cm^{-1} provides a wide variety of appropriate spectral properties to perform laser-based measurements of carbon monoxide under lab-scale experimental conditions of the in situ combustion process of a heavy crude oil.

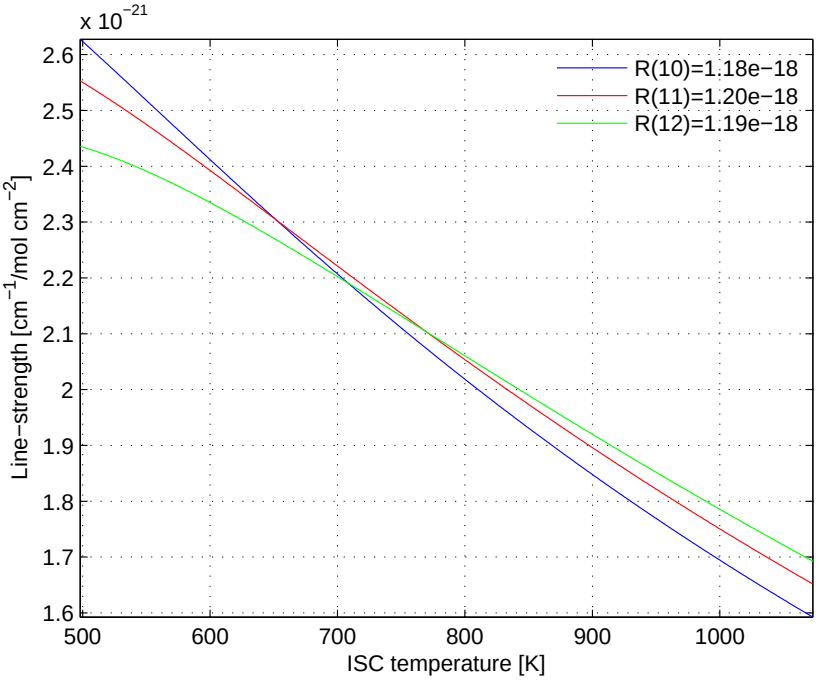

FIGURE 3.12: Line-strength variation with temperature for rotational transitions R(10), R(11) and R(12) from the first overtone.

3.6 Interference by hydrocarbons near to R(11) transition of CO

Hydrocarbons play an important role during the decomposition of the heavy-crude oil during ISC process. Although, large molecules have their fundamental bands in the MIR, an study was carried out to evaluate any interferences near R(11). Unfortunately, HiTran

database provides spectroscopic information for small hydrocarbons. Methane showed absorption bands over the R(11), however, it is not abundant during ISC experimental test.

A significant background interference from CH_4 around the R(11) was noticeable when CH_4-concentrations were higher than 0.5%. Figure 3.13 illustrates an absorption spectrum for a CO-concentration of 1.62% and different methane compositions at 293K, 1 atm and a pathlength of 0.05 m. Several absorption lines of CH_4 were found to be on both wings of R(11).

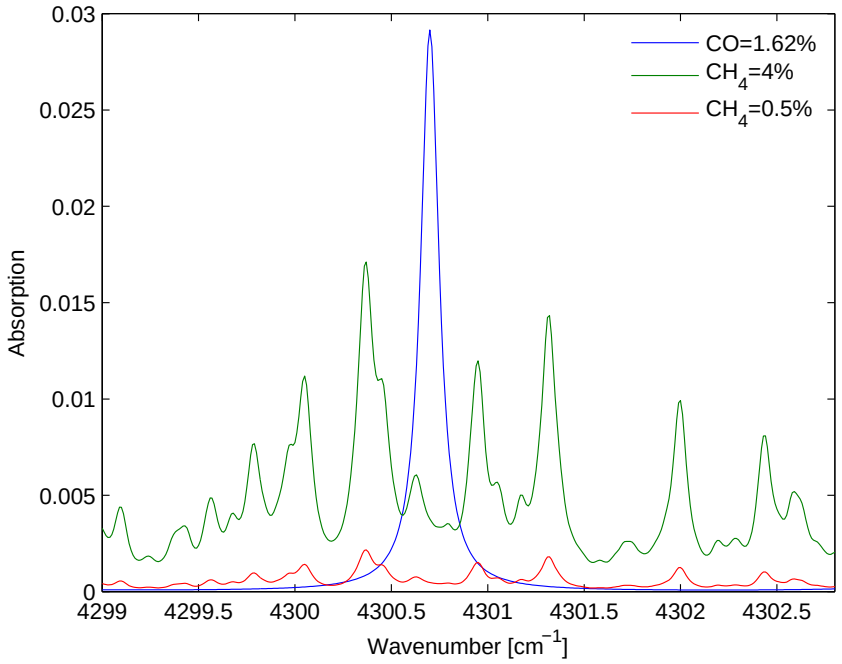

FIGURE 3.13: Analysis of the interference by methane to R(11) for high CH_4.

PNNL spectra library provided absorption spectra of different long hydrocarbons. An analysis to absorption bans of hydrocarbons up to C_{10} did not show any absorption over R(11).

Chapter 4

Laser-based sensor design and experimental methodology

4.1 Chapter outline

Chapter 4 describes the TDL sensor used to measure CO over the R(11) absorption line. The experimental setup was designed to perform direct absorption spectroscopy by scanned-wavelength method. The sensor architecture provides good versatility and safe operation by the use of optical fiber instead optical components of free-space. A distributed feedback diode laser (DFB-DL) and an InGaAs photodiode were chosen for the pitch and catch assembly. The TDL-experimental setup worked with easy alignment procedures during laser measurements in both the static-glass cell at room conditions, and the combustion chamber with optical access at high temperature and high pressure conditions. In the last part of Chapter 4, it is described the in-house interface developed using LabView to data acquisition and the data processing algorithm developed in MatLab.

4.2 Sensor architecture

The TDL-optical setup for laser-based sensing of carbon monoxide was designed to perform direct absorption spectroscopic measurements as good absorption values were obtained as outlined in Chapter 3. The most important equipment in optical technique are the radiation source, the measuring volume and the detection system.

In this thesis a TDL sensor was designed and validated to carry out laser-based optic diagnostic of CO at the R(11) of the 2ν absorption band by Direct Absorption-

Tunable Diode Laser Absorption Spectroscopy (DA-TDL). Scanned-Wavelength measurements seem to be an excellent method for lab-scale ISC experimental conditions because of its advantage outlined in Chapter 2. TDL technology provides a simple optical-assembly without the need to use a lens set to focus the laser beam across the target gases. A straightforward alignment is carried out when TDL systems are implemented at hazardous environments providing a tool useful to monitor flue gases at industrial processes. This research proposed the TDL-experimental setup depicted in Figure 4.1 for CO-sensing at similar conditions of lab-scale experimental test of a heavy crude oil during ISC. Relative few components compose the TDL-optical sensor: i) function-signal generator, ii) laser controller, iii) diode laser, iv) optical fiber, v) collimator, vi) gas cell, vii)photodiode and viii) PC with DAQ. By selecting the R(11) of the R-branch from the $CO - 2\nu$, it is ensure that building a TDL sensor is based to perform specific-species, such as CO, diagnostics by using a custom-designed diode laser emitting at a line-center wavenumber of 4300.7 cm^{-1} where the emitted photons from the DL will resonate on the natural frequency of the absorption line R(11) generating the light absorption.

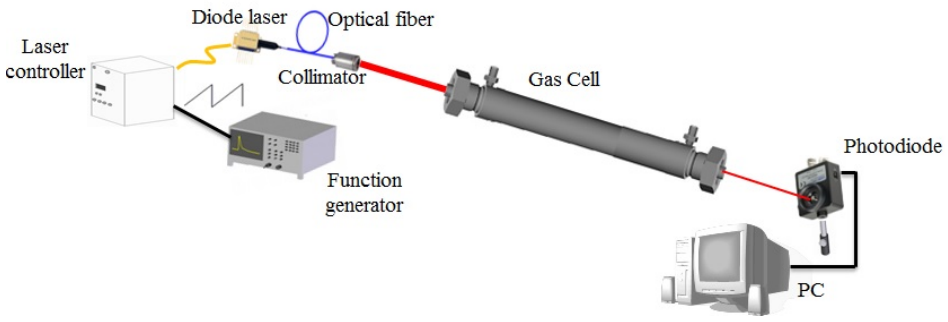

FIGURE 4.1: TDLAS sensor for CO concentration

To perform laser measurements using the scanned-wavelength method with the TDL sensor, the diode laser (DL) must be tuned over an specific absorption line, e.g. the R(11) rotational transition for this thesis. Diode lasers allow changing in the emitting wavelength by means of a modulation via an external reference signal to the laser controller. Wavelength modulations by injection current were carried out while the temperature from the TEC module of the laser controller was fixed to a standard value, for almost all experiment 25 °C. This external modulation signal is delivered by a function generator to the laser controller with output typical signals in the form of either saw-tooth or triangle for TDL diagnostics in combustion experimental tests. The DL controller receives an output-modulation signal and produces a current signal known as scanning-incident signal, Figure 4.2 A). The LD controller send to the diode laser the scanning-incident signal and a spectral scan takes place, Figure 4.2 B). The spectral region evaluated by the DL depends on the amplitude of the scanning-incident signal as

the DL-wavelength is directly proportional to the injection current. Because the diode laser emission is governed by the external reference signal of the function generator, the scanning frequency of the DL is determined by the frequency of the origin signal which comes from the output signal of the function generator. With the DL turned on the laser beam is guided by an optical fiber, most of the cutting-edged TDL setups used optical fiber to guide the light instead of optical-free space due to flexibility and advantage of alignment in optical assembles with optical fibers. The laser beam is collimated by a parabolic mirror and directed across the gas cell filled of the gaseous molecules. The gas media must be characterized to measure the average concentration over the line-of-sight by TDL technique. When the laser light goes through the measuring volume light-matter interaction in the spectral range of the R(11) absorption line takes place and an absorption phenomenon can be quantified via Beer-Lambert law by detecting the laser light for the transmitted intensity with a photodiode, Figure 4.2 C). The output voltage signal from the detector is recorded with a coaxial BNC cable, while the acquisition and processing data are carried out by means of in-house code in LabView.

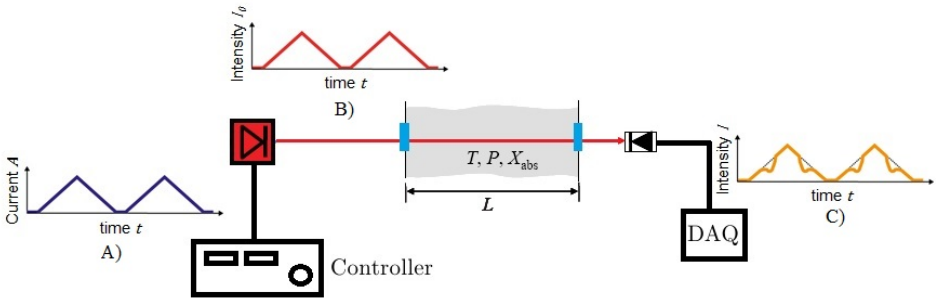

FIGURE 4.2: General TDLAS signals. A) laser controller signal for tuning diode laser, B) laser incident intensity I_0, and C) laser transmitted intensity I_T

4.3 Experimental hardware

This section described in details the selection of the diode laser as well as the optic, and optomechanical devices used for the TDL-CO sensor. An accurate diode laser and alignment tools were required to provide collimated beams with easy optical alignment through the test section; a robust design of the optomomechanical hardware from the TDL-CO setup was developed to maintain alignment for changes on the measuring volume such as the static-glass cell and the combustion chamber. During the development of the thesis some improvements on the TDL assembly were carried out such as the addition of an optical fiber for both high-pressure and high-temperature experiments in a combustion chamber with optical access. However, these additions do not compromise the truthfulness of the results.

4.3.1 Laser, optic and detector

The TDL-sensor uses a fiber-coupled distributed feedback (DFB) diode laser housed in a type 1, 14-pin butterfly package with an integrated TEC element and thermistor. The DFB diode laser provides narrow-linewidth, and single-frequency lasing emission with an optical fiber of 1 m terminated with a FC/APC connector. The custom-designed DFB DL with serial number #1369/5−19 manufactured by Nanoplus, provides mode-hop-free operations with a continuous current tuning from 35 mA to 110 mA in a temperature range from 20 $°C$ to 30 $°C$. The DFB-DL was designed to provide an emission at the line-center of the R(11) , around 2325.2 nm or 4300.69cm^{-1} , at 25$°C$ and 80 mA, and lasing wavelength over an spectral range from 2324.5 nm to 2327.5 nm by changing in both temperature and current. The diode laser achieves 2 MHz linewidth with an excellent side mode suppression above 40 dB as shown in the measured spectrum in Figure 4.3, as quoted by the manufacturer of the DFB diode laser. A linear behaviour of the output power from the DFB-DL was guaranteed by the manufacturer, with a threshold current of around 25 mA, a slope efficiency of $0.03\frac{mW}{mA}$ and a maximum optical-output power of almost 3 mW at 120 mA at 25$°C$, Figure 4.4. Fine-tuning over the spectral range of R(11) is achieved by a current modulation with a constant of $0.04\frac{nm}{mA}$.

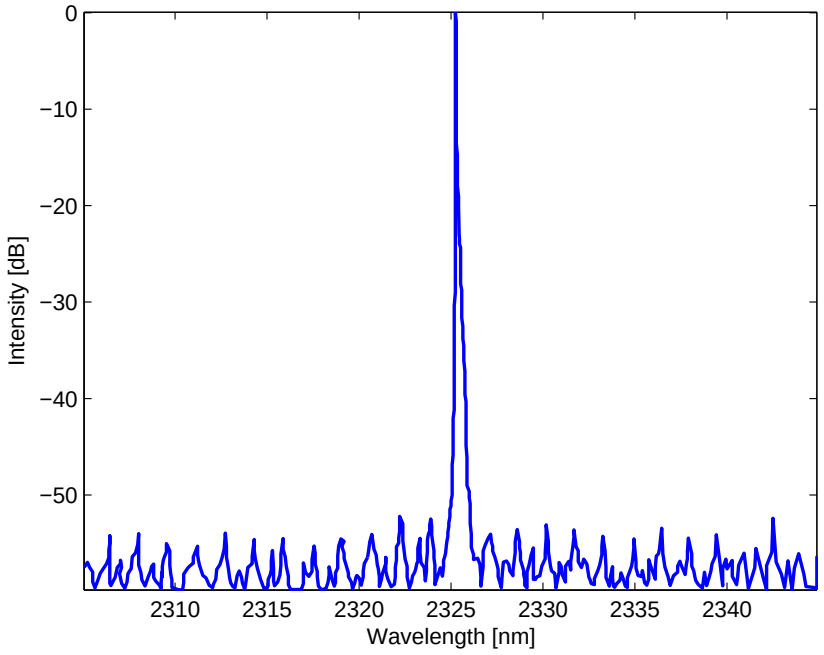

FIGURE 4.3: Spectrum of Nanoplus 2325.2 nm DFB diode laser

.

Figure 4.5 shows the lasing wavelength modulation by injection current over the spectral region of the R(11) from the $CO-2\nu$, blue-line profile, where the line-center of the absorption line was reached by the DFB-DL at an injection current of 80 mA at 25$°C$.

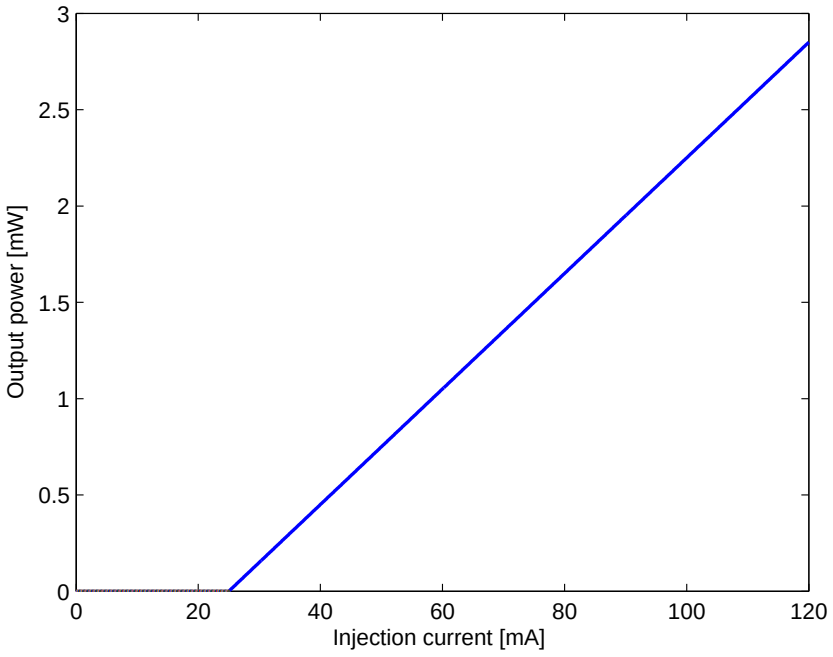

FIGURE 4.4: Typical power and current characteristics of Nanoplus 2325.2 nm DFB diode laser.

Background interference from H_2O, red-line profile, was simulated in the order to provide information of possible absorption phenomena. The magnitude of the H_2O-absorption was two orders of magnitude lower than CO-absorption spectrum. The red-line shows a lasing-scanning from, almost, 2323-5 nm to 2326.5 nm for an injection current of 40 mA to 110 mA at $25°C$. The DFB-DL provides an appropriate scanning of the whole R(11), even at high pressures where broadening mechanisms generate a broadened absorption line.

The DFB-DL has 1 meter of a single-mode optical fiber terminated with a FC/APC connector and manufactured by Nufern (SM1950). First experiments were carried out using the Nufern's fiber optic, after calibration experiments a single-mode ZrF_4 fiber patch cable was used to avoid possible damage of the DL's fiber. Single-mode fibers have a small core diameter, in this case $7\mu m$, and restrict the light transmission to a single-propagation mode avoiding related problems of modal noise. In addition, the small core size results in a smaller beam diameter at the output with less divergence. The use of optical-fiber components to the TDL-CO sensor provides advantages in alignment procedures and safety experimental tests because of the flexibility and versatility of the optical parts. The end of the optical fiber was connected into a collimator with an aspheric lens of fixed focus, f=5.95 mm, with FC/APC connector (Thorlabs-F028APC200). A small-theoretical divergence of around 0.1265° was reported to be reached at a wavelength of 2325.2 nm, and a collimated beam is emitted with a diameter of 1.2 mm.

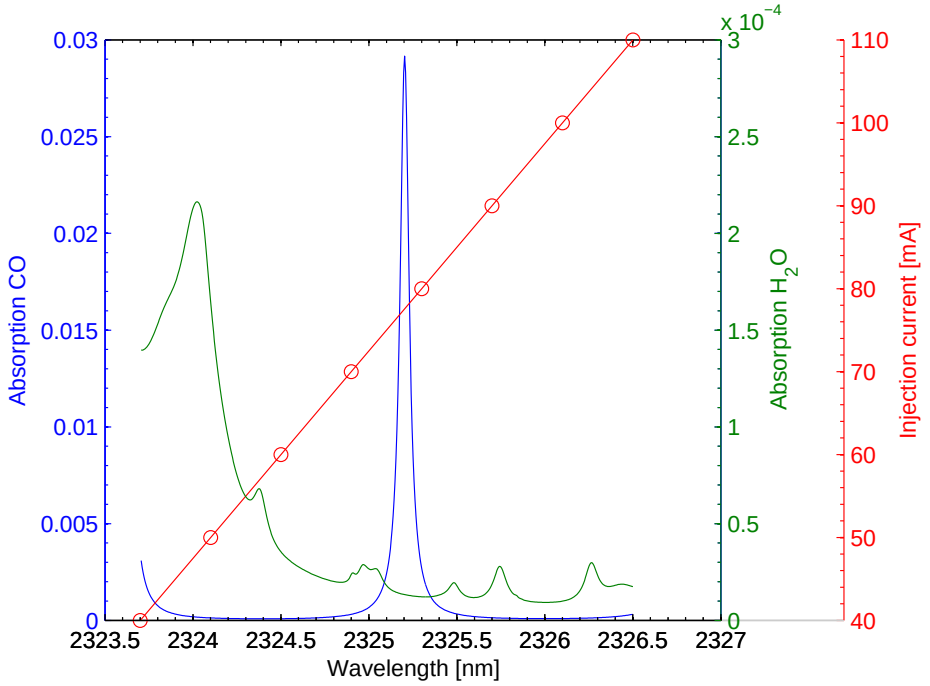

FIGURE 4.5: Tuning modulation by injection current at R(11) spectral region.

To detect the transmitted light an InGaAs transimpedance amplifier photodetector PDA10D provide by Thorlabs was used. The photodiode has it maximum sensitivity to light of 1.35 $\frac{A}{W}$ at the region around 2300 nm over the 0.8 mm^2 of active area. The high bandwidth, about 15MHz, ensures high modulation in the order of hundreds of kHz can be recorded without aliasing.

4.3.2 Optomechanical components

As noted above, TDL technique uses few optical components; in the designed TDL setup just one lens was implemented in the order to collimate the laser beam. As good values of transmittance were obtained it was not necessary to focus the beam into the active are of the photodiode by a focusing mirror. The optical components for both pitch and catch assembly were carefully selected to maintain a laser alignment for the TDL sensor for the different measuring cells. The collimator was supported by a collimator adapter (Thorlabs-AD11F) in a kinetic mount (Thorlabs-KM100T) and focusing the collimator output face into the input face of the measuring cell. The light laser was tilted using the kinetic mount to avoid background reflections known as etalon effect. To provide precise spatial alignments a XYZ-translation stage (Newport-9064XYZ) was used to perform micrometric movements up to 1.1 in of travel, Figure 4.6 A). The catch assembly shown in Figure 4.6 B) was easier than the pitch assembly as the photodiode

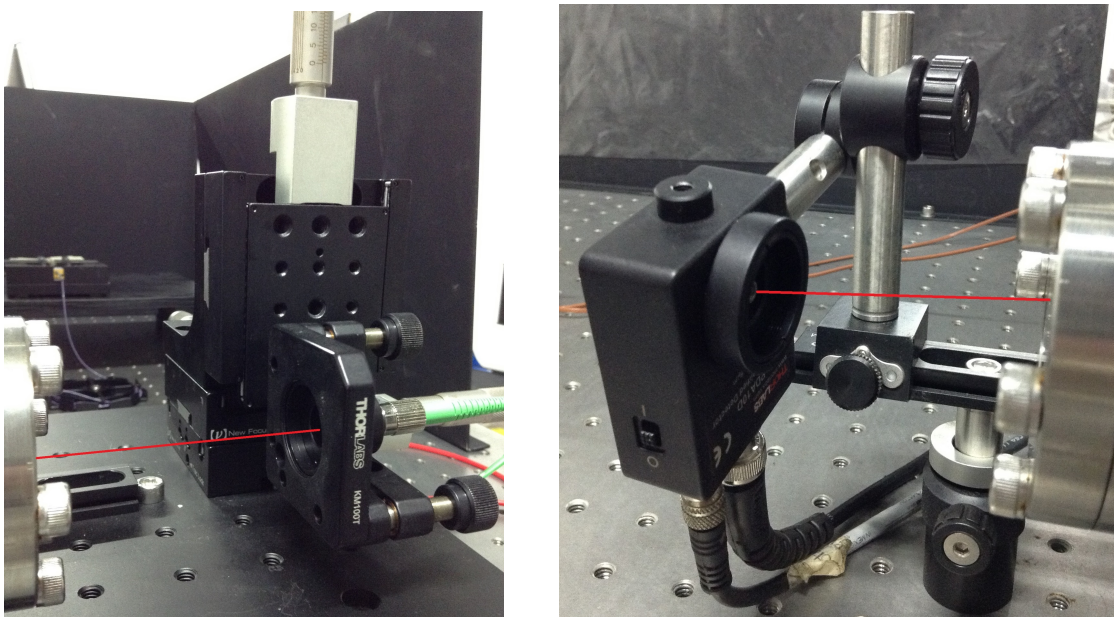

(A) (B)

FIGURE 4.6: A)Pitch and B) catch assembly for the TDL-sensor setup used in both the chamber and the static-glass cell.

was place by an adjustable-angle post clamp over a dovetail optical rail; to avoid a resonant cavity the photodiode was tilted. However, some background refractions were present even in the best experimental-optical alignment. The optical rail provides a reference line-of-sight for alignment procedures. The idea of use a rail was based in the need to place the pitch and catch in the same reference level. A breadboard with the dovetail optical rail served as a platform on which both pitch and catch assemblies were mounted, between them the measuring volume, in this dissertation this consisted of a static-glass cell and a custom-designed combustion chamber with optical access, was placed. The mounts are very rigid, and the adjustment knobs were locked in place after an appropriate alignment. Since carbon monoxide concentrations at room conditions are almost negligible, the TDL-sensor does not have a nitrogen purge for the free-space over the line-of-sight of the laser beam. To remove water vapour of the lab-atmosphere a dehumidifier was operating during laser-sensing measurements.

CO measurements were carried out by the TDL-sensor at room conditions in a static-glass cell and high-pressure and high-temperature conditions in a custom-designed chamber with optical access. On both absorption cells the pith and catch assemblies were designed as outlined above as shown in Figure 4.7. The easy alignment in both scenarios showed the versatility of the proposed optical setup.

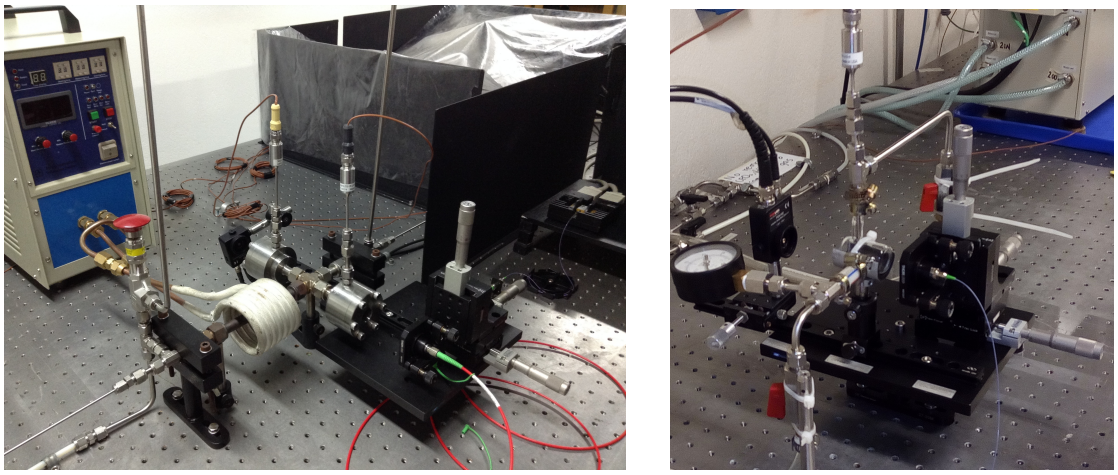

(A) (B)

FIGURE 4.7: TDL-sensor setup used in: A) chamber and B) static-glass cell.

4.3.3 Sensor control and data acquisition system

The temperature and current of the DFB-DL were controlled by both the TEC and current modules of a PRO800 controller of Thorlabs. The current module (ThorlabsLDC 8040) received a modulation signal from the function generator BKPrecision 4040B and a modulation by injection current was achieved. A data acquisition card NI PCIe-6343 from National Instruments was used to acquire and processing the incoming voltage signals from the detector and thermocouples. The card has a vertical resolution of 16-bit and the dynamic range can be adjusted to match the signal to be recorded. The DAQ card was connected to a National Instrument SCB-68A connector block. An in-house interface using LabView was developed for data acquisition and processing. Figure 4.8 showed the interface with recording options as well as graphic-charts for displaying the photodiode signal.

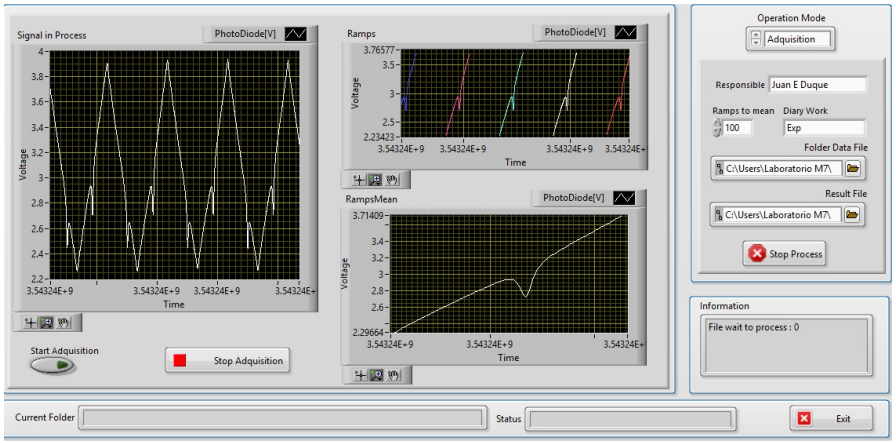

FIGURE 4.8: LabView interface for data acquisition from photodiode.

4.4 Data analysis

The data processing and spectral analysis were carried out using an in-house code in Matlab. A methodology for signal processing was proposed to carry out CO measurements by the TDL-sensor. Figure 4.9 shows the algorithm used during the CO-quantification in different experimental tests. Good results were obtained following the flowchart and the procedure was validated for the both free-calibration and calibration methods.

The data processing starts reading the acquired data from the Labview's interface, then a reference signal through a polynomial fit was calculated using both the non-absorption regions and the absorption region from the signal. With the current-tuning curve provided by Nanoplus and the modulation properties of the function generator, the time domain was transformed into wavenumber units, the optical density or absorption spectra were easily calculated. In the order to perform accurate measurements data fitting using a pseudo-Voigt profile was proposed. The raw data was fit to a Voigt profile by a non-linear fitting using Levenberg-Marquardt algorithm. Two measuring methods were developed and successful achieved during TDL-CO measurements. A calibration method uses the maximum absorption which takes place at the line-center of the R(11). Therefore, calibration curve were calculated by quantifying the amplitude of the Voigt profile from the absorption spectra. The free-calibration method used the Beer-Lamber law with the line-shape function normalized. By using HiTran database to calculate the line-strength at the temperature over the line-of-sight, and the pressure and path-length, the CO concentration can be obtained calculating the integrated absorption area for the Voigt profile.

The signal-to-noise ratio (SNR) was based on the maximum absorption value and the standard deviation obtained between the raw data and the Voigt profile and was calculated as shown in Eq 4.1.

$$SNR = \frac{\alpha_{\nu_0}}{\sigma} \tag{4.1}$$

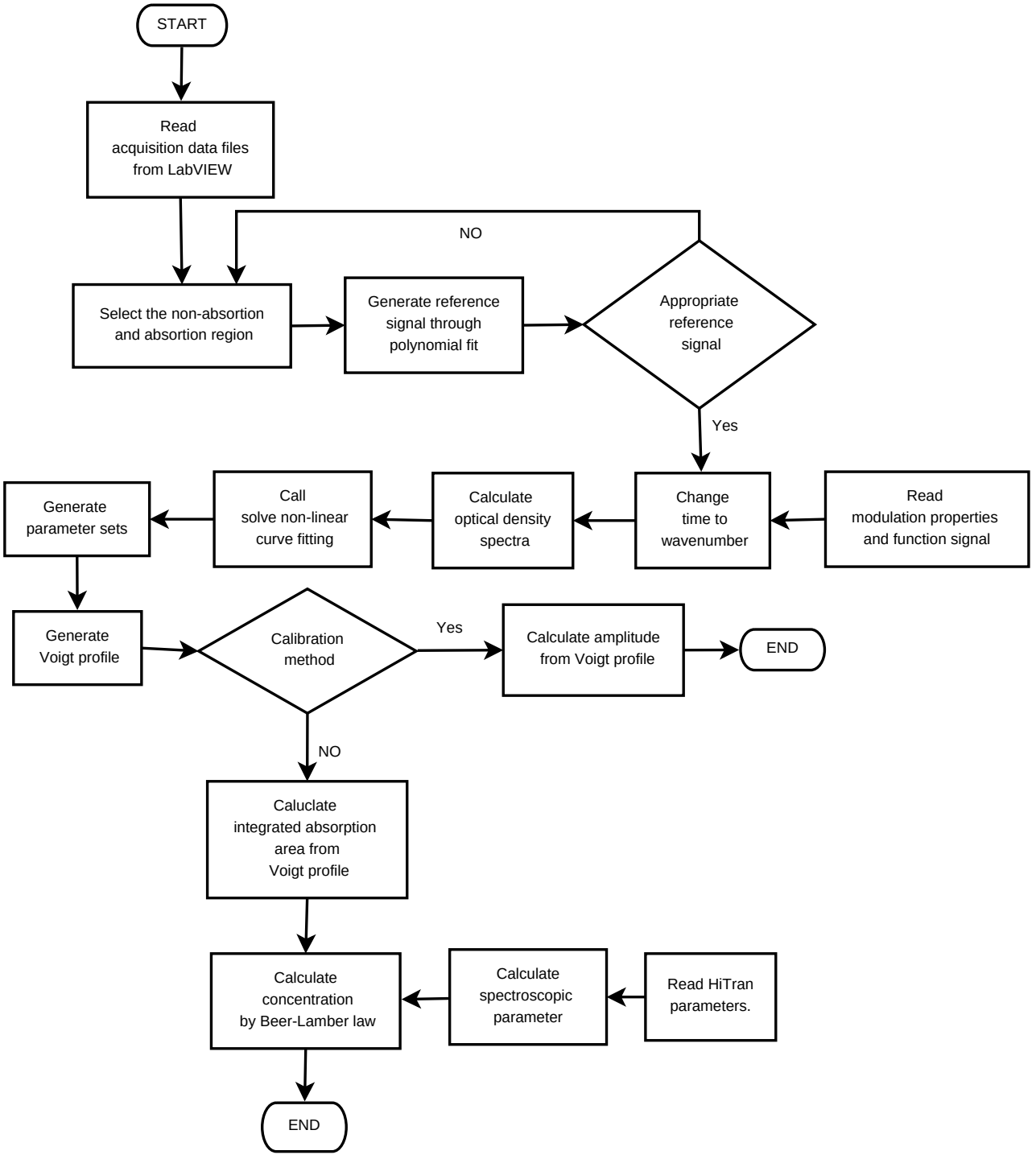

FIGURE 4.9: Algorithm flowchart used for data processing during TDLAS analysis.

Chapter 5

TDL-Sensor validation by laser-based measurements of CO concentrations.

5.1 Chapter outline

In Chapter 5 a validation analysis of spectroscopic parameter from HiTran database was carried out along with calibration and free-calibration measurements. Non-interference by hydrocarbons was confirmed, while background spectral interference from water was not obtained because to etalon effect, simulations ensured none limitations for CO sensing using the TDL-sensor. Line-strength measurement at room temperature showed good agreement to that reported from HiTran database with an error less than 5%. Calibration measurement with goo absorption values above 1×10^{-3} allows developing direct absorption spectroscopy at even the lowest-CO concentration evaluated. Although, etalon effects were obtained during TDL measurements, a calibration curve agrees to the linear fit reaching a R^2 of 0.99865 while to free-calibration method a R^2 of 0.99882. All measurements were validated using HiTran and a parity plot by quantifying the absorption at the line-center showed a good agreement with an R^2 of 0.99881 with error deviations from the theoretical values less than 3%.

5.2 Verification and completion of spectroscopic database

Laser-based measurements were conducted in a custom-designed glass cell of Duran borosilicate 3.3 in the order to validate specific-CO detection of TDL-sensor without

spectral interference from H_2O and hydrocarbon such as heptane (C_7H_{16}). Line-strength measurements were carried out at different partial pressure at room temperature to validate by HiTran database 2008 the measuring performance of CO-laser detection. In addition, spectroscopic simulations provided theoretical detection limits of CO for different temperature and pressure conditions.

5.2.1 CO direct absorption measurements in a static glass cell

The spectroscopic data for the R(11) absorption line from the $CO - 2\nu$ band were validated by means of line-strength measurements. Because to high uncertainty of Hitran which can be as high as 20% in some spectral regions, CO-validations of the theoretical line-strengths were needed to be studied in the order to provide reliable measurements for the free-calibration method as spectroscopic parameters from HiTran need to be used to obtained a line-strength value in a specific temperature.

As outlined above, a static-glass cell of Duran borosilicate 3.3 material was custom-designed with a similar path-length of 3.81 cm to the synthetic-core diameter designed for characterizing experiments of chemical reactions of ISC heavy crude oil. Those experiments and the ISC chamber will be carried out by the PhD candidate Mr. Henry Copete. This thesis developed CO-laser measurements within similar conditions of ISC experiments and path-length similar dimension to those provided by Mr. Copete in the order to provide similar absorption spectra when ISC charactering tests will be developed.

The one-section cell was placed and aligned between the pitch and catch assemblies of the TDL-sensor previous described. A general sketch is shown in Figure 5.1 for the experimental tests carried out for spectral validations of line-strength. Seven partial pressures of CO were measured by encapsulating the known gas with two valves placed at both the inlet and output gas port of the static-glass cell. To perform line-strength validation by HiTran database, the gas temperature was recorded with a type-K thermocouple provided by Omega and analyzed using the in-house interface from LabView. A partial pressure range from 4.47 Torr to 21.70 Torr was conducted at 296K with a pathlength of 296K for a standard gas mixture of CO, CO_2 and N_2. Due to the use of connecting hoses for both the inlet and outlet ports, room temperature was studied because to the difficulty of alignment process and safety operating procedures at temperature above 300 K.

Wavelength-scanned method was performed during direct absorption measurements of CO. By an injection current the DFB-DL was modulated following a reference-triangle

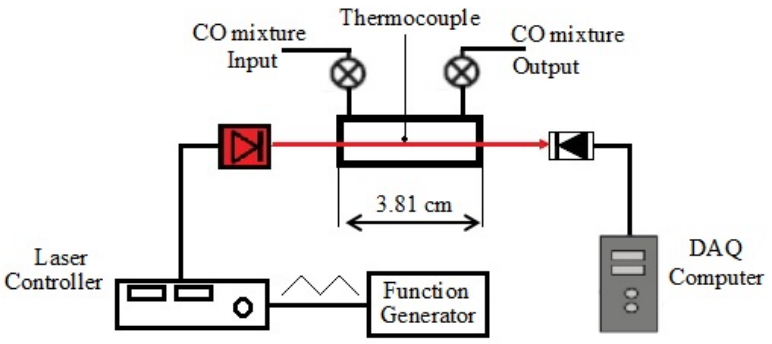

FIGURE 5.1: Measurement of linestrength R(11) near 4300.7cm^{-1} by DA-TDL optical sensor in sampled room temperature gas with pathlength L=3.81 cm.

signal with a symmetry fixed to 50%, a frequency of 70 Hz, and 0.02 V of amplitude. Although the diode laser was operated at moderate-scanning frequency, around 70 Hz, It can be reduced at low frequency as CO measurements is not reacting and chemical phenomena for the standard-gas mixture flowing through the glass cell can be considered negligible. However, all experiments in this research thesis were carried out at frequency above 70 Hz in the order to have fast-scanning measurements of CO and minimize beam-steering effect and low-frequency $(1/f)$ noise.

To measure the line-strength of the R(11) transition, the line-shape functions were fitted to a Voigt profile, and Wavelength-scanned direct absorption (DA) measurements were conducted in the cell. The integrated absorption area, which was obtained following the algorithm in Figure 4.9, was fitted to a linear partial pressure dependence to determine the line-strength at a specific temperature of 296K. The line-strength measurement procedure is illustrated in Figure 5.2. For the evaluated temperature, the integrated absorption area was measured at seven different partial pressures. At each partial pressure, 1500 absorption-scan measurements were conducted and the integrated absorption area was obtained by the averaging-absorption spectrum. Following Eq 2.7 the line-strength at 296K was inferred from the slope of the linear fit to the data. Good data consistency was achieved as shown in Figure 5.2, and the measured line-strength of 6.19 $\times 10^{-2}$ $cm^{-2}atm^{-1}$ at, around, 296K agrees with the HiTran2008 value of $\times 10^{-2}$ $cm^{-2}atm^{-1}$ within the estimated $\pm 5\%$ measurement uncertainty. The measured and theoretical line-strengths are listed in Table 5.1.

TABLE 5.1: Measured and calculated linestrength at 296K.

Line $[cm^{-1}]$	$S_{Measured}[cm^{-2}atm^{-1}]$	$S_{HiTran}[cm^{-2}atm^{-1}]$	Error rate [%]
4300.69	6.19×10^{-2}	6.47×10^{-2}	4.33

The acceptable agreement around 5% between the measured and the HiTran value of

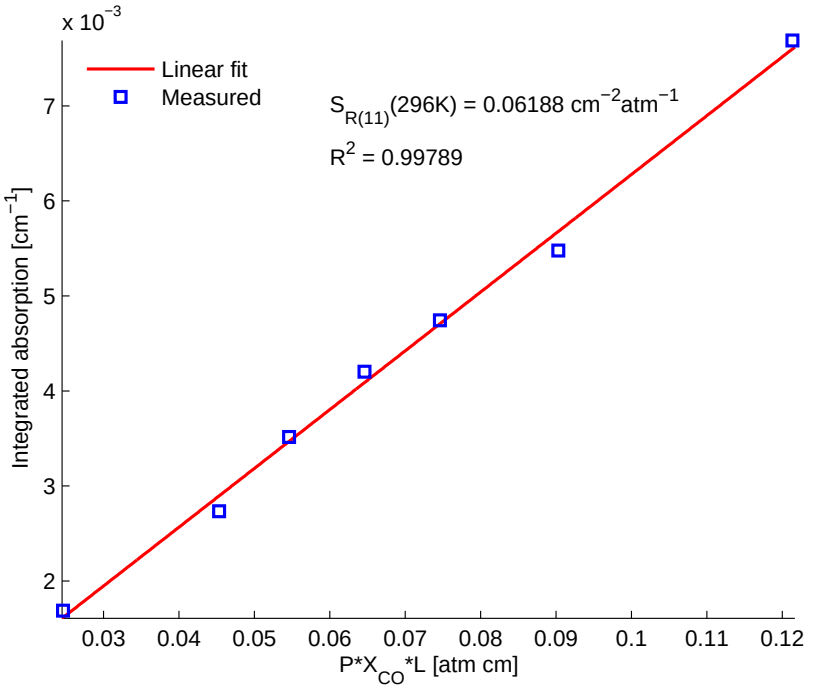

FIGURE 5.2: Measurement of linestrength R(11) near $4300.7cm^{-1}$ by DA-TDL optical sensor in sampled room temperature gas with pathlength L=3.81 cm.

line-strength confirms the spectroscopic assignment in HiTran. The measured line-strength is about 4.3% lower than that reported in HiTran, however, it is important to note that the uncertainty in HiTran is $5-10\%$. No effort was made to verify the line-strengths at elevated temperatures than 296 K because to the limitations of the connections of the gas ports. In addition, and by the fact that simulated and theoretical values have a good agreement, a line-strength profile over the ISC temperature was simulated and it is expected to obtain approximate values at elevated temperatures as those obtained in Figure 5.3.

5.2.2 Measurements of interference from combustion gases

Absorption spectra over the R(11) transition from $CO-2\nu$ showed background-spectral interference from H_2O without any overlapping even to the highest pressures and lowest temperature for ISC-experimental tests. HiTran database predicted non-interference from CO_2, and then it was not experimentally proved. Although a relatively weak absorption of H_2O was calculated by HiTran, an experiment with a poor laser-diagnostic was carried out without any successful and remarkable result. Because the custom-designed glass cell was built without standard for design, the surfaces in which the laser beam in and out of the static glass cell does not have wedged walls, generating

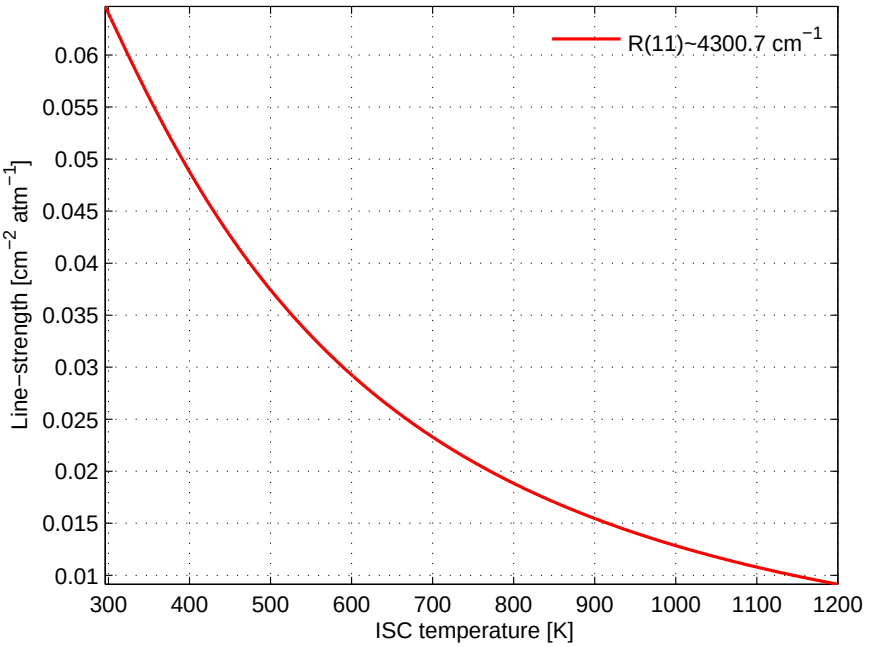

FIGURE 5.3: Calculated linestrength R(11) near 4300.7cm^{-1} by HiTran database optical sensor in sampled room temperature gas with pathlength L=3.81 cm.

an optical-resonant cavity producing an etalon effect with some oscillations in the acquired signals. A TDL measurement was conducted in the static-glass cell at 63.84 Torr of H_2O and 383K. The TDL-sensor achieved an alignment by using high-temperature hoses, however, some expansion from the connections hoses were observe as the TDL alignment was getting lost during some experimental tests.

Although the absorption spectrum of H_2O reached absorption as high as 18×10^{-7} for HiTran simulations at experimental conditions, the measured spectra showed appreciable oscillations because to etalon effect with an amplitude of, almost, 5×10^{-3}. The ghost measurements magnified the normal absorption by almost 1K. Figure 5.4 illustrated the Hitran and measured absorption spectrum for CO over the R(11) CO-transition. The transition was calculated to a molar fraction of 3.4% and a pressure of 10 Torr in the order to indicate that the analyzed spectral region is over the R(11) transition.

Despite the fact that etalon effect generated an uncommon-absorption spectrum for water vapor absorption, it is well known by simulation that temperatures below 1100K the H_2O interference can be assumed negligible over the spectral range of R(11) transition at atmospheric pressure. However, the resonant cavity restricted an appropriate performance of the TDL-sensor for sensing the background interference of H_2O.

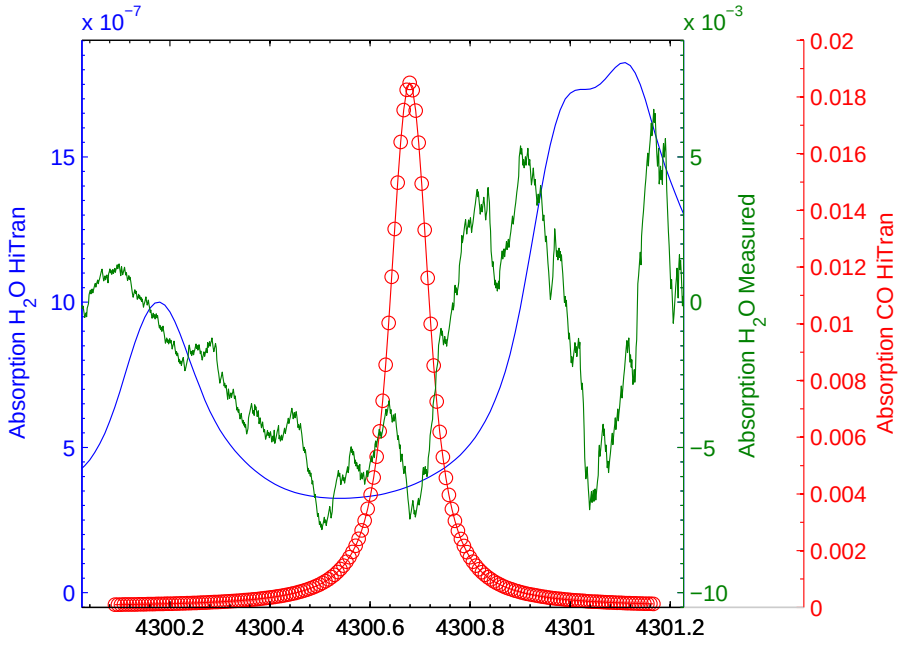

FIGURE 5.4: Measured and calculated H_2O background at 383K.

To avoid interference by hydrocarbons around the R(11) transition for ISC characterizing tests of heavy crude oils, an experiment was carried out by bubbling a standard gases mixture with a composition of 3.4% CO, 30% CO_2 and balance N_2 into 150 ml of heptane at 22°C and atmospheric pressure. Hydrocarbons show absorption mainly at the MIR, however, an experimental study confirmed no-absorption over the spectral range where R(11) is located. However, as the same static-glass cell used during experimental measurements of H_2O was implemented for hydrocarbons interference study, an etalon effect was obtained. Figure 5.5 illustrated the CO-absorption spectrum and the fact that as for both ends of three experimental test some oscillations showed an amplitude lower than the obtained at elevated temperature when the connection hoses provided inappropriate alignment.

5.2.3 Predicted CO detection limits

The detection limit of the carbon monoxide is limited by minimum detectable absorbance know as MDA as a function of the signal size and the sensor noise. The detection limit can be defined by the Eq 5.1, where the line-shape function is evaluated at the maximum absorbance of the transition located at the line-center. By increasing the pathlength, the averaging time or using modulation technique, the detection limit can experimentally be improved. However, there are designing challenges with multipass cells and complex

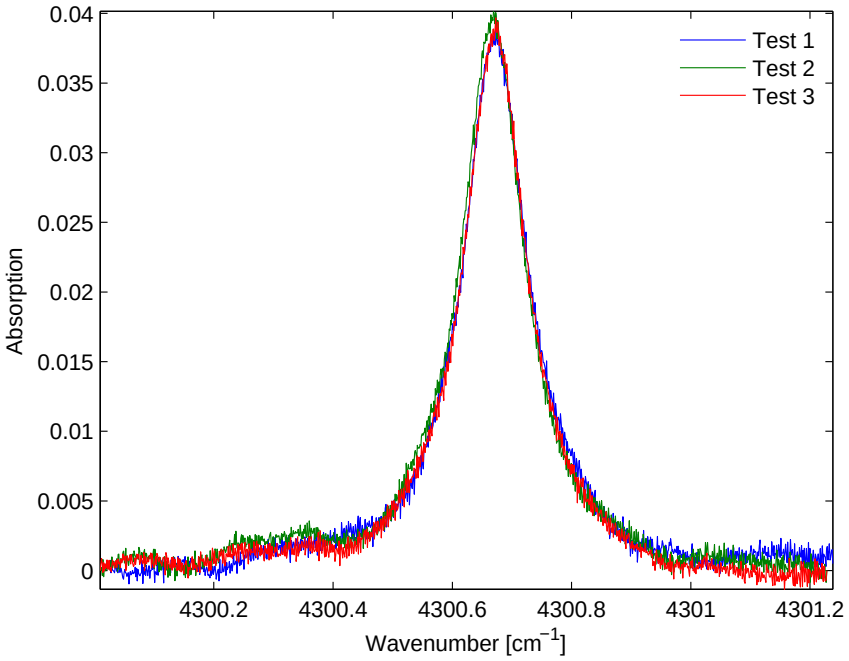

FIGURE 5.5: Absorption spectrum of CO during bubbling in Heptane.

algorithms for data processing of signals from modulation techniques. For direct absorption spectroscopy, a MDA of 10^{-3} can be considered as a reasonable first assumption. Thus, minimum detectivity profile can be calculated for different temperatures and pressures. For the minimum-theoretical detectivity profiles, spectroscopic data from HiTran were used to obtain both the line-strength and the line-shape functions.

$$X_{j,min} = \frac{MDA}{S_i \phi_{\nu_0} PL} \tag{5.1}$$

The y-axis of Figure 5.6 illustrates the temperature dependence of the calculated detection limit for the R(11) from $CO - 2\nu$ assuming a MDA of 10^{-3}. The minimum detectivity was evaluated over the ISC temperature at atmospheric pressure and 100 cm of path-length. By increasing the temperature the line-strength drop as simulated in Chapter 3, and the minimum detectivity goes up. Thus, for the R(11) transition will obtain high sensitivity by decreasing the temperature as temperature-dependent minimum detectivity is primarily determined by changes in the line-strength. A minimum-theoretical detectivity of 30 ppm-m was achieved at temperatures near to 300K, while 180 ppm-m was obtained for 1100K. On the other hand, the optimum pressure for detection is near to 200 Torr where a minimum-theoretical detectivity of 300 ppm-m can was achieved by evaluating Eq 5.1 to 296 K and 100 cm of path-length and assuming a 10^{-3} value for MDA. Figure 5.7 showed as a steady state was accomplished and determined bu the Voigt profile evaluated at the R(11) line-center.

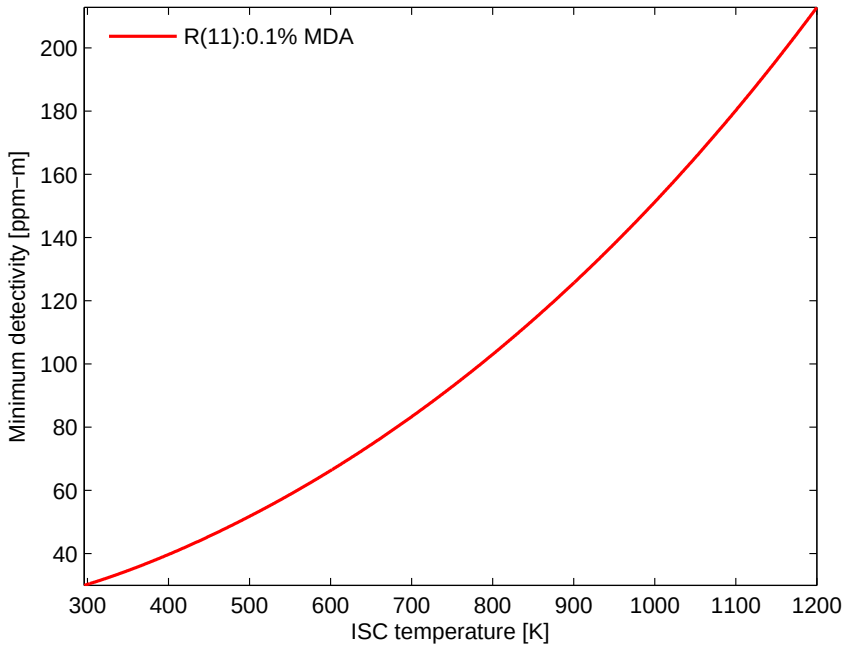

FIGURE 5.6: Predicted CO detection limit with DA by assuming 10^{-3} MDA , P=1 atm, for R(11) at 4300.69 cm^{-1}

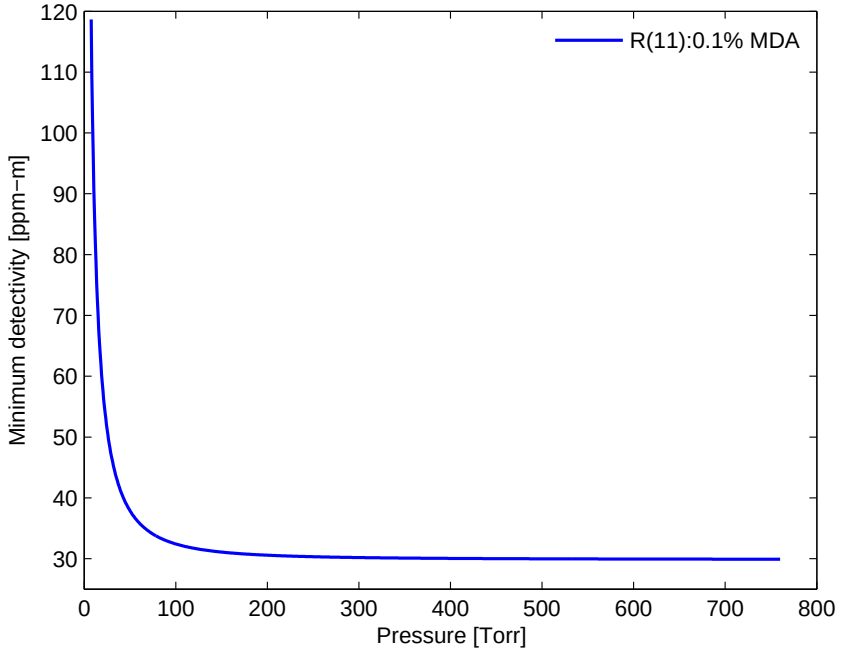

FIGURE 5.7: Predicted CO detection limit with DA by assuming 10^{-3} MDA , T=296 K, for R(11) at 4300.69 cm^{-1}

5.3 CO-Concentration validation experiments at static-glass cell

Before deploying the TDL-sensor in hazard conditions, such as high temperature and high pressure during experimental tests in the combustion chamber, and uncharacterized environment as expected during the in-situ combustion of a heavy crude oil, an important task is to validate the truthfulness of data from laser-based measurements. To validate the CO measurements carried out by the TDL-sensor, experiments at highly-controlled experimental conditions of a well-known composition gas were conducted in the static-glass cell at room conditions in the order to find possible failures for CO-sensing by WS-DA-TDL, and an improper use of the data processing algorithm. Different experiments allowed figuring out the performance of the sensor hardware and data processing schemes, as well as quantifying measurement uncertainty and identification of any potential problem that may arise when the TDL-sensor is deployed. For the propose of validate the TDL-sensor, an experimental setup were built to sense seven-different concentrations of CO at 296K and atmospheric pressure in a 3.81-long glass cell. The experimental data were used to develop a calibration curve with excellent agreement to the linear fit and specific-CO detection without any neighboring interference, while the laser-based measurements were validated by means of HiTran database.

5.3.1 TDL-setup and experimental conditions

The validation and calibration experiments were carried out using the pitch and catch assemblies of the TDL-sensor outlined in Chapter 4 with good alignment procedure over the absorption cell. The experimental setup consisted of a Duran borosilicate glass-cell of 3.81 cm long and 2.54 cm diameter as the static-glass cell was custom-designed molded part with non-precision equipment the thickness for both surfaces of in and out for the laser beam were not symmetric. Two gas-ports were located on the cell-body and the output-gas port was used as gas outlet and measuring-temperature point. As shown in Figure 5.8 connection hoses were used to join the metallic parts with the gas sample input/output ports. Although, plastic hoses are not considered as the best option of connection to evaluate different conditions of temperature and low pressures, and acceptable rate of leakage was achieve to be less than $250 Pa/min$, and experimental tests can be conducted at room conditions with successful results for both the calibration curve and experimental-data validation for CO detection measurements. The gas outlet was send to an exhaust hood while the gas inlet was controlled by precision micro-orifice ($O'keefeControls\#3$).

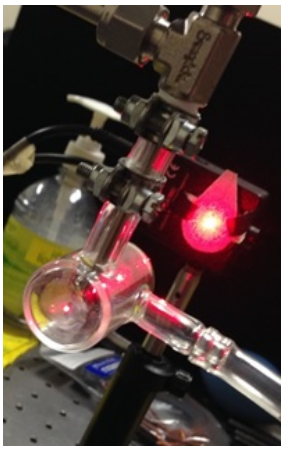

FIGURE 5.8: Single-zone glass cell for calibration experiments.

Experimental measurements of CO by TDLAS in the static-glass cell were carried out in a considerably cleaner environment than those expected to obtain during ISC experimental test of heavy oils. High transmission were achieved because to the low light scattering and is supposed that laser measurement from the exhaust gases for experimental lab-scale tests of ISC will not have considerable drop of the laser transmission by particle size. The TDL-sensor was aligned across the absorption cell and it was not purged with dry nitrogen since trace CO of laboratory environment can be assumed negligible. The pitch and catch assemblies were the same to those used during line-strength measurements. Tubing connections and tubing line showed in Figure 5.9 enabled a continuous flow of the target gas throughout the static-glass cell assuming an uniform composition and temperature over 3.81 cm-long of line-of-sight.

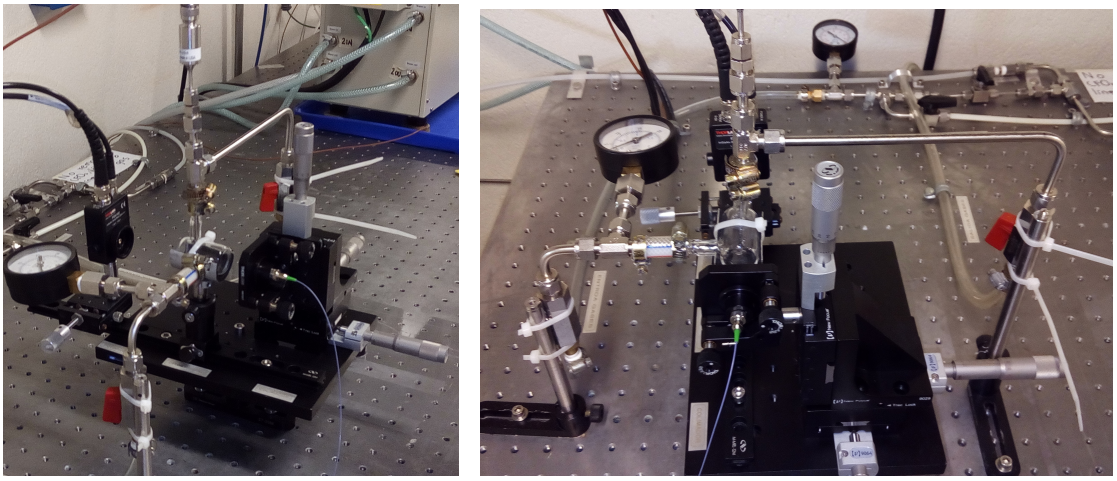

(A) (B)

FIGURE 5.9: TDLAS-setup used for calibration experiments.

An etalon effect was observed during calibration experiments because to the constructive and deconstructive interference generated by background reflections. Although, many attempts were deployed to minimize the resonant cavities, such as tilts of the laser, glass cell and photodiode, none successful outcome was achieved. However, the CO-monitoring was carried out without overlapping interference from etalon effect to concentration as low as 0.7%. The etalon effect was mainly generated by the custom-designed of the glass-cell, to future work the surfaces where the laser beam in and out must be remove and locate wedged windows.

A calibration curve was performed using a 3.4% (Linde primary standar, ±0.02% absolute) CO, 30% CO_2 and balance N_2, and six CO-molar fractions were provided by diluting the standard-gas mixture with N_2 reaching CO-concentration as low as 0.7% for a constant-gas flow of $CO/CO_2/N_2$ standard mixture of 141 cm^3/min. At room conditions of 296 K, atmospheric pressure and continuous flow the calibration experiments and validation analysis were carried out. The in-house interface for data acquisition provided a low sample rate of 1Hz, although one scan was obtained during experiments the non-reactivity behavior of the evaluated experimental tests assured negligible changes in molar composition during the experimental time. 1500 measured-scans were averaged to obtain an absorption spectrum by following the data processing algorithm depicted in Chapter 4. The TDL-sensor operated under current modulation provided by a reference-triangle signal of 50% symmetry and 70 Hz of frequency and amplitude of 0.02V. The controller was fixed to 25°C for the TEC module and a background current of 80 mA for the drive module.

5.3.2 Calibration measurements and validation analysis for both calibration and free-calibration methods

Laser-based diagnostics using the DA-TDL technique were carried out in the order to provide a calibration curve for CO-concentrations. Molar fractions from 0.7% to 3.4% were monitored by the wavelength-scanned method of direct absorption spectroscopy evaluating four times each experimental concentration to assess the repeatability of laser-measurements.

By quantifying the maximum absorption as describe in the data processing algorithm in Chapter 4, the calibration curve at room conditions was appropriately reproduced achieving an excellent agreement with the linear fit with a R^2 of 0.99865 for the seven CO-molar fractions evaluated as shown in Figure 5.10, the error bars are too small to be identified in the figure. TDL-sensor and the experimental architecture can provide good

laser-measurement of CO using the calibration method for the described concentration range using the calibrating equation shown in Figure 5.10. Although, the calibration curve carried out concentration measurements up to 0.7%, the calibrating equation can provide, with a good approximation, lower concentrations. However, the challenge is rooted to eliminate the etalon effect in the order to avoid overlapping oscillations over the spectral range of R(11).

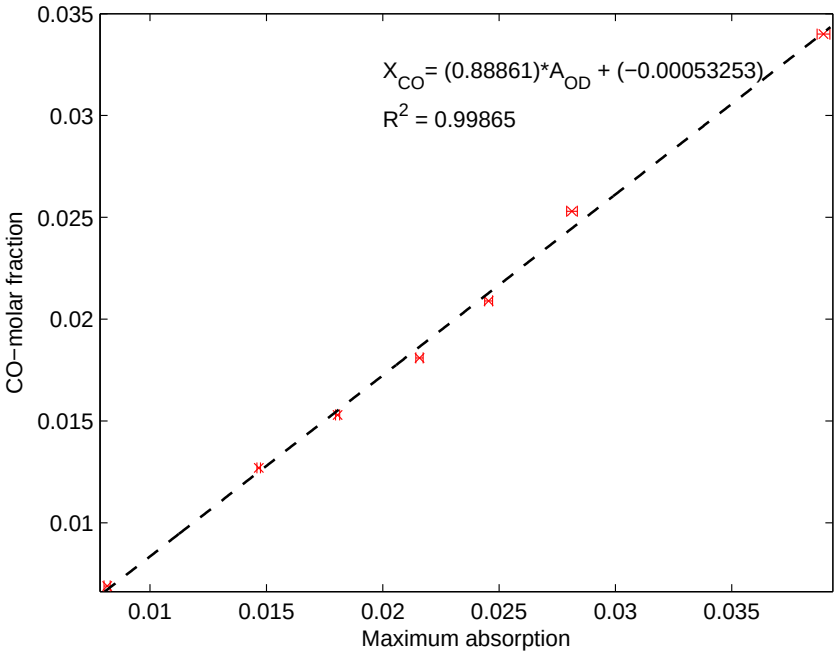

FIGURE 5.10: Calibration curve of CO concentration at static-glass cell at atmospheric pressure and room temperature.

As experimental-CO concentration decreased, the maximum absorption reached lower values according to absorption physic. Although, 3.81 long- pathlength was considered, at the beginning, as a short path to perform TDL-measurements experiments provided that good absorption values upper than 10^{-3} can be easily achieved, and direct absorption spectroscopy worked appropriately for CO sensing at even 0.7%. Unfortunately, none effort for trace-CO sensing by the TDL-sensor was carried out, but accurate CO-measurements over the study range were measured and validated for the first time at CO-molar fractions expected to be produced during the ISC of a heavy crude oil. Spectral simulations for the experimental conditions showed absorptions values, in the line-center of R(11), above of 10^{-3} proving the feasibility to perform DA measurements. Figure 5.11 illustrated the maximum absorption reached at each CO-experimental concentration with their error bars. Because to the good repeatability during experiments, the error bars showed low values, which were not to be easily seen.

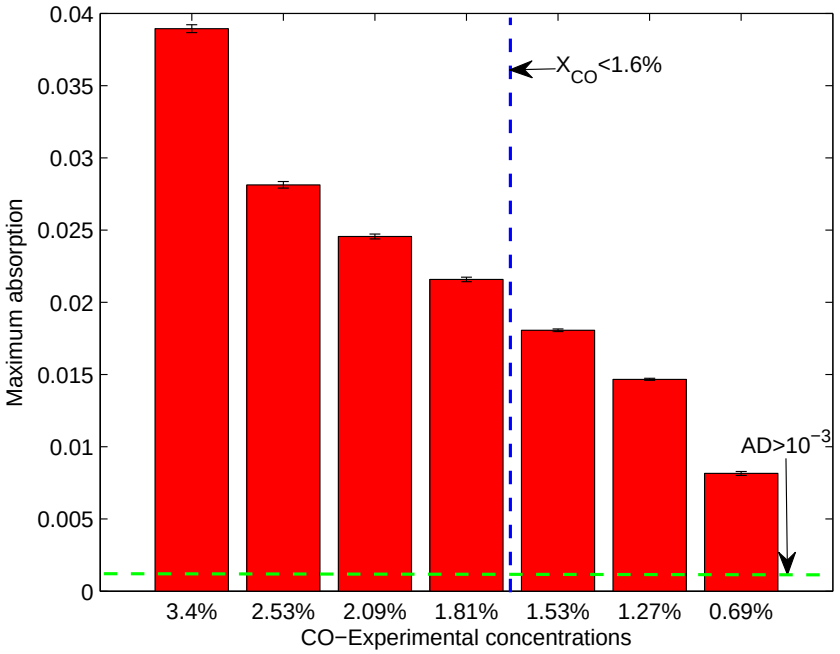

FIGURE 5.11: Calibration bars of CO concentrations at static-glass cell at atmospheric pressure and room temperature.

As the expected CO concentration during lab-scale ISC tests can be, by the Thomas stoichiometry, as high as 1.6% at, the viability to carry out TDL measurements with the pathlength proposed by Mr.Copete for the ISC chamber appear to be possible even with DA-spectroscopy. Absorptions of, around, 0.08 at $CO = 0.7\%_{mole}$ and 1.8 for $CO = 1.6\%_{mole}$, as illustrated by both green and blue lines in Figure 5.11, confirmed that CO can sensed by DA without the need to use modulation techniques. However, for trace-gas detection at ppm scale, an analysis of the absorption values must be developed.

Some statistic parameters from the calibration experiments outlined above were listed in Table 5.2 in the order to illustrate the good repeatability obtained by the TDL-sensor. For lowest-CO concentration, it was observed a relative standard deviation (RSD) of 1.65%, whereas typical RSDs around 0.6% were obtained to CO-molar concentration between 3.4% and 1.27%. The uncommon RSD of 1.65% was provided by the fact that a new alignment of the TDL-optical setup was carried out at that experimental concentration.

Absorption spectra from each experimental test are shown in Figure 5.12 along with both the Voigt profile and a HiTran-absorption spectrum. For all laser-based measurements the absorption at the line-center was achieved and validated with HiTran database. Although, some etalon effects were obtained over the scanned-spectral range, the ghost modulation were more pronounced in both ends of the absorption line. By reducing the

TABLE 5.2: Statistic parameters of experimental data of calibration curve.

Concentration	Standard deviation	Mean	Relative standard deviation [%]
3.4 %	0.271220343894066	0.038941796922771	0.696476190947099
2.53 %	0.229394202516766	0.028131898596440	0.815423821219786
2.09 %	0.169641182966834	0.024551346359791	0.690964888364178
1.81 %	0.156899559997498	0.021579792956705	0.727067031237442
1.53 %	0.089265097902419	0.018062822250642	0.494192417241147
1.27 %	0.074319482149038	0.014669158278139	0.506637672999902
0.69 %	0.134775653461189	0.008155646304353	1.652544120130094

CO-concentration the signal from the cavity resonant showed stronger effects, even the experiment at $CO = 0.7\%$ showed an oscillation from the etalon effect located near to the line-center. However, for the seven experimental tests, non-overlapping was reached and experimental data agreed with theoretical simulations. The SNR decreased up to 14 as the standard deviation showed increases at low concentration because to the difference between the measured data and the Voigt profile, where typical values for the residual were in the order of $\pm 1 \times 10^{-3}$.

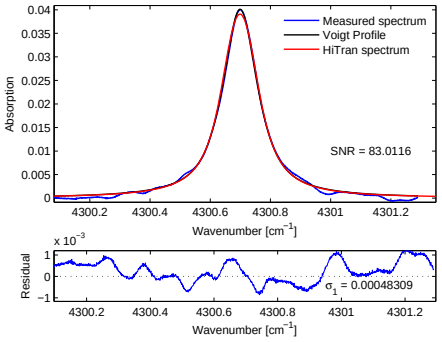

(A) first

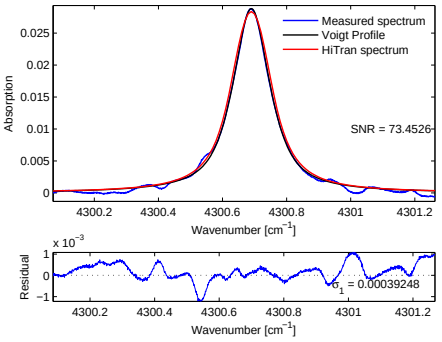

(B) second

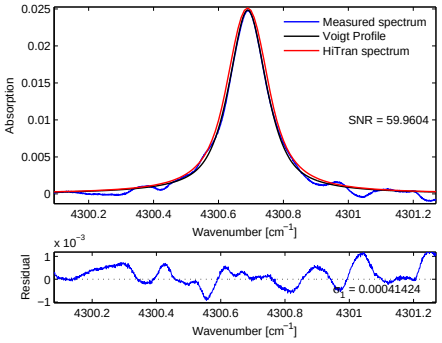

(C) third

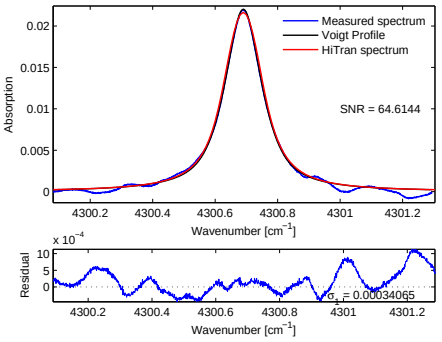

(D) forth

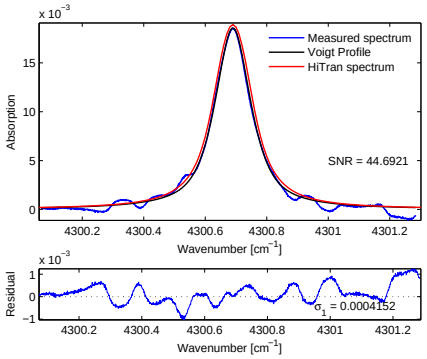

(E) fifth

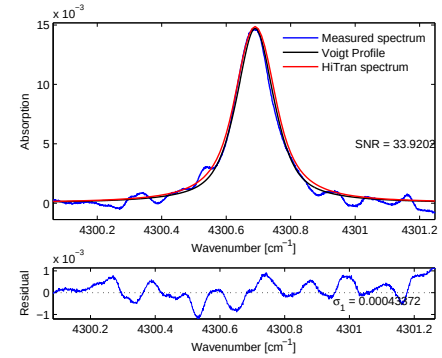

(F) sixth

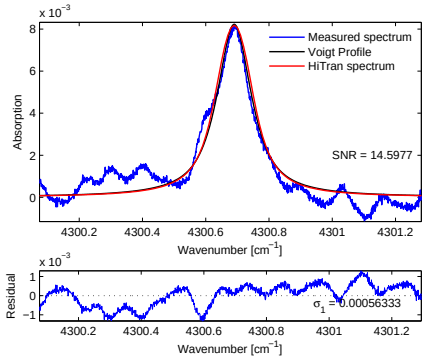

(G) seventh

FIGURE 5.12: Absorption spectra of calibration experiments at: a) CO:3.4%, b) 2.5%, c)2.1%, d)1.9%, e)1.5%, f)1.3% and g) 0.7%. Each experiment was validated using HiTran database.

In the order to determine the detection limit of the TDL-sensor during calibration curve, an absorption simulation at different CO-concentration, room conditions and 3.81 cm pathlength, was carried out along with the etalon signal. The oscillating signal has an amplitude of, about, 2×10^{-3} than can interfere and overlapped absorption spectra below to 0.2% as illustrated in Figure 5.13. Because the etalon effect was mainly generated by the custom-designed glass cell, it can be affirm that the sensor architecture for TDL-CO measurements provide acceptable measurements and an improvement of the absorption cell would carry out a more sensitive detection.

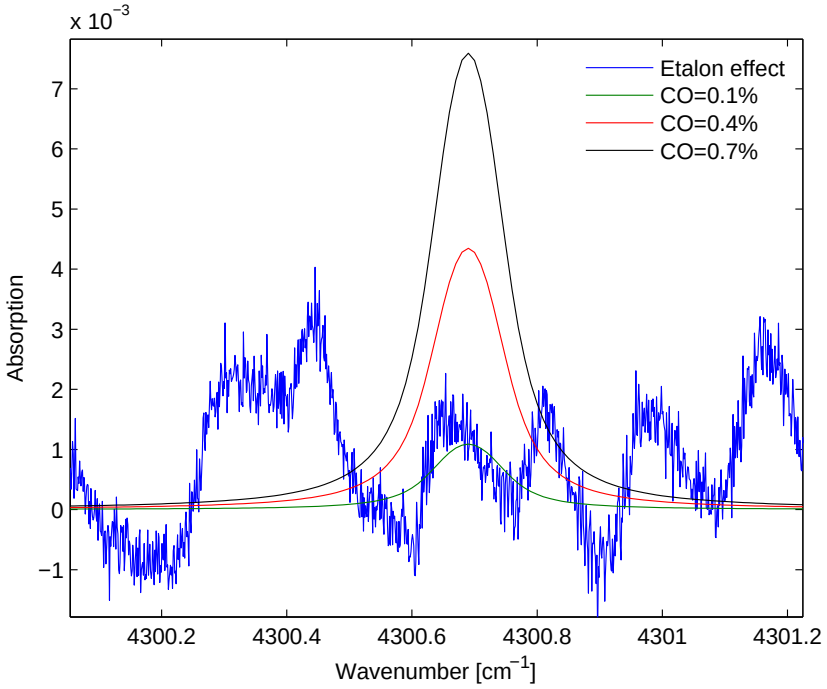

FIGURE 5.13: Interference from etalon effect during calibration experiments by DA-TDLAS optical sensor in sampled room temperature gas in the static glass cell.

The TDL-measurements were validated as shown previously in the absorption spectra by the HiTran- simulation at the different concentration. The maximum absorption at the line-center was well reproduced by the spectroscopy theory at each test which can be seen by using the parity plot in Figure 5.14. A good agreement between both the maximum experimental and maximum theoretical absorption of the R(11) transition was accomplished with a R^2 of 0.99881 with an error rate less than 3%. An important result was the similar behavior of the fitting of the raw data (Voigt profile) and the theoretical-absorption spectrum, where each of them is superimposed. Thus, free-calibration measurements can be implemented for CO sensing since a whole absorption spectrum from the Voigt profile can be quantified.

Although, calibration method showed an excellent agreement to the linear fit the TDL-sensor is usually implemented to performed free-calibration measurements with the

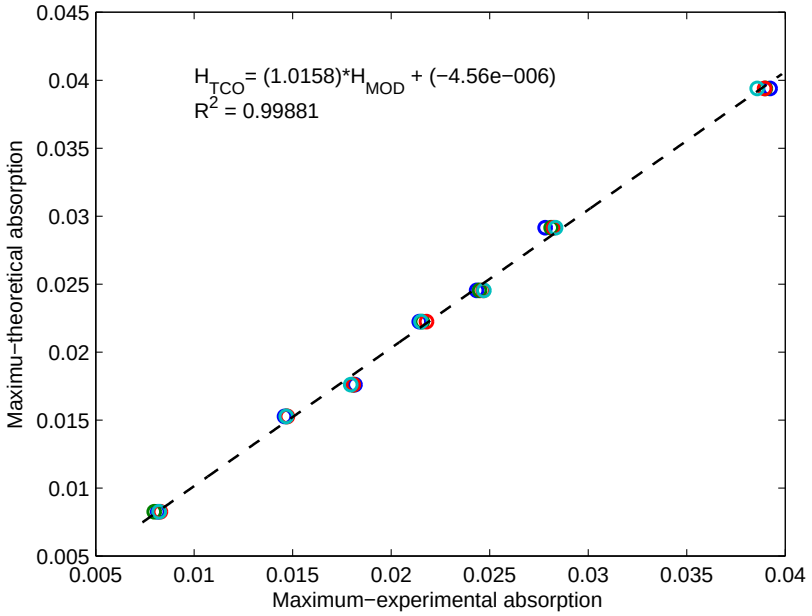

FIGURE 5.14: Validation error rate between theoretical absorption and measured amplitude.

procedure outlined in Chapter 4. Wavelength-scanned direct absorption spectroscopy was successfully carried out over the experimental concentration evaluated. The path-averaged CO concentration measured by WS-DA-TDL in the static-glass cell for a non-combustion test at room conditions is illustrated in Figure 5.15 with a R^2 of 0.99882 for the TLD-measurements. The line-of-sight path averaged CO concentrations measured by the TLD-sensor are plotted against the theoretical-CO concentration. The laser-based measurements agree with the theoretical concentration over the range from 0.7% to 3.4%, where error bars were too small to be seen. As the line-strength data from Hi-Tran were validated with an error validation less than 4%, the line-strength were taken from the database and used to perform the free-calibration method. A dotted-blue line depicted the reference concentration of the experimental test, while the solid-red line the concentration profile for optical measurements. Although, optical sensor reached concentrations with error rate less than 10% to the theoretical concentration, the high linearity of TDL-sensor predicts reliable measurements.

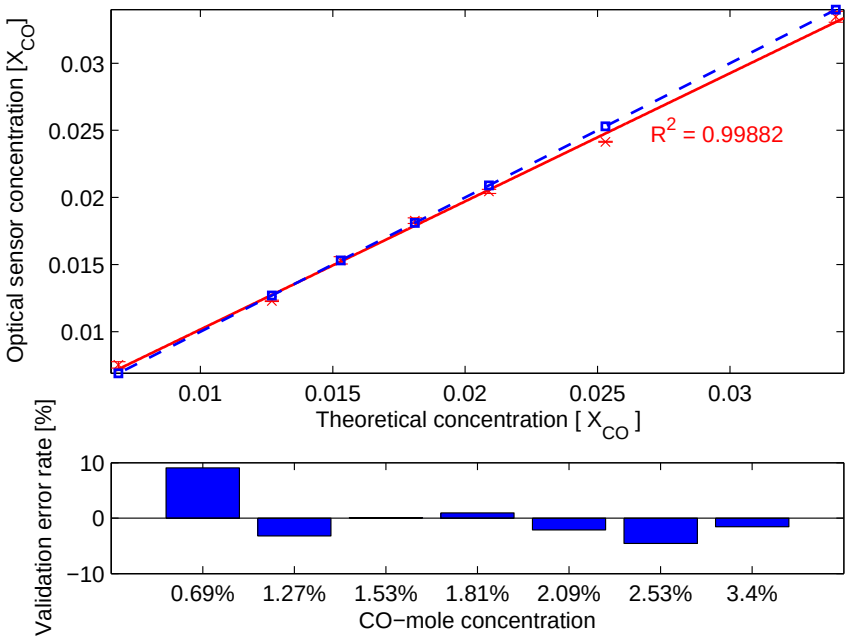

FIGURE 5.15: Free-calibration concentrations measured by DA-TDLAS optical sensor versus ideal measurements in sampled room temperature gas with pathlength L=3.81 cm.

Chapter 6

CO concentration measurements in a high pressure combustion chamber with optical access.

6.1 Chapter outline

Chapter 5 describes the laser-based measurements of carbon monoxide at hazard conditions similar to those implemented during ISC lab-scale experimental tests of pressure and temperature. A mechanical design of a combustion chamber with optical access is developed in order to provide a controlled environment of high-pressure and temperature. Wedged-sapphire windows were used to avoid etalon effect while gas sample ports were implemented to monitor gas temperature. Calibration and free-calibration curves were first conducted at room conditions for the purpose of validate TDL-sensor and alignment in the combustion chamber. TDLAS experiments of CO concentration at 30 psig and 60 psig were carried out reaching linear trends above 0.999 for both calibration and free-calibration method. For thermal experiments, an induction furnace was used with 7-coils over the induction reactor and non-uniform temperatures over the line-of-sight were obtained during the operation of the TDL-sensor. To validate the absorption measurement for two CO-concentrations, CFD simulations of the thermal profile of the combustion chamber were carried out, and acceptable results of the integrated absorption were obtained by numerical simulation.

6.2 Mechanical design of a combustion chamber with optical access for both high-pressure and high-temperature conditions.

A custom-designed combustion chamber with optical access was designed to carry out lase-based measurements of CO concentration at high conditions. The designed optical access allows transmitting more than 85% of the laser beam across to the gas media with a pathlength of 14 cm and measured values without cavity-resonant phenomena such as etalon effects. Although, ISC experimental test of a heavy crude oil for lab-scale conditions are reported to achieve temperatures as high as $800°C$, the optical chamber operated up to 570K without any operational problem. Although, non-uniform field were obtained for thermal experiments because to the custom-design, good agreement to the theoretical absorption were accomplished.

The combustion chamber with optical access provided an easily assembly to the induction reactor for future experiments of ISC characterizing experiments of a heavy oil, and mainly to supply an optical accessibility for CO-sensing by TDL measurements. Unfortunately, ISC experiments were not conducted and reported in this thesis dissertation, which is considered to future work, but high-temperature and high pressure suggested the viability of the TDL-sensor for CO measurements. The assembly of the optical access in the induction reactor was developed downstream, providing quasi-in-situ measurements.

A 316 stainless steel union cross for $\frac{1}{2}$ in OD tubbing (Swagelok: SS-810-4) has fitted two optical viewports designed for housing wedged-sapphire windows and gas sample ports at both optical access for gas purging when ISC test will be carried out. Sapphire material were chosen because to its superior IR transmission (above 85%) capability and its excellent mechanical and physical properties for harsh environments, while for avoiding etalon effect 2° wedge angle were used because back reflections from wedged windows are not collinear with the incident beam. O-ring gaskets of graphite were used for sealing the optical access and avoid any possible leakage. However, a leak test at 74 psig showed a leakage of 325 Pa/min. Because to the experiments carried in this thesis did not use oil, none window-fouling by particles and the gas sampling ports were used to monitor the temperature along the line-of-sight. The assembly between the union cross and the optical access is depicted in Figure 6.1 where the exploded view drawing illustrated the position of the sealing gaskets and the optical windows. In addition, Figure 6.2 A) illustrated the mechanical design of the top cover while Figure 6.2 B) for the lower cap.

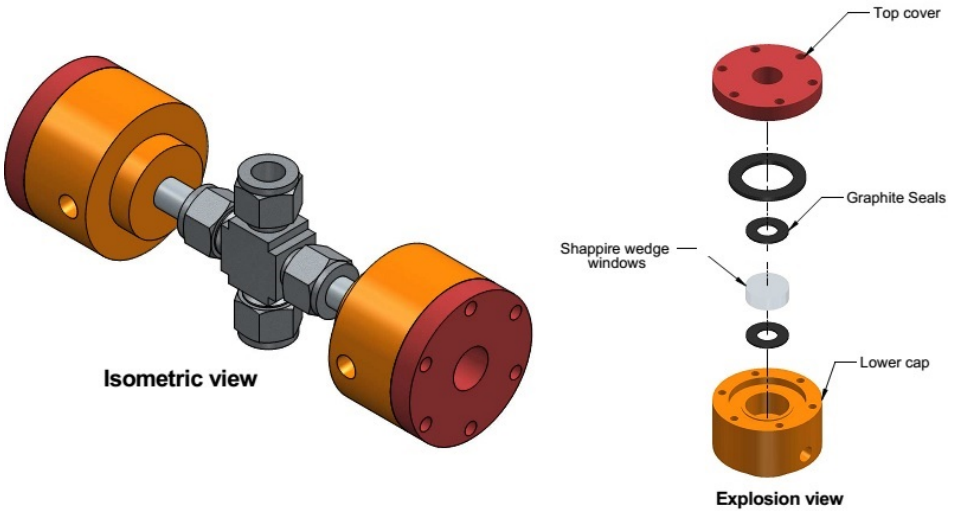

FIGURE 6.1: Optical access for CO concentration measurements during ISC lab-scale experiments.

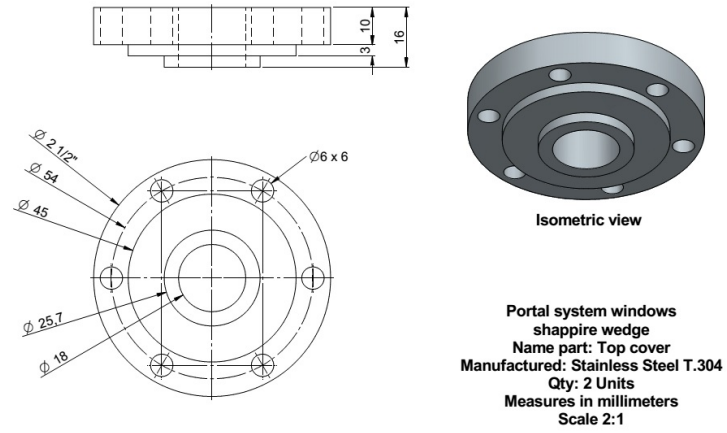

(A)

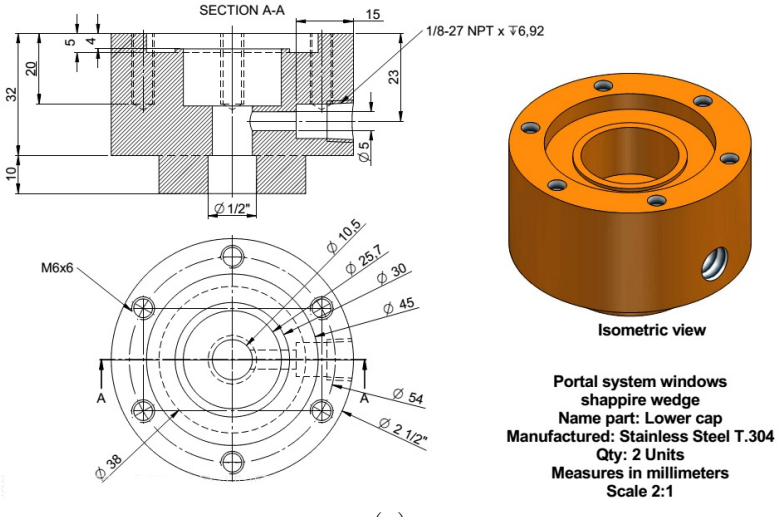

(B)

FIGURE 6.2: Mechanical design of wedged window housing.

6.3 CO absorption sensor using wavelength-scanning direct absorption at atmospheric conditions.

As developed in Chapter 5, line-strength data were validated using TDL measurements in the custom-designed combustion chamber. This new validation was carried out in the order to verity spectroscopic data from HiTran for experimental test in the optical access.

The optical access was placed and aligned along the TDL-sensor and coupled with the induction reactor. A general sketch is shown in Figure 6.3 for the experiments carried out for line-strength validation and, subsequently, the calibration experimental tests. The temperature was measured with a type-K and type-J thermocouple (Omega) each located as close as possible to the inlet surface of both sapphire windows. To performed line-strength validation, the same experimental procedure used in Chapter 5 was used, where six partial pressure of CO were measured over the 14-long of line-of-sight inside of the custom-designed combustion chamber at 296K. A new gas-standard with gas composition of $CO = 3.52\%$, $CO_2 = 30\%$ and balance N_2 were used during experimental tests in the optical access. Non-purge system was designed as CO-ambient was considered negligible.

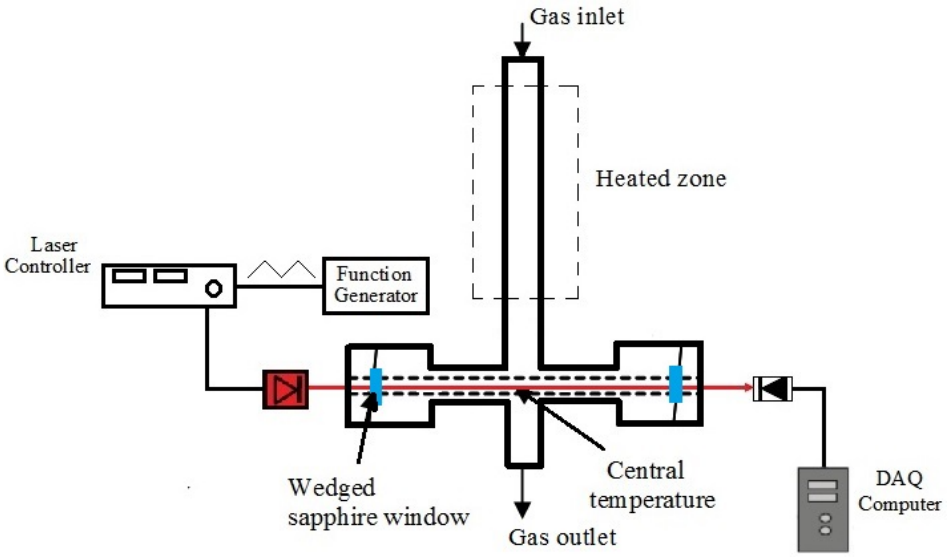

FIGURE 6.3: TDLAS arrangement for the induction reactor.

Wavelength-scanned DA-TDL was performed by means of an injection current to the DF-DL modulated using a reference-triangle signal with a 50% of symmetry, a frequency of 140 Hz, and 0.04 V of amplitude. Following the data-processing outlined in Chapter 5, the line-strength measured data are illustrated in Figure 6.4, with each experimental measurement being an average of 300 absorption-scans. The line-strength was inferred by the slope of the linear fit to the data. Good data consistency was achieved with a R^2

of 0.9997, and the measured line-strength of $6.62 \times 10^{-2} cm^{-2} atm^{-1}$ at, around 296K agrees with the HiTran value of $6.47 \times 10^{-2} cm^{-2} atm^{-1}$ with a validation error rate of 2.4%. The measured and theoretical line-strengths as well as the validation error rate are listed in Table 6.1.

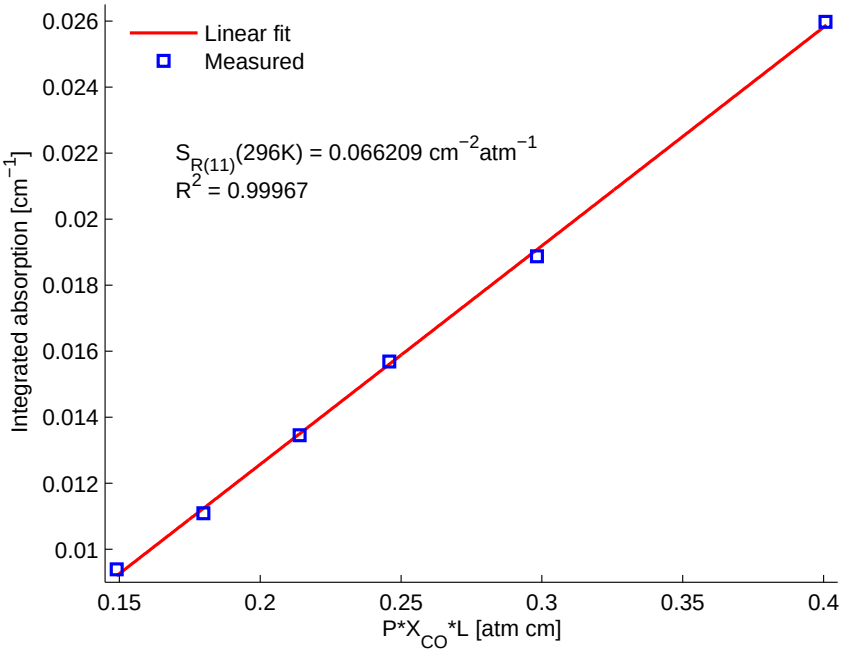

FIGURE 6.4: Measurement of linestrength R(11) near $4300.7 cm^{-1}$ by DA-TDLAS optical sensor in sampled room temperature gas with pathlength L=13.5 cm.

TABLE 6.1: Measured and calculated linestrength at 296K in combustion exhaust.

Line $[cm^{-1}]$	$S_{Measured}[cm^{-2}atm^{-1}]$	$S_{HiTran}[cm^{-2}atm^{-1}]$	Error rate [%]
4300.69	6.62×10^{-2}	6.47×10^{-2}	2.37

In order to develop reliable measurements in high conditions with the custom-designed combustion chamber, an important task was to validate the TDL sensor using highly-controlled experimental conditions of a well-known gas composition at room temperature and atmospheric pressure. Although, the WS-DA-TDL procedure and data processing algorithm was evaluated in Chapter 5, a new test facility with wedged windows had to be characterized.

The pitch and catch assemblies described in Chapter 4 were used with an excellent alignment procedure even with laser-beam deflections from the two wedged windows. The gas pipeline was built with stainless steel tubbing and the gas inlet flow to the induction reactor was controller by precision micro-orifice (O'keefe Controls), while the gas outlet was sent to an exhaust hood. Although, a leakage was observed at high pressures above 50 psig, non-appreciable pressure drop was obtained at working pressure below

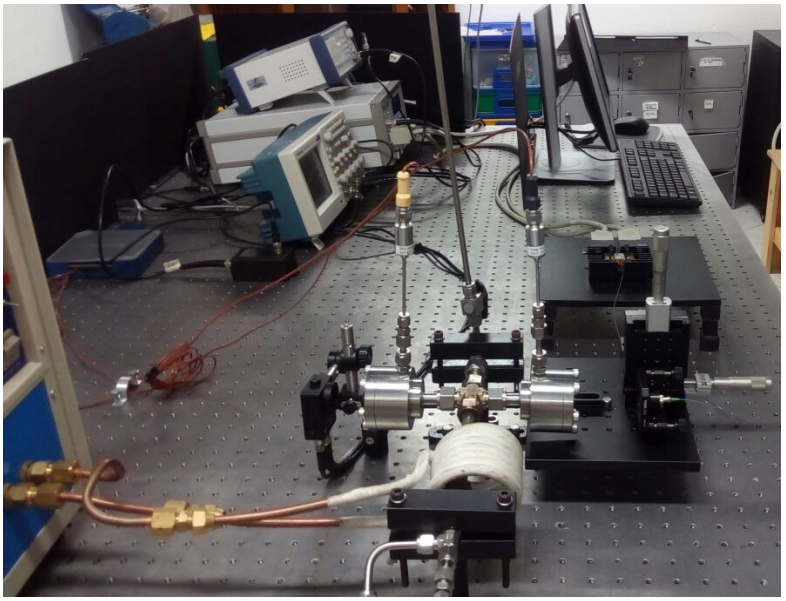

(A)

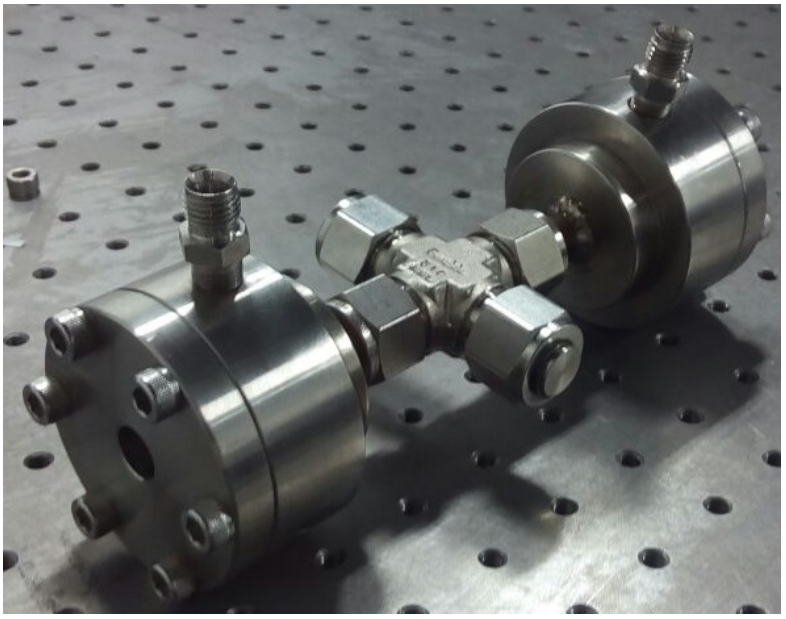

(B)

FIGURE 6.5: A)TDLAS-setup used for monitoring CO concentration during ISC lab-scale experiments, and B)mechanized optical access fitted to the union cross.

to 30 psig. Before the alignment process of the TDL-sensor, an induction oven was located behind the optical setup with seven coils along 10 cm of the reactor. Although, calibration curve and pressure experimental tests were conducted at room temperature, the TDL assembly was couplet to the induction reactor and aligned in order to provide a final ISC-experimental setup for future characterization of a heavy crude oil, as shown in Figure 6.5 A), while Figure 6.5 B) illustrated the machined optical access fitted to the union cross.

By previous knowledge obtained during the experimental training of TDL measurements in the static-glass cell, wedged windows were used to avoid etalon, Furthermore, photodiode and diode laser were tilted to minimize as much as possible any resonant cavity. Lower background reflections were observed than those obtained during calibration experiments at static-glass cell and non-overlapping from etalon oscillations was obtained at even low concentrations.

A calibration curve at room conditions of a standard-$CO/CO_2/N_2$ mixture of 141 cm^3/min was carried out for molar fractions varying from 1.3% to 3.52% of CO. 300 measured-scans were averaged to obtain an averaged-absorption spectrum by following the algorithm of calibration method illustrated in Chapter 4. Laser-based diagnostics using wavelength-scanned DA-TDL were performed in the order to monitor the CO concentration at both calibration and free-calibration measurements. The TDL-sensor was modulated by means of current with a triangle signal of 70 Hz of frequency and 0.03 V of amplitude, while the TEC module was fixed at $25°C$ and the drive module to a background current of 80 mA. Each calibration test was repeated three times in the for the purpose of evaluate repeatability.

Test data at room followed appropriately a linear trend with an excellent agreement to the linear fir with a R^2 of 0.9994 for the six CO-molar fractions, as shown in Figure 6.6. Contrary to the calibration curve of the static-glass cell, the experiment data showed error bars higher than those reported in Figure 5.10, although TDL-measurements in the combustion chamber achieved a better linear regression. Some statistic parameters are listed in Table 6.2 where typical RSD are between 1% and 3% and standard deviation below to 2.5×10^{-3}.

TABLE 6.2: Statistic parameters of experimental data of calibration curve at combustion exhaust.

Concentration	Standard deviation	Mean	Relative standard deviation [%]
3.52 %	0.002381149616920	0.151410290727576	1.572647146688713
2.62 %	0.001174761803844	0.111612800517938	1.052533220556164
2.16 %	0.002235564304431	0.091293700520726	2.448760748747829
1.87 %	0.001543052444403	0.081272847035250	1.898607592439190
1.58 %	0.001916852531955	0.069989484748393	2.738772172486160
1.31 %	0.001351489007902	0.056861897425360	2.376791962800171

Absorption spectra from the calibration experiment tests confirm with an excellent agreement with HiTran the absorption phenomenon of the CO along the line-of-sight of the combustion chamber with optical access at room conditions as shown in Figure 6.7. Measured-absorption spectra were fitted to a Voigt profile and were validated with spectroscopic parameters over the spectral range. Although etalon effect were not as high

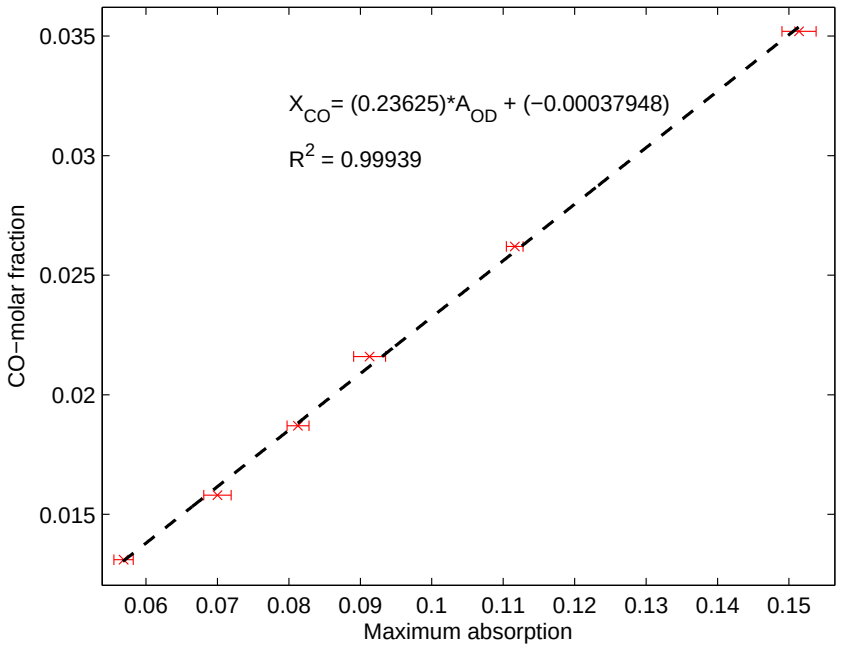

FIGURE 6.6: Calibration curve of CO concentration at combustion exhaust with optical access at atmospheric pressure and room temperature.

as those obtained in static glass cell, those resonant cavities were minimized as much as possible to the TDL-sensor. However, it is expected to performed, with the optical system, measurements for trace-CO concentration. SNRs were achieved with values as high as 174.3 to $CO = 3.52\%$, while an SNR of 57.7 was obtained at 1.3%. Because to the 14cm-long of the optical access, high absorption values were obtained increasing the detection limit of the TDL-sensor in this test facility.

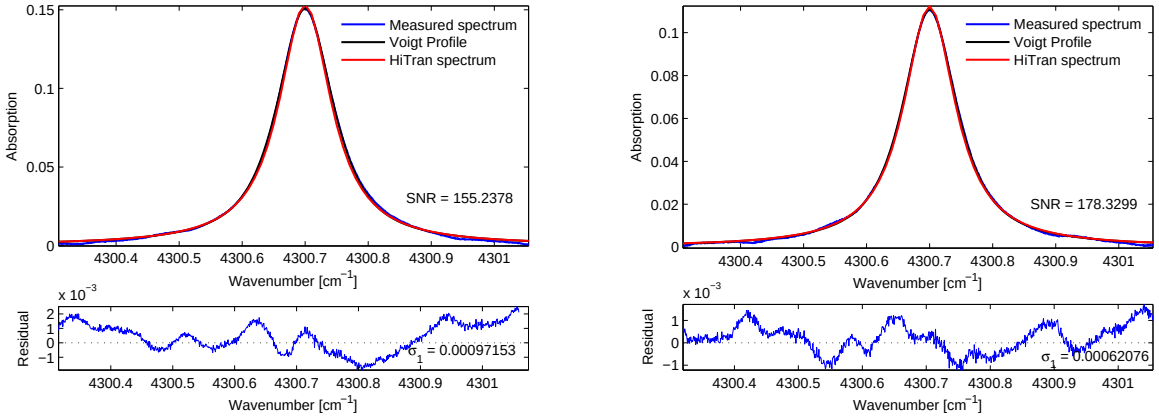

(A) first

(B) second

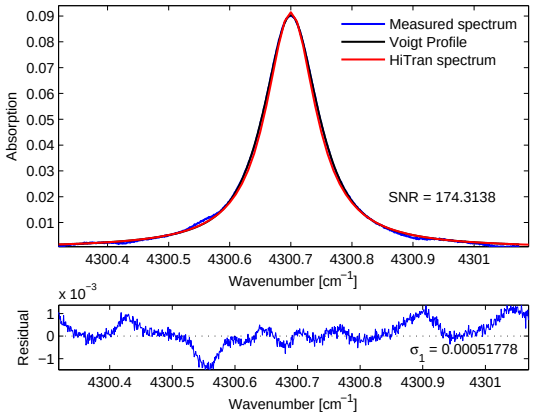

(C) third

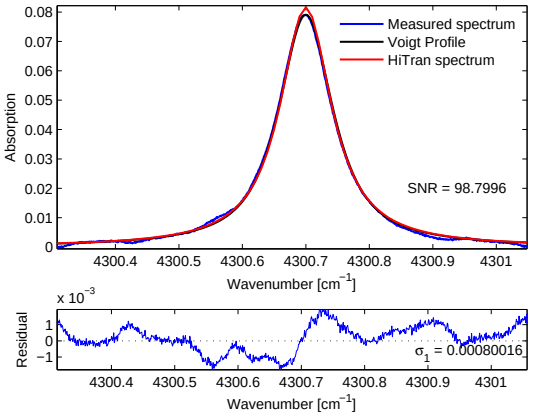

(D) forth

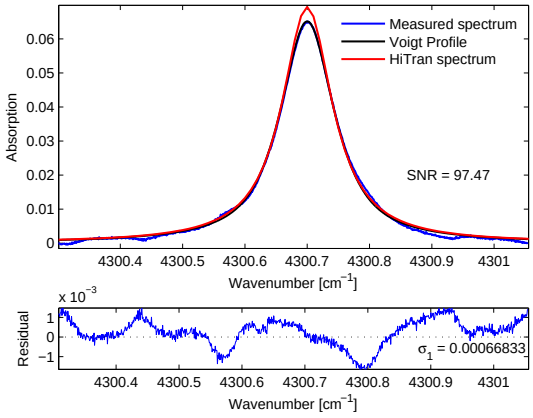

(E) fifth

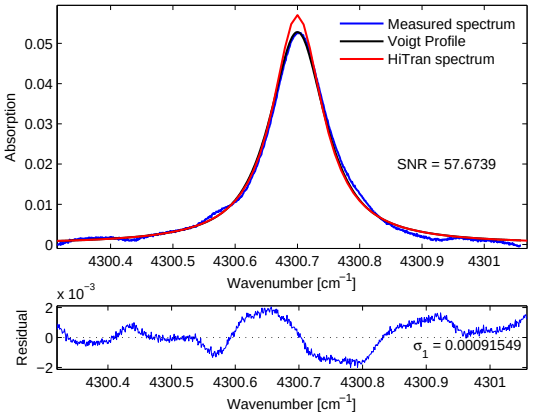

(F) sixth

FIGURE 6.7: Absorption spectra of calibration experiments at: a) CO:3.52%, b) 2.62%, c)2.16%, d)1.87%, e)1.58% and f)1.31% . Each experiment was validated using HiTran database.

An important factor of the TDL-sensor was to validate the laser measurements in the

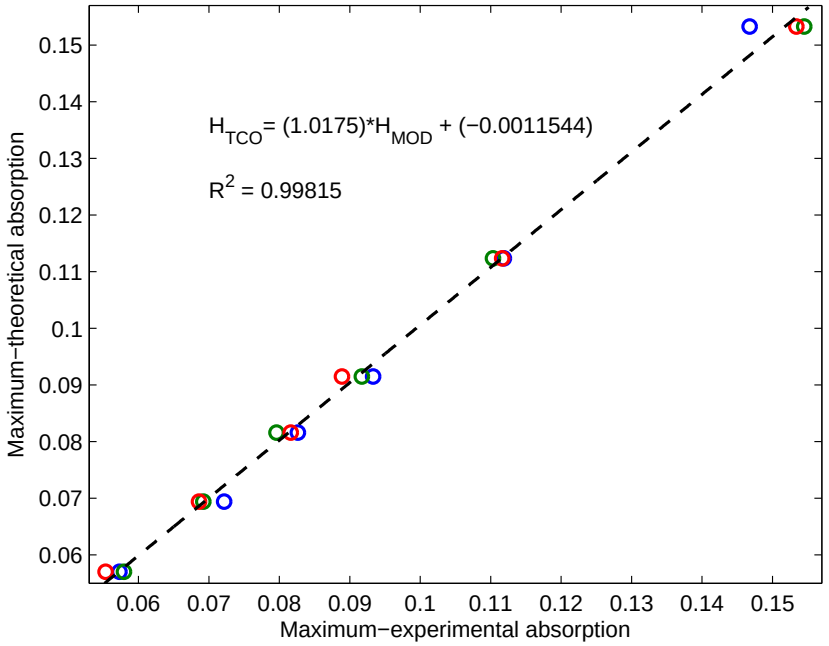

FIGURE 6.8: Validation error rate between theoretical absorption and measured amplitude.

combustion chamber by absorption spectroscopic. The maximum absorption of each experimental test was compared by a parity plot with a theoretical maximum absorption as the validation study developed in Chapter 5 for the measurements in the static-glass cell. Absorption spectra simulated with HiTran database showed for almost all tests a similar absorption profile which registered error rates up to 4%. Although, for low concentration it was not successfully reproduce, a linear fit showed good agreement to the experimental data with an R^2 of 0.9981 as showed in Figure 6.8.

Free-calibration measurements were developed with successful results for TDL-sensor at room temperature and atmospheric conditions in the combustion chamber. The importance of this study showed the viability to perform real-time measurements with high-accuracy in combustion environments. Figure 6.9 illustrates a linear behavior for the CO-measured concentration by the TDL-sensor which reached a R^2 of 0.9997. The dotted-blue line represents the theoretical concentration with a perfect linearity of $R^2 = 1$. The result obtained suggests that carbon monoxide can be sense in the optical access by quantifying the integrated area from the absorption spectra fitted to a Voigt profile, and monitoring the system pressure and temperature over the line-of-sight. An error rate less than 5% showed reliable measurements of the target compound. It is important to note that the validation error rate increased when CO concentration decreased.

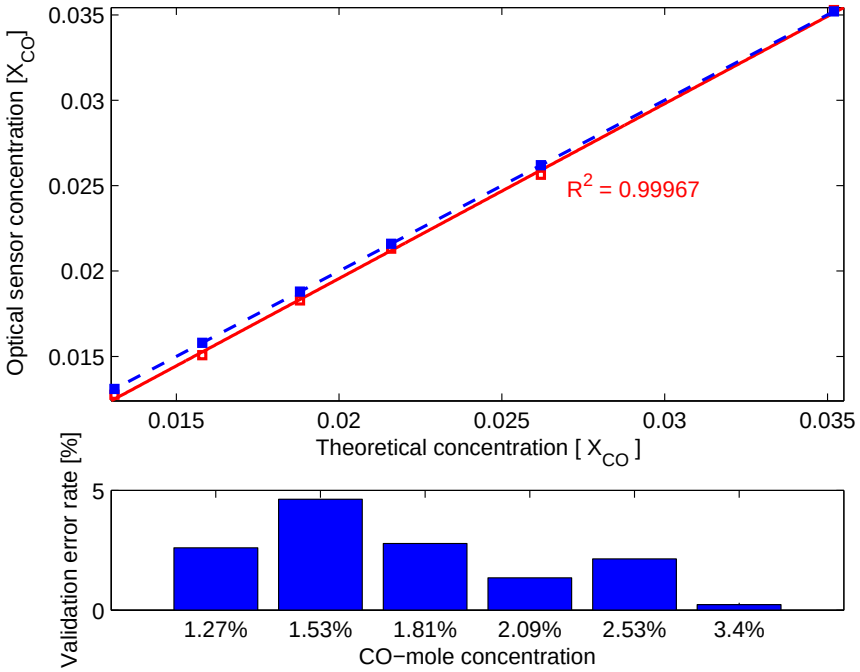

FIGURE 6.9: Free calibration measurements of CO at room temperature and atmospheric pressure at combustion chamber.

6.4 TDLAS measurements of CO concentration at high pressure.

The ISC process is carried out at high pressures up to 60 bars for industrial-scale projects. However, lab-scale experimental tests in combustion tube are performed up to 10 bars. This thesis developed laser-based measurements of CO at high pressures up to 4 atm under similar gas composition of those gases obtained during lab-scale ISC experiments of a heavy crude oil. These experimental tests showed the capabilities of the TDL-sensor developed as a method for CO-sensing at hazard conditions.

The absorption spectra simulated in Chapter 3 showed a spectral broadening of the R(11) transition of the $CO-2\nu$ band when the gas pressure increased because to collisional effects from neighboring molecules. In the order to conduct wavelength-scanned DA-TDL over a wider spectral range, the modulation conditions of the TDL-sensor were changed to have 0.08V of amplitude of a triangular signal with 50% symmetry and 140 Hz of frequency. 300 experimental scans were recorded and averaged to develop the calibration curve and free-calibration method. In the order to avoid any drop pressure during high-pressure experiments, a back pressure regulator was located in the gas outlet of the combustion chamber with optical access.

A calibration curve and free-calibration curve were obtained for the same gas composition of $CO/CO_2/N_2$ used in the experimental tests at room conditions of the combustion chamber. A work pressure of 30 psig was kept constant and TDL-measurements were carried out. Each experiment was repeated three times to evaluate repeatability with excellent results as shown in the error bars in Figure 6.10. The calibration curve were developed with five CO-concentration from 0.7% to 3.5% showing a good agreement of the experimental data with the linear fit reaching a R^2 of 0.9998 depicted in Figure 6.10 A), while the free-calibration method, which is illustrated in figure 6.10 B), obtained a linear regression of R^2 =0.9994 with error rate less than 4% to the theoretical CO-concentration.

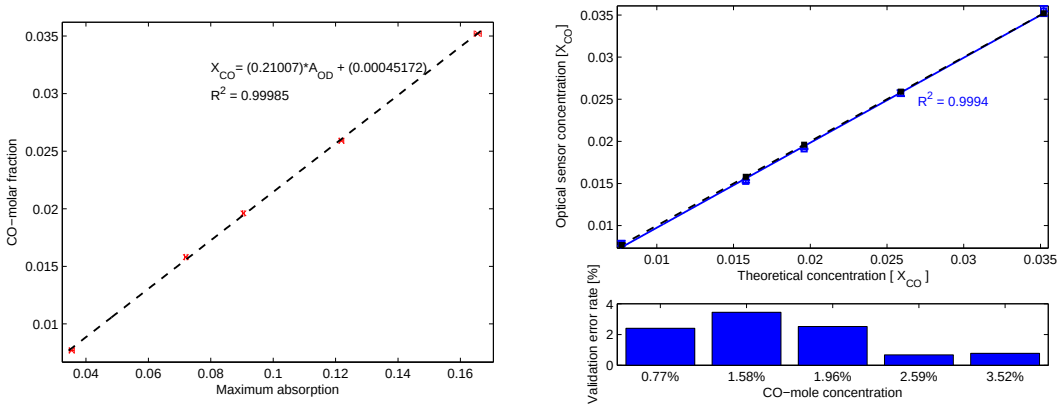

(A) (B)

FIGURE 6.10: A)Calibration curve and B) free-calibration of CO concentration at combustion exhaust with optical access at 30 psig and room temperature.

For safety operation of the custom-designed combustion chamber, the maximum work pressure was 60 psig, where appreciable broadening was obtained. Although, the FWHW increased the spectral line was successfully measured with wavelength-scanned method. During the calibration procedure for 60 psig, four CO-concentrations were conducted at room temperature with the modulation parameters outlined above. The experimental data showed in Figure 6.11 an excellent linear trend with a R^2 of 0.9998 for the calibration curve, and R^2 = 0.9995 for the free-calibration with an error rate less than 4%.

6.5 TDLAS measurements of CO concentration at high temperature.

High-temperature experiments were carried out at the combustion chamber with optical access to monitor the performance of TDL-CO-sensor under thermal ISC conditions for

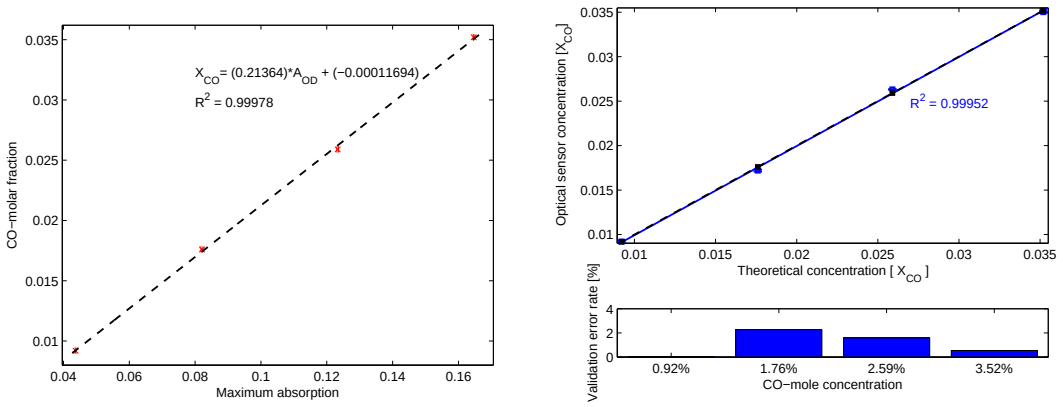

(A) (B)

FIGURE 6.11: A)Calibration curve and B) free-calibration of CO concentration at combustion exhaust with optical access at 30 psig and room temperature.

a controlled flow of a known standard mixture. Two CO-mole concentrations were evaluated by heating up the gaseous flow upstream by means of an induction furnace with seven-coins and reaching the highest temperature, of almost, $300°C$ at the center of the line-of-sight of the laser beam along the combustion equipment. Figure 6.12 shows the experimental setup used to conduct the TDL-CO sensing experiments at high temperatures. A relief valve was incorporated in the inlet of the induction reactor and set to a safety pressure of 32 psig to avoid hazard conditions due to plugging over the experimental assembly line. The line-of-sight was thermally characterized by three- measuring places with thermocouples. The temperature at the center of the combustion chamber was evaluated with a K-type thermocouple, while the temperatures at the end of both wings were measured with a J-type and a K-type thermocouple. The voltage signals from each thermocouple were acquired and processed by an in-house LabView interface. The gases into the induction reactor obtained the highest temperature of the experiment while the combustion chamber was heated up by convection and conduction of the exhaust gases which were released to the fume extractor hood.

A single-mode ZrF_4 optical fiber patch cable was included to the previous TDL-CO system to avoid damage to the DFB diode laser at hazard-experimental conditions and to improve safety movements for the DL-light emission during future alignments. This guarantees that damage risk due to thermal radiation will be minimum for the CO-sensor. Two mole fractions of CO, $CO = 3.52\%$ and $CO = 1.76\%$, were measured at four different temperature tests. Since the custom-designed combustion chamber does not have a constant diameter along the line-of-sight and heat transfer phenomena over the device, a non-uniform thermal behaviour was obtained. A new challenge at this point was faced by the methodology previously used where a constant temperature over

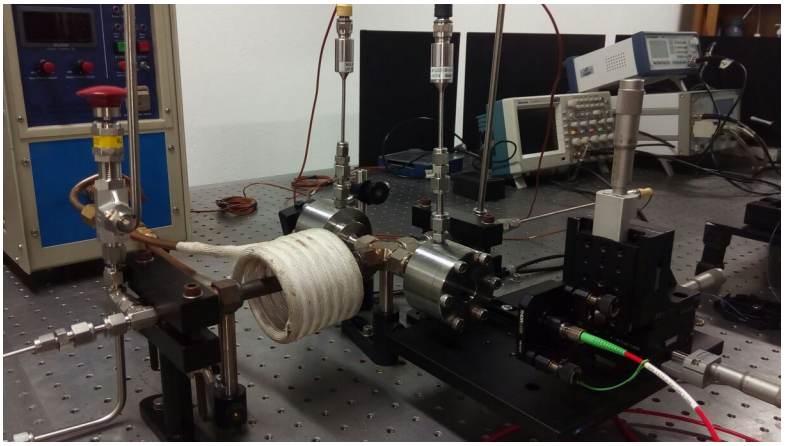

FIGURE 6.12: TDL-CO sensor setup for high-temperature experiments.

the optical-path was assumed.

A standard-gas mixture of $303 cm^3/min$ with a CO-mole fraction of 3.52% flow through the combustion chamber previously heated up by the induction furnace with compressed air. After the energy steady state was achieved at the center of the combustion chamber, four TDL-CO measurements were continuously performed by a triangle signal of 50% symmetry with amplitude of 0.08V and a frequency of 140 Hz. Figure 6.13 illustrates the absorption spectrum obtained for experimental temperatures evaluated at: i) 328.65 K ±1K, ii) 377.15 K ±1K, iii) 468.15K ±1K and iv) 550.65K ±1K.

The custom-designed geometry of the combustion chamber generates non-homogeneous fields of temperature along the laser-beam path. The light-matter interaction by absorption phenomena over the measuring volume is a function of the temperature discrete in space. Therefore, computational tools must be used in this point to obtain detail information about the temperature profile over the line-of-sight. Several CFD simulations were carried out to obtain a detailed-temperature profile along the line-of-sight for developing accurate measurements of the absorption spectra and for validating, by spectroscopic parameters, the maximum absorption reached for the high-temperature experiments. To developed accurate measurements of CO by using TDL-sensor, precise information of the thermal profile must be obtained over the path-length as the absorption depends of temperature by both the line-strength and the line-shape function. Equation 6.1 shows the mathematical model, which is the absorbance from Beer-Lambert law, used to validate the measured-absorptions at the line-center of R(11) absorption transition.

$$\alpha = P \times X_{CO} \times \int_0^L S_{R(11)}(x) \times \phi_{R(11)}(x)\, dx \tag{6.1}$$

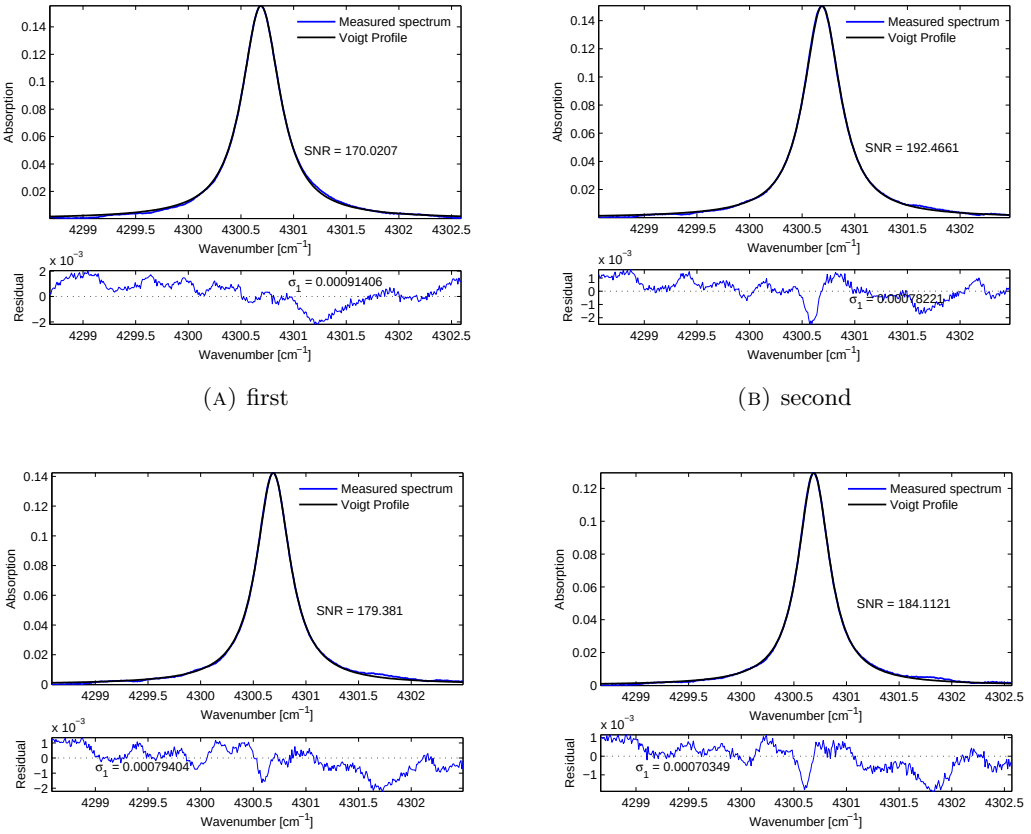

FIGURE 6.13: Absorption spectra of CO=3.52% during temperature experiments at: a)328.65 K ±1K, b)377.15 K ±1K, c)468.15K ±1K, and d)550.65K ±1K.

The line-shape function was evaluated at the linecenter υ_0 of the rotational transition R(11) since the experimental measurements of absorption were quantified by means of the maximum optical density obtained at υ_0. The line-shape function was fitted to be a Voigt function, by using Eq 6.2 evaluated at the linecenter.

$$\phi_V(\upsilon_0) = \frac{2}{\Delta\upsilon_D}\sqrt{\frac{ln2}{\pi}} \times exp\left(a^2\right) \times \left[1 - erf\left(a\right)\right] \tag{6.2}$$

where a was obtained by,

$$a = \frac{\sqrt{ln2} \times \Delta\upsilon_D}{\Delta\upsilon_D} \tag{6.3}$$

The custom-design combustion chamber was replicated in a 1:1 scale with a tetrahedral, non-homogeneous mesh with 400.000 cells. The CFD simulations converged after 300 iterations and were validated using the temperature measurements obtained by the three-measuring thermocouples placed close as much as possible to the line-of-sight of the light beam. Figure 6.14 shows the temperature profile obtained using CFD simulations for a measured-experimental temperature at the center of the combustion chamber of 328.65K

as an illustrative example of the mathematical process developed for validating of the experimental data. The simulations were according with the measured data and thus the CFD simulations were properly validated.

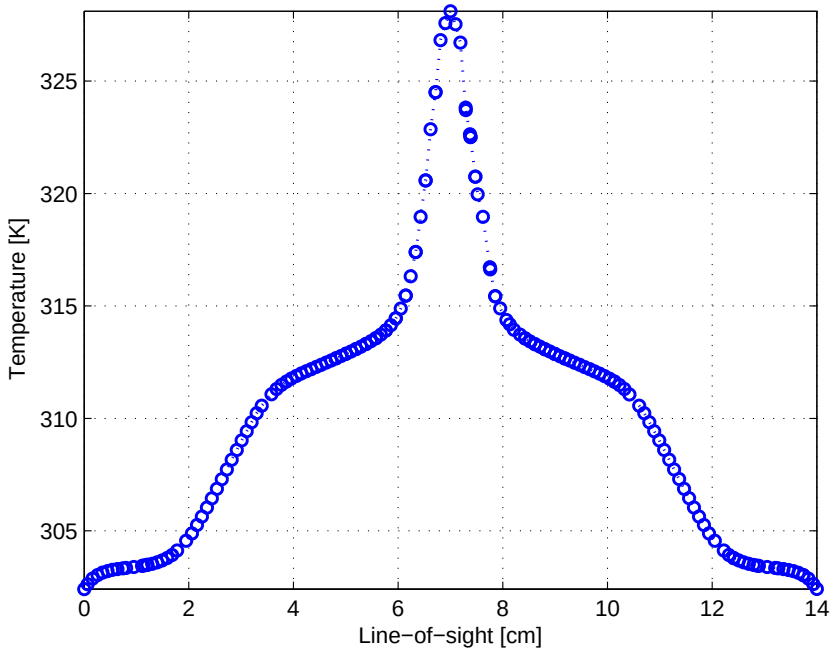

FIGURE 6.14: CFD simulation of the temperature profile along the line-of-sight of the combustion chamber with optical access.

Figure 6.15 A) and B) show a temperature-contour display for the scenario previously outlined with the simulated geometry of the combustion chamber. CFD simulations consider that the laser beam goes through the center of the inlet diameter of the combustion chamber and the CO concentration is uniform over the line-of-sight.

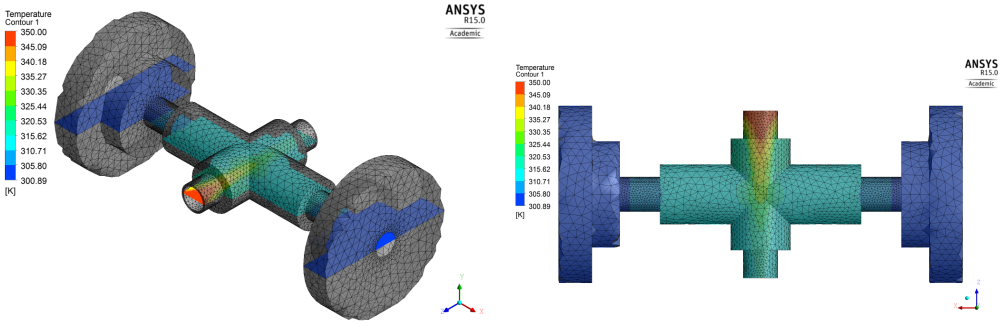

(A) (B)

FIGURE 6.15: A) Isometric and B)top view of CFD-temperature contour for the custom-designed combustion chamber with optical access.

The line-strength depends of temperature along the path-length and by using spectroscopic parameters from HiTran database 2008, a line-strength profile was obtained for

the measured-temperature experiment. Because the combustion chamber has symmetry at the center, the temperature profile and, therefore, the linestrength presents a symmetric behaviour over the line-of-sight, Fig 6.16 A). Increases in temperature produce a declined to the linestrength, Fig 6.16 B), giving that the maximum line-strength is located at both ends of the combustion chamber while the minimum at the center where the maximum temperature was reached. The linestrength varies in a range of, around, 0.0636 $cm^{-2}atm^{-1}$ to 0.0594 $cm^{-2}atm^{-1}$ as the temperature was not uniform for the illustration case of a center optical-access temperature of 328.65K.

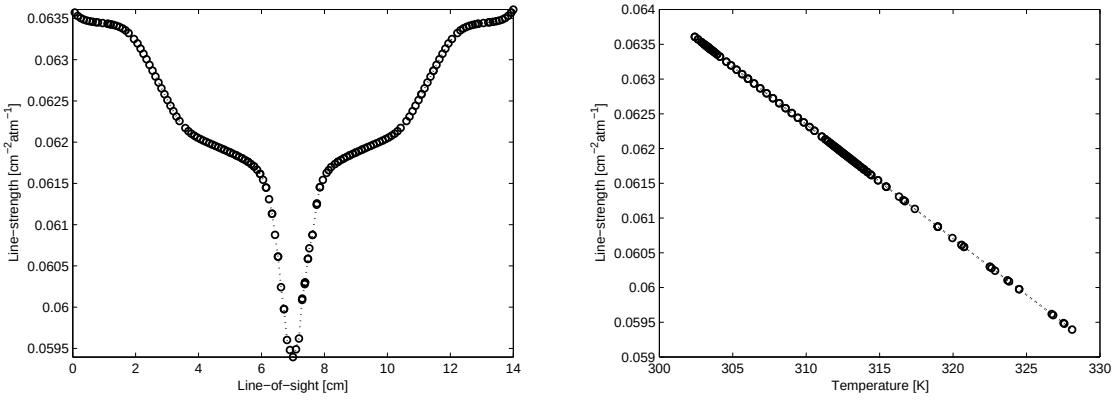

(A) (B)

FIGURE 6.16: CFD simulations of linestrength over: A) temperature and B) line-of-sight.

In the same way as linestrength, the absorption was obtained to each temperature-experimental test. As pressure (P) and CO-mole fraction (X_{CO}) in Eq 6.1 were considered constant and the linestrength follows the temperature profile over the line-of-sight, the absorption possesses the minimum value at the maximum temperature located at the center of the combustion chamber. Figure 6.17 A) shows how the absorption reduces its values to increases in temperature, while Figure 6.17 B) illustrates the absorption profile with a symmetric behaviour over the combustion chamber.

The experimental data were obtained to each temperature-experimental test and plotted as dotted red line, wherein the error bars have relative standard deviation below to 0.6%. CFD simulations are plotted as dotted blue line represents the validation profile for the experimental conditions evaluated. Figure 6.18 shows a comparative graphic between both the experimental and numeric data. The x-axis values depict the steady-state temperature at the center of the combustion chamber, while the y-axis is based on the integrated absorption by measuring and simulating procedures. The experimental data suggested the absorption values were conducted at lower temperatures that the predicted by CFD method. The mismatch between experimental and simulation data suggests that

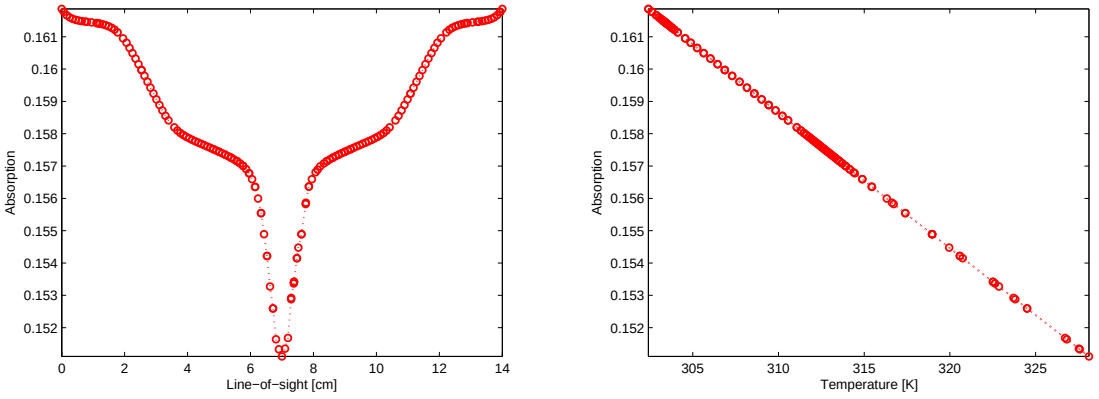

(A) (B)

FIGURE 6.17: CFD simulations of optical density over: A) line-of-sight and B) temperature.

a precise knowledge of the CO-concentration along the optical path must be obtained and the assumption of constant concentration do not provide accurate measurements.

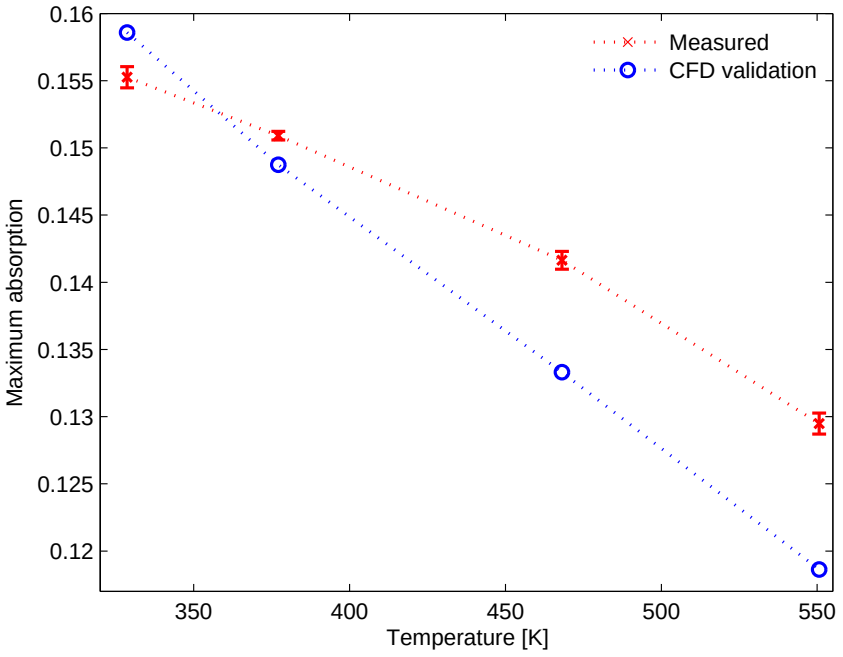

FIGURE 6.18: Calibration curve to temperature-experimental test at $CO = 3.52\%$.

A standard-gas mixture of 141 cm^3/min with a CO-mole fraction of 3.52% was diluted with 141 cm^3/min of nitrogen up to reached a CO-concentration of 1.76%. As the experiments of CO=3.52%, the combustion chamber was previously heated up by the induction furnace with compressed air and after the energy steady state was achieved

four TDL-CO measurements were continuously performed by the same modulation conditions outlined above. Figure 6.19 illustrates the absorption spectrum obtained for experimental temperatures evaluated at: i) 326.15 K ±1K, ii) 386.15 K ±1K, iii) 458.15K ±1K and iv) 570.15K ±1K.

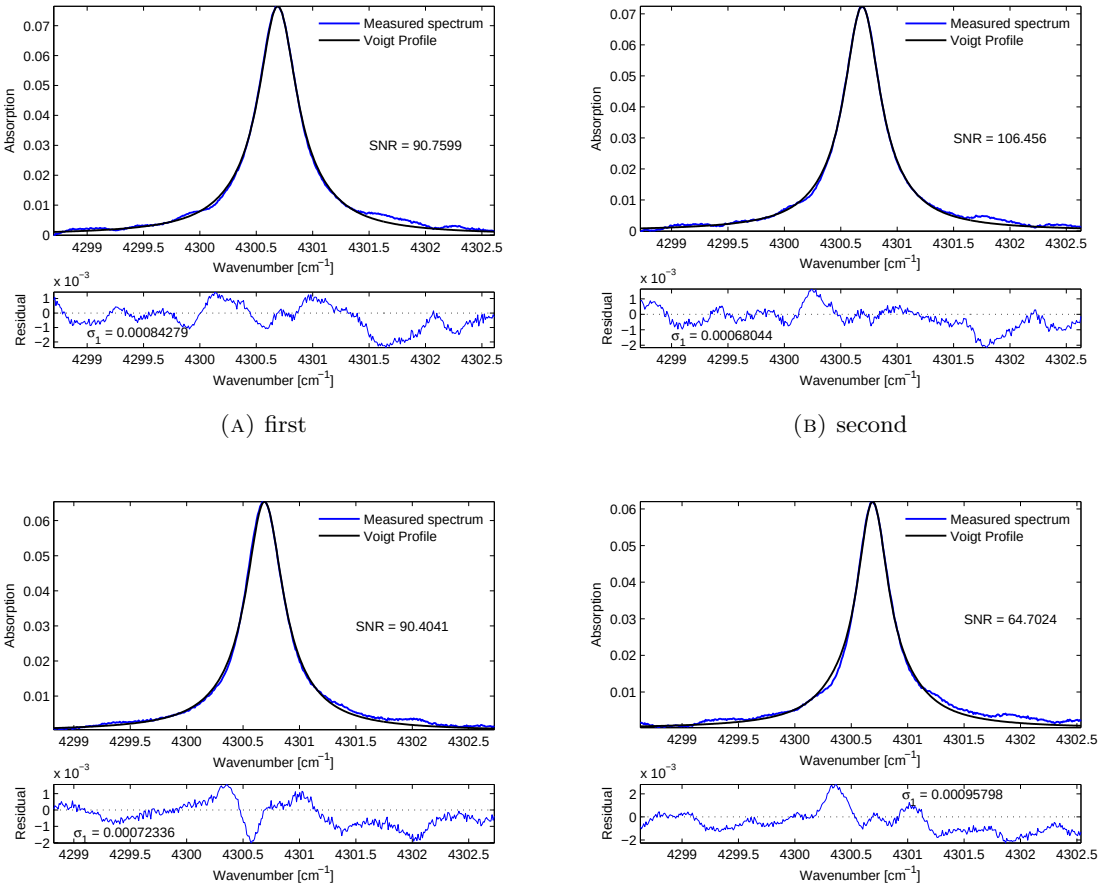

(A) first (B) second

(C) third (D) forth

FIGURE 6.19: Absorption spectra of CO=1.76% during temperature experiments at: a)326.15 K ±1K, b)386.15 K ±1K, c)458.15K ±1K, and d)570.15K ±1K.

Typical values above SNR 90 were obtained, although a value of 60 was observed at the highest temperature evaluated. In the CO=1.76% high-temperature concentrations the experimental absorptions showed values below to the CFD simulations given the idea that the temperature over the line-of-sight was higher than the predicted to the simulations, Figure 6.20 .

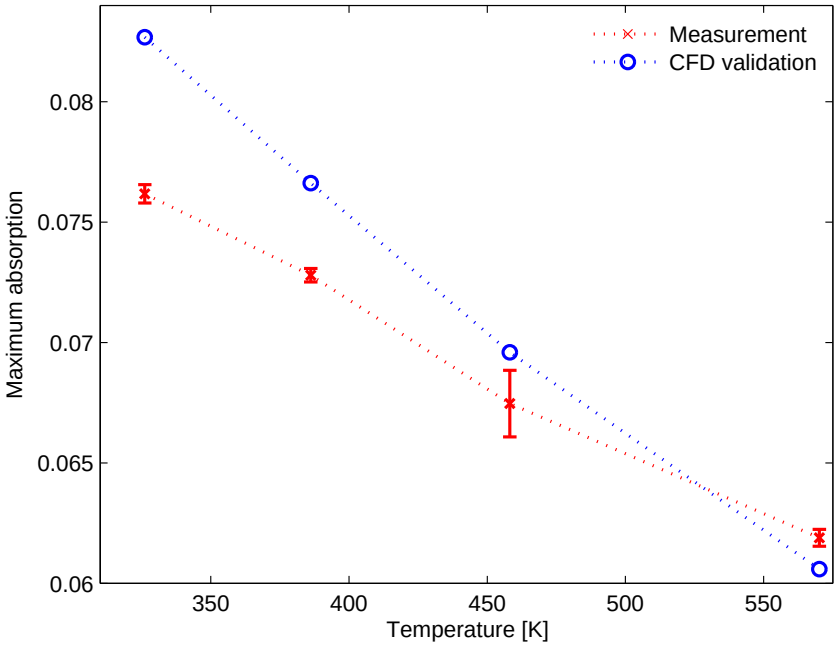

FIGURE 6.20: Calibration curve to temperature-experimental test at $CO = 1.76\%$.

Chapter 7

Concluding remarks and outlook

A laser-based methodology has been successfully implemented for CO-sensing using TDL technique carrying out laser diagnostics in both calibration and free-calibration methods under typical experimental conditions of ISC lab-scale tests. The rotational transition R(11) from the first-overtone of CO has been chosen as an appropriate spectral region to measure without spectral interference the carbon monoxide generated during ISC experiments. The developed TDL-sensor provided easy alignment in the static glass cell and the custom designed combustion chamber without the need of using reference-visible laser light. The spectral region of R(11) transition from $CO-2\nu$ has been experimentally evaluated at different conditions to verify CO-sensing and non-interference from neighboring molecules as expected by the spectral simulations. Collisional broadening was scanned for CO sensing even at pressures as high 4 atm providing excellent calibration results via scanned-wavelength direct absorption. Non-uniformed laser measurements were validated in a good manner using CFD. From the results, the following conclusions and outlook can be stated:

The first overtone of CO (2ν) showed at labs-scale ISC conditions absorption values adequate to develop laser-based diagnostics for specific-sensing without neighboring interference at even high temperatures and high pressures. As absorption values suggested that direct absorption measurements, it was validated by the measurements in the static-glass cell at room conditions and the hazard conditions in the combustion chamber. The R(11) transition showed an appropriate intensity over thermal and pressure effects, where absorption scans from experiments were obtained without experimental issue due to low intensity or spectral interference from CO_2 and H_2O.

The pitch and catch assemblies from the TDL-sensor were successfully designed and

evaluated in two experimental facilities where a rigid mount generated an easy alignment. Although, etalon effects were obtained during the measurements conducted in the static-glass cell, the TDL-sensor provided appropriate diagnostics when wedged windows were implemented in the custom-designed combustion chamber with optical access. The optical sensor setup has the convenience to be implemented in different combustion chamber with optical access since because to the few optical elements.

CO concentrations were carried out in a static-glass cell at room conditions via calibration and free-calibration methods both with good agreement to the linear fit above R^2 of 0.999. Validations with HiTran database demonstrated the accuracy provide from the absorption spectroscopy and the reliable measurements for sensing a target molecule. The line-strength value from HiTRan database was validated by laser measurements. At high pressure and high temperature, the TDL-sensor provided appropriate measurements with high accuracy and excellent linear fit to the measure data while a CDF simulation of the combustion chamber must be developed to obtain the integrated absorption over non-uniformed line-of-sight.

Bibliography

[1] W.E. Brigham and L.M Castanier. In situ combustion. *Society of petroleum engineers*, 2004.

[2] US Environmental Protection Agency. National Emission Standards for Hazardous Air Pollutant.

[3] M.G. Ursenbach, D.W. Bennion, J.D.M Belgrave, and R.G. Moore. A comprehensive approach to in situ combustion modellin. *SPE Advance Technology Series*, 1995.

[4] R. Kharrat and S. Vossoughi. Feasibility study of the in-situ combustion process using TGA/DSC techniques. *Journal of petroleum technology*, 37(8):1441–1445, 1985.

[5] M.G. Allen. Diode laser absorption sensors for gas dynamic and combustion. *Measurement Science and Technology*, 9(545), 1998.

[6] J.K. Delgado. *Amount of carbon dioxide fraction determination by TDLAS: Evidences for potential primary method directly applied in gas analysis.* PhD thesis, 2006.

[7] R.K. Hanson. Applications of quantitative laser sensors to kinetics, propulsion and practical energy systems. *Proceeding of the combustion institute*, 33:1–40, 2011.

[8] V. Ebert, H. Teichert, P. Strauch, T. Kolb, H. Seifert, and J. Wolfrum. Snsitive in situ detection of CO and O2 in a rotary kiln-based hazardous waste incinerator using 760 nm and 2.3 um diode lasers. *Proceeding of the combustion institute*, 30:1611, 2005.

[9] P.J. McCabe. Energy resources - cornucopia or empty barrel? *AAPG Buttelin*, 83(11):2110, 1998.

[10] R.F. Meyer and E.D Attanasi. Heavy oil and natural bitumen resoruces in geological basis of the world, 2007.

[11] description and USGS world petroleum assesment 2000 Results. USGS World energy assesment tema. 2011.

[12] R.G. Moore, J.D.M Belgrave, and M.G. Ursenbach. In situ combustion in heavy oil reservoirs: problems and perspecives. *In situ*, 21:1–26, 1997.

[13] W.E. Brigham and L.M Castanier. Upgrading of crude oil via in situ combustion. *Journal of Petroleum Science and Engineering*, 39(125-136), 2003.

[14] M Gerritsen and A Kovscek. Experimental investigation and high resolutio simulation of in situ combustion process, DOE Award No: DE-FC26-03NT15405. Technical report, 2008.

[15] J.D.M. Belgrave, M.G. Ursenbach, and R.G. Moore. In situ combustion in Canadian heavy oil reservoirs. *Fuel*, 74(8):1169–1175, 1995.

[16] Laureshen C.J., M.G. Ursenbach, S.A. Mehta, J.D.M. Belgrave, and R.G. Moore. Combustion/oxidation behaviour of athabasca oil sands bitumen. *SPE Reservoir Engineering*, 2(6), 1999.

[17] F. B. Thomas, R.G. Moore, and D.W. Bennion. Kinetic parameters for the high-temperature oxidation of insitu combustion coke. *Canadian Petroleum Technology*, 24(6):60–67, 1985.

[18] Kapadia, P.R., M.S. Kallos, and I.D. Gates. Potential for hydrogen generation from in situ combustion of Athabasca bitumen. *Fuel*, 90(6):2254–2265, 2011.

[19] Z. Liu, K. Jessen, and T.T. Tsotsis. Optimization of in situ combustion processes: A parameter space study towards reducing the CO2 emissions. *Chemical Engineering Science*, 66(12):2723–2733, 211.

[20] B. Dechelette, O. Heugas, and G. Quenault. Air injection improved determination of the reaction scheme with ramped temperature experiment and numerical simulation. *Journal of Canadian Petroleum Technology*, 45(1):41–47, 2006.

[21] B. Hascakir, G. Glatz, and L.M Castanier. In situ combustion dynamics visualizated with X-Ray computed tomography. *SPE Journal*, pages 524–536, 2011.

[22] J.M. Kremsner and C.O. Kappe. Silicon carbide passive heating elements in microwave-assisted organic synthesis. *The journal of organic chemistry*, 71(12):4651–4658, 2006.

[23] O. Drici and S. Vossoughi. Study of the surface area effect on crude oil combustion by thermal analysis techniques. *Journal of petroleum technology*, 37(4):731–735, 1985.

[24] C. Tropea and A. Yarin. Combustion diagnostic. In *Handbook of experimental fluid dynamic*, pages 1241–1315. 2007.

[25] J. Ballester and T. Garcia. Diagnostic techniques for the monitoring and control of practical flames. *Progress in Energy and Combustion Science*, 36(375-411), 2010.

[26] W. Hentschel. Optical disgnostics for combustion process development of direct injection gasoline engines. *Proceeding of the combustion institute*, 28(1):1119–1135, 2000.

[27] M Alden. Visualization and understanding of combustion processes using spatially and temporally resolved laser diagnostic techniques. *Proceeding of the combustion institute2*, 33:69–97, 2011.

[28] J.M. Porter. *Laser-based diagnostics for hydrocarbons fuels in the liquid and vapor phases*. PhD thesis, Stanford University, 2009.

[29] M. Gabrysch. Simultaneous detection of CO and CO2 using a semiconductor DFB diode laser at 1.578 um. *Applied Physics B*, 79(1):75–79, 1997.

[30] D.S. Wang, J. Maiorov, M. Baer. In istu combustion measurements of CO with diode laser absorption near 2.3 um. *Applied Optics*, 39(30):5579–5589, 2000.

[31] J.C. Nicolas. Tunable Diode Laser Absorption Spectroscopy of Carbon Monoxide around 2.35 um. *Applied Optics1*, 37(33):7906–7911, 1998.